ANTENNA SELECTION FOR SPACE-TIME BLOCK CODED SYSTEMS WITH IMPERFECT CHANNEL KNOWLEDGE

by

Chi Lee

A thesis submitted to the
Department of Electrical and Computer Engineering
in conformity with the requirements
for the degree of Master of Science (Engineering)

Queen's University
Kingston, Ontario, Canada
April 2006

Abstract

Multiple-input multiple-output (MIMO) wireless communication systems promise a higher data rate to meet the demand of future wireless applications. However multiple expensive RF chains, that include power amplifiers, are required at both the basestation and subscriber unit. The system complexity also increases significantly as the number of signal dimensions increase. Orthogonal frequency division multiplexing (OFDM) can reduce complexity of a wide band system. The thesis investigates whether MIMO and MIMO-OFDM system complexity can be reduced by using antenna selection techniques, while maintaining good performance. This study emphasizes MIMO systems.

To date, the performance of antenna selection has not been examined under imperfect instantaneous channel knowledge with a specific channel estimation technique. In this thesis, orthogonal space-time block coded (OSTBC) MIMO antenna selection systems are investigated with maximum-likelihood (ML) and linear minimum-mean-square error (LMMSE) channel estimation techniques. A novel MIMO antenna selection system that takes short-term instantaneous and long-term statistical channel state information into account is developed. The achievable outage and ergodic capacity are evaluated under spatially uncorrelated and correlated Rayleigh block fading channels with different channel estimation strategies. The numerical results indicate that the developed system does not always benefit appreciably from deploying additional transmit antennas. It has been found

since the channel spatial correlation improves the LMMSE channel estimation quality, spatial correlation may not always reduce capacity for some signal-to-noise ratios is in contrast to prior studies of systems under perfect channel state information assumption.

It can be shown that the performance enhancement due to additional transmit antennas for MIMO-OFDM systems is upper bounded by the enhancement obtained for MIMO systems. It will also be shown that the total number of transmit antennas should be relatively small for both MIMO and MIMO-OFDM systems under these more practical considerations.

Acknowledgments

First and foremost, I wish to thank my supervisor, Dr. Steven D. Blostein, department head of the Electrical and Computer Engineering at Queen's University. His guidance and patience have supported me since the first day I entered Information Processing and Communications Laboratory. Thank you to Dr. W. Y. G. Chan, Dr. S. Gazor, Dr. K. S. Novakowski, and Dr. G. K. Takahara for carefully reviewing my thesis and providing valuable suggestions. It was an honor to have you as thesis examining committee members.

My colleagues and friends at Queen's university have provided great encouragement and assistant through the years. Special thanks to Dr. Steven D. Blostein, Bernice Ison, Robert Lu, Wei Sheng, Constantin Siriteanu, Yi Song and Neng Wang for their moral support during the important time of my life. Finally, I would like to thank my family for their encouragement and support throughout my study at Queen's University.

This work is in part sponsored by Bell Mobility, Samsung Electronics AIT, and Queen's University. The financial support is greatly appreciated.

Contents

List of Tables

List of Figures

NOTATION

a	the scalar a
$\overline{\boldsymbol{a}}$	the column vector $\overline{\boldsymbol{a}}$
a_m	m-th entry of a column vector $\overline{\boldsymbol{a}}$
$\boldsymbol{A}$	the matrix $\boldsymbol{A}$
$a_{k,l}$	the (k,l)th element of $\boldsymbol{A}$
$(\cdot)^*$	Complex conjugate
$(\cdot)^T$	Matrix or vector transpose
$(\cdot)^\dagger$	Matrix or vector conjugate transpose
$\|\cdot\|_F^2$	squared Frobenius norm for matrices
$\otimes$	the Kronecker product
$\log_2$	the base-2 logarithm
$\det(\cdot)$	the determinant of a matrix
$Tr(\cdot)$	the trace of a matrix
$\boldsymbol{A}^{1/2}$	the Hermitian square root of $\boldsymbol{A}$
$\boldsymbol{a}$	the vector obtained by stacking the columns of $\boldsymbol{A}$ on top of each other; $vec(\boldsymbol{A})$
$\boldsymbol{I_N}$	the identity matrix of dimension $N \times N$; N omitted whenever referring to arbitrary dimension or no confusion can occur

$\boldsymbol{0_{M\times N}}$	the $M \times N$ matrix of zeros; N omitted whenever referring to arbitrary dimension or no confusion can occur
$x \backsim y$	the distribution of random variable x is identical to distribution of random variable y
$\boldsymbol{X} \backsim N_c(\overline{\boldsymbol{\mu}}, \boldsymbol{R})$	$\boldsymbol{X}$ is circular symmetric complex Gaussian with mean $\overline{\boldsymbol{\mu}}$ and covariance matrix $\boldsymbol{R}$
$E(\cdot)$	the expectation of random variables
$\triangleq$	defined as
erf	the error function
$J_m(.)$	the Bessel function of the first kind with order m

COMMONLY USED SYMBOLS

C_s	instantaneous capacity
$\overline{C_s}$	ergodic capacity
$\boldsymbol{C}$	space-time block code matrix
C_{outage}	outage capacity
N_t	number of transmit antennas
N_r	number of receive antennas
M_t	number of selected transmit antennas
M_r	number of selected receive antennas
$\boldsymbol{H}$	time-domain channel matrix
$\boldsymbol{h}$	$vec(\boldsymbol{H})$
$\ddot{\boldsymbol{H}}$	frequency-domain channel matrix
$\ddot{\boldsymbol{h}}$	$vec(\ddot{\boldsymbol{H}})$
$\widehat{\boldsymbol{H}}$	estimate of time-domain channel matrix $\boldsymbol{H}$
$\widehat{\boldsymbol{h}}$	$vec(\widehat{\boldsymbol{H}})$
$\widehat{\ddot{\boldsymbol{H}}}$	estimate of frequency-domain channel matrix $\ddot{\boldsymbol{H}}$
$\widehat{\ddot{\boldsymbol{h}}}$	$vec(\widehat{\ddot{\boldsymbol{H}}})$
$\widetilde{\boldsymbol{H}}$	time-domain estimation error of channel matrix $\boldsymbol{H}$
$\widetilde{\boldsymbol{h}}$	$vec(\widetilde{\boldsymbol{H}})$
$\widetilde{\ddot{\boldsymbol{H}}}$	frequency-domain estimation error of channel matrix $\ddot{\boldsymbol{H}}$

$\widetilde{\ddot{\boldsymbol{h}}}$	$vec(\widetilde{\ddot{\boldsymbol{H}}})$
$\widehat{\boldsymbol{H}}_{\boldsymbol{s}}$	selected time-domain channel matrix
$\widehat{\ddot{\boldsymbol{H}}}_{\boldsymbol{s}}$	selected frequency-domain channel matrix
$\boldsymbol{H}_{\boldsymbol{w}}$	$\boldsymbol{H}_{\boldsymbol{w}} \backsim N_c(\boldsymbol{0},\boldsymbol{I})$
$\boldsymbol{h}_{\boldsymbol{w}}$	$vec(\boldsymbol{H}_{\boldsymbol{w}})$
$\boldsymbol{R}_{\boldsymbol{Tx}}$	transmit channel covariance matrix
$\boldsymbol{R}_{\boldsymbol{Rx}}$	receive channel covariance matrix
r_c	code rate of a space-time block code
$\boldsymbol{Y}$	received signal matrix
$\boldsymbol{S}_{\boldsymbol{d}}$	space-time block coded signal matrix transmitted during data phase
$\boldsymbol{S}_{\tau}$	training signal matrix transmitted during training phase
T	block length
T_{τ}	training length
T_d	data transmission length
T_b	space time block code length
T_c	channel coherence time
T_f	feedback delay
$\boldsymbol{W}$	noise matrix
$\boldsymbol{w}$	$vec(\boldsymbol{W})$
$\boldsymbol{Q}$	whitening matrix
Ω	FFT matrix
ρ	channel signal-to-noise ratio

ABBREVIATIONS

A/D	analog to digital
AWGN	additive white Gaussian noise
BER	bit error rate
BS	base station
CP	cyclic prefix
CSI	channel state information
DFFT	discrete fast fourier transform
Eq.	equation
FFT	fast fourier transform
Fig.	figure
IDFT	inverse discrete fourier transform
IFFT	inverse fast fourier transform
i.i.d.	independent and identically distributed
ISI	intersymbol interference
LMMSE	linear minimum-mean-square-error
MIMO-OFDM	multiple-input multiple-output orthogonal frequency division multiplexing
MIMO	multiple-input multiple-output
ML	maximum-likelihood
NLOS	non line-of-sight

OSTBC	orthogonal space-time block code/codes/coding
P/S	parallel-to-serial
PAS	power azimuth spectrum
p.d.f.	probability density function
RF	radio frequency
RMS	root -mean square
S/P	serial-to-parallel
SISO	single-input single-output
SNR	signal-to-noise ratio
SU	subscriber unit
SVD	singular value decomposition

Chapter 1

Introduction

1.1 Motivation

The continuing increase in demand for services such as data, video on demand, high speed multimedia and mobile internet access has driven wireless communications toward the next generation. In response, wireless communication technology has improved greatly in terms of spectral efficiency to satisfy the increasing capacity and data rate. Multiple-input multiple-output (MIMO) systems and orthogonal frequency division multiplexing (OFDM) are the major technologies that boost the data rate of wireless communications systems.

One of the earliest MIMO wireless communication systems was proposed by Jack Winters in 1984 [75]. OFDM was first implemented in 1957 in the Collins Kineplex system [13]. An implementation by fast Fourier transform is proposed in [74] to lower the system cost and is first described in the context of mobile wireless communications in [11]. OFDM is adopted in various standards, such as ETSI digital audio broadcasting (DAB) [14], digital video broadcasting (DVB) [15], and IEEE 802.11 [29, 30] wireless LAN. The deployment of OFDM in GSM systems is currently under consideration [1]. The first MIMO-OFDM system was presented in 1996 [57]. MIMO-OFDM has been adopted in

ETSI HIPERLAN/2 [16] with a maximum of two transmit antennas and IEEE 802.11n [26] with a maximum of four transmit antennas.

However the major drawback of MIMO/MIMO-OFDM systems is that system complexity and cost increase dramatically with number of transmit antennas. Antenna selection has been proposed to target this problem. Current studies on antenna selection focus on systems with perfect channel state information (CSI). With this ideal assumption, this simplified MIMO system performance can improve without bound. However in practice, CSI is never perfect. The most common way to acquire CSI is through transmitting training symbols from the transmitter. The receiver then estimates the channel by techniques such as maximum likelihood (ML) or linear minimum-mean-square error (LMMSE) estimation. The channel estimation does not only induce error but also reduces capacity due to training overhead. The system performance and design of antenna selection incorporating imperfect CSI has not been investigated according to the best of our knowledge.

1.2 Thesis Overview

This thesis investigates practical aspects of the antenna selection for orthogonal space-time block coded MIMO and MIMO-OFDM wireless communication systems. A total of five chapters in this thesis addresses this topic.

In Chapter 2, the wireless channel models for both MIMO and MIMO-OFDM are described. The analogy between MIMO and MIMO-OFDM spatially correlated channels are derived. The orthogonal space-time block coded MIMO/MIMO-OFDM with perfect channel knowledge and their corresponding antenna selection algorithms are reviewed. Different channel estimation techniques for both MIMO and MIMO-OFDM systems are also reviewed.

In Chapter 3, the orthogonal space-time coded system with antenna selection under consideration is defined in greater detail. The relations among the channel quality, estimate training length, channel spatial correlation and signal-to-noise (SNR) are formulated mathematically. However due to the order statistics resulting from antenna selection, it is difficult to analytically evaluate the outage and ergodic capacities. Therefore extensive numerical studies involving Monte Carlo channel realizations with a wide range of SNR, transmission block lengths, and spatial correlations with different training strategies have been undertaken and are presented in Chapter 4. In the same section, the performance enhancement for the MIMO-OFDM system due to additional transmit antennas is shown to be upper bounded by the enhancement of the MIMO system, given that the channel on each MIMO-OFDM subcarrier is statistically identical to those of the MIMO channel. Finally Chapter 5 summarizes the conclusions and suggests possible directions for future research.

1.3 Summary of Contributions

The primary contributions of this thesis are summarized as follows:

- A statistical characterization of the true channel, channel estimate and estimation error for linear-minimum-mean-square error channel estimation is presented in Section 3.3, clarifying previous studies.
- Application of the above statistical characterization to orthogonal space time block decoding in correlated fading channels is presented in Section 3.4.
- An OSTBC MIMO system with antenna selection that takes short-term instantaneous and long-term statistical channel state information into account.
- An analysis, in terms of Monte Carlo analysis, of the orthogonal space-time block

coded MIMO system with antenna selection under various settings is performed, which takes training overhead into account, in Chapter 4.

- An analysis of OSTBC MIMO-OFDM systems with antenna selection is conducted and an upper bound on performance enhancement due to additional transmit antennas is determined in Section 3.7.

Chapter 2

Background and Objectives

2.1 MIMO Channel Model

We consider a multiple-input-multiple-output (MIMO) wireless communication system where the transmitter has N_t antennas, and the receiver has N_r antennas (Fig. 2.1). The channel coherence bandwidth (B_c) is defined as the range that frequency responses are closely correlated. The coherence bandwidth is inversely proportional to delay spread (L). Depending on the relation between the bandwidth of the transmitting signal B_s and B_c, the system might experience frequency-flat or frequency-selective fading. In this section, we will discuss both types of fading.

2.1.1 Frequency-Flat Fading

For narrow-band wireless communications, the signal bandwidth is assumed to be smaller than the coherence bandwidth. Under this assumption, the channel experiences frequency-flat fading. The channel frequency response can be treated as flat across the occupied

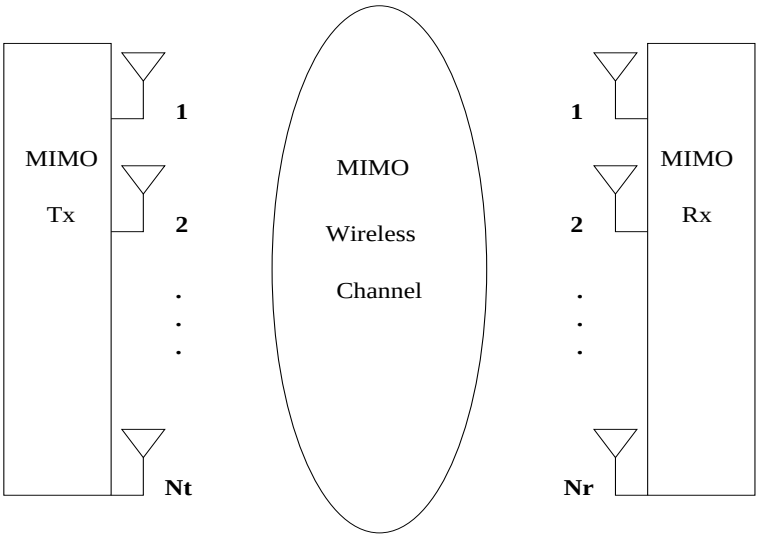

Figure 2.1: MIMO System

frequency band. The MIMO channel can be expressed in a matrix form

$$\boldsymbol{H} = \begin{pmatrix} h_{1,1} & h_{1,2} & \dots & h_{1,N_t} \\ h_{2,1} & h_{2,2} & \dots & h_{2,N_t} \\ \vdots & \vdots & \ddots & \vdots \\ h_{N_r,1} & h_{N_r,2} & \dots & h_{N_r,N_t} \end{pmatrix}. \tag{2.1}$$

The channel matrix $\boldsymbol{H}$ comprises the short-term instantanous channel state information (CSI). It is assumed that all the antenna elements in the MIMO system have the same polarization and radiation pattern. Let m_i and m_j be values of $1 \dots N_t$ representing indices for any two transmit antennas and n_i and n_j be values of $1 \dots N_r$ representing indices any two receive antennas. The spatial correlation coefficient between impinging waves between any of the two transmit antennas is defined as

$$p^{Tx}_{m_i,m_j} = E[h_{n_k,m_i} h_{n_k,m_j}], \tag{2.2}$$

Similarly, the spatial correlation coefficient at the receiver is defined as

$$p^{Rx}_{n_i,n_j} = E[h_{n_i,m_k} h_{n_j,m_k}]. \tag{2.3}$$

Given (2.2) and (2.3) the correlation matrices are defined as follows

$$\boldsymbol{R_{Tx}} = \begin{pmatrix} p_{1,1}^{Tx} & p_{1,2}^{Tx} & \cdots & p_{1,N_t}^{Tx} \\ p_{2,1}^{Tx} & p_{2,2}^{Tx} & \cdots & p_{2,N_t}^{Tx} \\ \vdots & \vdots & \ddots & \vdots \\ p_{N_t,1}^{Tx} & p_{N_t,2}^{Tx} & \cdots & p_{N_t,N_t}^{Tx} \end{pmatrix}, \tag{2.4}$$

and

$$\boldsymbol{R_{Rx}} = \begin{pmatrix} p_{1,1}^{Rx} & p_{1,2}^{Rx} & \cdots & p_{1,N_r}^{Rx} \\ p_{2,1}^{Rx} & p_{2,2}^{Rx} & \cdots & p_{2,N_r}^{Rx} \\ \vdots & \vdots & \ddots & \vdots \\ p_{N_r,1}^{Rx} & p_{N_r,2}^{Rx} & \cdots & p_{N_r,N_r}^{Rx} \end{pmatrix}. \tag{2.5}$$

In the model provided in [54], the spatial correlation matrix of the MIMO wireless channel is the Kronecker product of the spatial correlation matrix at the transmitter and receiver and is presented as

$$\boldsymbol{R} = E[\boldsymbol{h}\boldsymbol{h}^{\dagger}] = \boldsymbol{R_{Tx}} \otimes \boldsymbol{R_{Rx}}. \tag{2.6}$$

To generate the channel matrix $\boldsymbol{H}$ according to the spatial correlation defined in Eq. (2.6), it is easy to see

$$\boldsymbol{H} \backsim \boldsymbol{R_{Rx}}^{1/2} \boldsymbol{H_w} \boldsymbol{R_{Tx}}^{1/2}, \tag{2.7}$$

$$\boldsymbol{h} \backsim \boldsymbol{R}^{1/2} \boldsymbol{h_w}, \tag{2.8}$$

where $\boldsymbol{H_w}$ is a complex zero-mean Gaussian random matrix and the variance of each quadrature element is $1/2$. $\boldsymbol{h}$ is the vector obtained by stacking the columns of $\boldsymbol{H}$ on top of each other, and $\boldsymbol{h_w}$ is the vector form of $\boldsymbol{H_w}$. In Eq. (2.7), the notation $x \backsim y$ means that "the statistical distribution of x is identical to the statistical distribution of y" Such a model has been supported with experimental validation in [61]. The information regarding $\boldsymbol{R_{Tx}}$ and $\boldsymbol{R_{Rx}}$ is called the long-term statistical CSI.

2.1.2 Frequency-Selective Fading

Consider a wide band MIMO communication system, where the signal bandwidth is greater than the channel coherence bandwidth. Such a MIMO channel is called frequency-selective fading. The received MIMO signal is a sum of delayed replicas of the transmitted signal.

$$\boldsymbol{Y}(t) = \sum_{l=1}^{L} A^l(t)\boldsymbol{H^l}(t)\boldsymbol{S}(t-\tau_l(t)), \tag{2.9}$$

where $\boldsymbol{H^l}(\boldsymbol{t})$ and $A^l(t)$ are the channel response and the power at each path, respectively, and L is the number of resolvable paths of the channel. The information regarding L and A^l is called the channel delay profile, and is closely associated with a given environment.

2.1.3 Time-Selective Fading

Relative motion between the environment and system causes variation of a channel over time. Therefore the transmitted signal experiences different fading at different times. This characteristic of the wireless channel is referred to as time-selective fading. Motion causes frequency shift (Doppler spread). Time-selective fading can be characterized by the channel coherence time, T_c, which is inversely proportional to Doppler spread. Most communications systems require channel state information (CSI) at the receiver to decode the transmitted information. For channels with relatively small T_c, CSI needs to be estimated frequently, which increases overhead. As T_c decreases, it is more difficult for systems that require CSI at transmitter to obtain useful CSI related information through feedback from the receiver.

2.1.4 Power Azimuth Spectrum

Let the two random signals observed by two antennas be

$$r_m = X_m + jY_m, \; m\text{=1 or 2}. \tag{2.10}$$

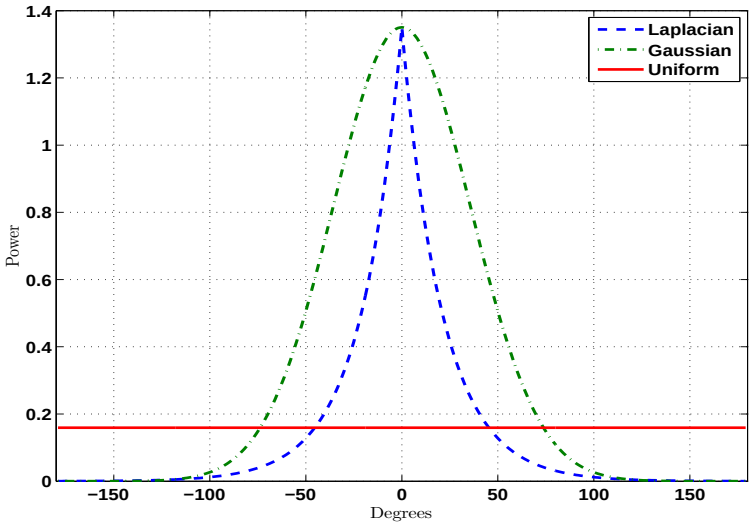

Figure 2.2: Normalized PASs for a single cluster case. For the three PASs, AS=30° and angle of incidence $\phi = 0°$. PASs are confined within $[-180°, 180°]$

In order for $\|r_1\|^2$ and $\|r_2\|^2$ to be equal power Rayleigh random variables and the quadrature components are uncorrelated, the following are sufficient conditions: [31].

$$\begin{aligned}
\mu_0 &= R^{X_1X_1}(0) = R^{X_2X_2}(0) = R^{Y_1Y_1}(0) = R^{Y_2Y_2}(0) \\
\mu_1 &= R^{X_1X_2}(D(p,q)) = R^{Y_1Y_2}(D(p,q)) \\
\mu_2 &= R^{X_1Y_2}(D(p,q)) = -R^{Y_1X_2}(D(p,q)) \\
0 &= R^{X_1Y_1}(D(p,q)) = R^{X_2Y_2}(D(p,q)),
\end{aligned} \tag{2.11}$$

where $D(p,q) = 2\pi\frac{d}{\lambda}$ is the normalized distance between the p-th and q-th antenna elements where λ is the wavelength and d is distance. The cross-correlation functions, $R^{X_1X_2}(D(p,q))$ and $R^{X_1Y_2}(D(p,q))$ can be obtained through power azimuth spectrum (PAS). The PAS are commonly modeled by three different distributions, namely uniform, Gaussian and Laplacian. All three PASs are reviewed in [62]. A PAS of an environment with N_c scattering clusters depends on angle of incidence $\phi_{0,k}$, azimuth spread (AS) σ_k, and distribution boundary $\triangle\phi_k$, such that the PAS is defined in the range $[\phi_{0,k} - \triangle\phi_k, \phi_{0,k} + \triangle\phi_k]$,where

$k = 1 \ldots N_c$. To maintain generality, the mathematical expression of PAS for each case is summarized in the following sections for a multi-cluster scenario ($N_c > 1$). An example of a single cluster ($N_c = 1$) PAS is shown in Fig. 2.2 ($\phi = 0°$, AS= 30, $\triangle\phi = 180°$) for all three distributions for visualization purposes. In the following discussions, m presents the number of signal paths. If m is large enough we may apply the Central Limit Theorem to conclude the channel is a complex Gaussian process, so the envelope of the fading channel is Rayleigh distributed. As suggested in [31], this Rayleigh approximation is quite good for $m \geq 6$.

2.1.4.1 Uniform PAS

First introduced in [58], a uniform PAS with multi-cluster is modeled as

$$PAS_U(\phi) = \sum_{k=1}^{N_c} C_{U,k} \left(\varepsilon[\phi - (\phi_{0,k} - \triangle\phi_k)] - \varepsilon[\phi - (\phi_{0,k} + \triangle\phi_k)] \right), \tag{2.12}$$

where $\varepsilon(\phi)$ is a step function. Normalization factors $C_{U,k}$ are derived such that $PAS_U(\phi)$ meets the requirement of a probability density function (p.d.f.), e.g.,

$$\int_{-\pi}^{\pi} PAS_U(\phi) d\phi = \sum_{k=1}^{N_c} \int_{\phi_{0,k}-\triangle\phi_k}^{\phi_{0,k}+\triangle\phi_k} C_{U,k} d\phi = 1. \tag{2.13}$$

From Eq. 2.13, the normalization constants $C_{U,k}$ need to satisfy the following condition:

$$2 \sum_{k=1}^{N_c} C_{U,k} \triangle\phi_k = 1. \tag{2.14}$$

The cross correlation function between the real components is

$$R_U^{X_1 X_2}(D(p,q)) \triangleq \int_{-\pi}^{\pi} \cos(D(p,q) sin\phi) PAS(\phi) d\phi \tag{2.15}$$

$$= J_0(D(p,q)) + 4 \sum_{k=1}^{N_c} C_{U,k} \sum_{m=1}^{+\infty} \frac{J_{2m}(D(p,q))}{2m} \cos(2m\phi_{0,k}) \sin(2m\triangle\phi_k). \tag{2.16}$$

On the other hand, the correlation between the quadrature components is

$$R_U^{X_1Y_2}(D(p,q)) \triangleq \int_{-\pi}^{\pi} \sin(D(p,q)\sin\phi) PAS(\phi) d\phi \tag{2.17}$$

$$= 4\sum_{k=1}^{N_c} C_{U,k} \sum_{m=1}^{+\infty} \frac{J_{2m+1}(D(p,q))}{2m+1} \sin[(2m+1)\phi_{0,k}] \sin[(2m+1)\triangle\phi_k]. \tag{2.18}$$

2.1.4.2 Gaussian PAS

A Gaussian distributed PAS is introduced in [2]. For a multi-cluster scenario, the PAS is modeled as

$$PAS_G(\phi) = \sum_{k=1}^{N_c} \frac{C_{G,k}}{\sigma_{G,k}\sqrt{2\pi}} \exp\left[-\frac{(\phi-\phi_0)^2}{2\sigma_{G,k}^2}\right] \times \left(\varepsilon[\phi-(\phi_{0,k}-\triangle\phi_k)] - \varepsilon[\phi-(\phi_{0,k}+\triangle\phi_k)]\right). \tag{2.19}$$

From (2.13), the normalization constants $C_{G,k}$ are derived such that

$$\sum_{k=1}^{N_c} C_{G,k}\, erf\left(\frac{\triangle\phi_k}{\sigma_{G,k}\sqrt{2}}\right) = 1, \tag{2.20}$$

where $erf(x)$ denotes the error function, defined as

$$erf(x) = \frac{2}{\sqrt{\pi}} \int_0^x e^{-t^2} dt. \tag{2.21}$$

By definition of (2.19) and (2.20), the cross-correlation functions for the Gaussian PAS are

$$R_G^{X_1X_2}(D(p,q)) = J_0(D(p,q)) + \sum_{k=1}^{N_c} C_{G,k} \sum_{m=1}^{+\infty} J_{2m}(D(p,q)) \cos(2m\phi_{0,k}) \exp(-2\sigma_{G,k}^2 m^2) \times \Re\left[\begin{matrix} erf\left(\frac{\triangle\phi_k}{\sigma_{G,k}\sqrt{2}} - jm\sigma_{G,k}\sqrt{2}\right) \\ -erf\left(-\frac{\triangle\phi_k}{\sigma_{G,k}\sqrt{2}} - jm\sigma_{G,k}\sqrt{2}\right) \end{matrix}\right]. \tag{2.22}$$

$$R_G^{X_1Y_2}(D(p,q)) = \sum_{k=1}^{N_c} C_{G,k} \sum_{m=1}^{+\infty} J_{2m+1}(D(p,q)) \sin[(2m+1)\phi_{0,k}] \exp\left(-2\sigma_{G,k}^2 \left(m+\frac{1}{2}\right)^2\right)$$

$$\times \Re \begin{bmatrix} erf\left(\frac{\triangle\phi_k}{\sigma_{G,k}\sqrt{2}} - j(m+\frac{1}{2})\sigma_{G,k}\sqrt{2}\right) \\ -erf\left(-\frac{\triangle\phi_k}{\sigma_{G,k}\sqrt{2}} - j(m+\frac{1}{2})\sigma_{G,k}\sqrt{2}\right) \end{bmatrix}, \tag{2.23}$$

where $\Re(x)$ denotes the real component of x.

2.1.4.3 Laplacian PAS

The most recently proposed PAS is the Laplacian distribution. It is first introduced in [54] with supporting experimental data obtained both from urban and rural areas. The PAS is modeled as

$$PAS_L(\phi) = \sum_{k=1}^{N_c} \frac{C_{L,k}}{\sigma_{L,k}\sqrt{2\pi}} \exp\left[-\frac{\sqrt{2}\|\phi-\phi_0\|}{\sigma_{L,k}^2}\right] \times \left(\varepsilon[\phi-(\phi_{0,k}-\triangle\phi_k)] - \varepsilon[\phi-(\phi_{0,k}+\triangle\phi_k)]\right). \tag{2.24}$$

The normalization constants are defined to satisfy the following condition.

$$\sum_{k=1}^{N_c} C_{L,k}\left[1-\exp\left(-\frac{\sqrt{2}\triangle\phi_k}{\sigma+L,k}\right)\right] = 1. \tag{2.25}$$

The cross-correlation functions are

$$R_L^{X_1X_2}(D(p,q)) = J_0(D(p,q)) + 4\sum_{k=1}^{N_c}\frac{C_{L,k}}{\sigma_{L,k}\sqrt{2}}\sum_{m=1}^{+\infty}\frac{J_{2m}(D(p,q))}{\left(\frac{\sqrt{2}}{\sigma_{L,k}}\right)^2+(2m)^2}\cos(2m\phi_{0,k}) \times \left\{\frac{\sqrt{2}}{\sigma_{L,k}} + \exp\left(-\frac{\triangle\phi_k\sqrt{2}}{\sigma_L,k}\right)\begin{bmatrix} 2m\sin(2m\triangle\phi_k) \\ -\frac{\sqrt{2}}{\sigma_{L,k}}\cos(2m\triangle\phi_k)\end{bmatrix}\right\}, \tag{2.26}$$

$$R_L^{X_1Y_2}(D(p,q)) = 4\sum_{k=1}^{N_c}\frac{C_{L,k}}{\sigma_{L,k}\sqrt{2}}\sum_{m=1}^{+\infty}\frac{J_{2m+1}(D(p,q))}{\left(\frac{\sqrt{2}}{\sigma_{L,k}}\right)^2+(2m+1)^2}\sin[(2m+1)\phi_{0,k}] \times \left\{\frac{\sqrt{2}}{\sigma_{L,k}} + \exp\left(-\frac{\triangle\phi_k\sqrt{2}}{\sigma_L,k}\right)\begin{bmatrix} (2m+1)\sin[(2m+1)\triangle\phi_k] \\ +\frac{\sqrt{2}}{\sigma_{L,k}}\cos[(2m+1)\triangle\phi_k]\end{bmatrix}\right\}, \tag{2.27}$$

where J_m is the Bessel function of the first kind and m-th order.

2.1.5 MIMO Channel Correlation Matrix and Cross-Correlation Functions

The purpose of this section is to state the relationship of cross-correlation functions, $R^{X_1X_2}$ and $R^{X_1Y_2}$, to the overall MIMO channel correlation matrix. The correlation coefficient between the envelope of the two radio waves was first studied in [39], however the resulting expression is difficult to compute. A close approximation was then proposed by [9] and then summarized in [41, 42]. The approximate normalized correlation function between the envelopes is

$$\begin{aligned} p_{p,q} &\approx \frac{E[X_1X_2] + E[X_1Y_2]}{E\left[X_1^2\right]^2} \\ &= \frac{R^{X_1X_2}(D(p,q)) + R^{X_1Y_2}(D(p,q))}{R^{X_1X_1}(0)}. \end{aligned} \tag{2.28}$$

Now let us construct the correlation matrix in Eq. (2.6) from the above result. As Eq. (2.6) and [62] suggested, the MIMO channel correlation matrix can be separated into correlations at transmit R_{Tx} antennas and receive antennas R_{Rx}. Now let us generalize the result to $N_t > 2$. Redefine Eq. (2.10) to represent the observed signal at the p-th transmit antenna. Let $\bar{r}_{Tx}$ be the column vector consisting of the observed signals at all the transmit antennas.

$$\bar{r}_{Tx} = \begin{bmatrix} r_{Tx1} \\ \vdots \\ r_{TxN_t} \end{bmatrix}. \tag{2.29}$$

The cross-correlation matrix is defined by

$$\boldsymbol{R_{Tx}} = E[\bar{\boldsymbol{r}}_{\boldsymbol{Tx}}\bar{\boldsymbol{r}}_{\boldsymbol{Tx}}^{\dagger}]. \tag{2.30}$$

which has element $p_{i,j}^{Tx}$ given by

$$p_{p,q}^{Tx} = \begin{cases} R^{X_1X_2}(0) + R^{Y_1Y_2}(0), & \text{p = q} \\ R^{X_1X_2}(D(p,q)) + R^{Y_1Y_2}(D(p,q)) + j[R^{Y_1X_2}(D(p,q)) - R^{X_1Y_2}(D(p,q))], & \text{p > q} \\ R^{X_1X_2}(D(p,q)) + R^{Y_1Y_2}(D(p,q)) - j[R^{Y_1X_2}(D(p,q)) - R^{X_1Y_2}(D(p,q))], & \text{p < q.} \end{cases} \tag{2.31}$$

Following the same steps, the correlation matrix of the observed signals at the receiver can be determined as well.

2.1.6 Spatially Uncorrelated and Semi-Correlated MIMO Channels

In a rich scattering environment, it is assumed that both basestation (BS) and subscribed unit (SU) are surrounded by local scatterers. The impinging waves observed at both the SU and BS can be considered to be independent in this case ($\boldsymbol{R_{Tx}} = \boldsymbol{R_{Rx}} = \boldsymbol{I}$). Therefore Eq. (2.7) becomes

$$\boldsymbol{H} \backsim \boldsymbol{H_w}. \tag{2.32}$$

This model is applicable to indoor/office wireless LAN environments, where the transmitter and receiver are at the same height as the furniture.

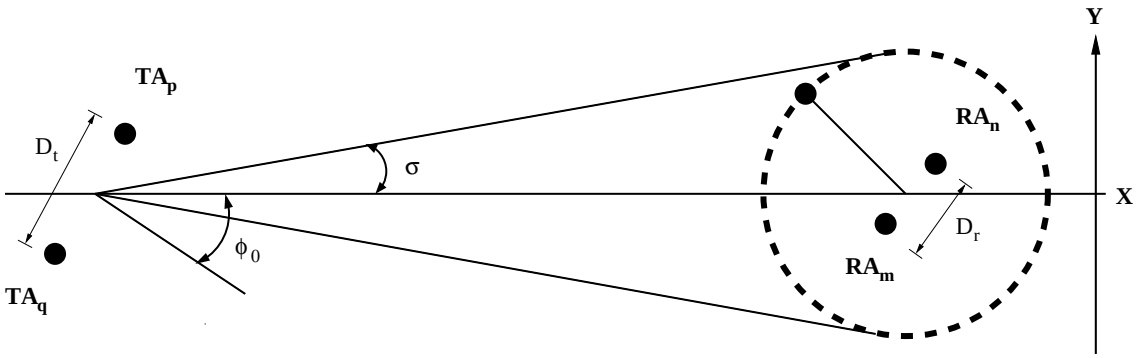

Figure 2.3: Illustration of "one-ring" channel model. TA: transmit antenna. RA: receiving antenna.

However in general environments, the BS is usually situated high above the ground, while only SU is in a rich scattering environment. This kind of model is usually referred as the "one-ring" channel model in the literature. The geometric interpretation of the model is shown in Fig. 2.3, where ϕ_0 and σ are the angles of incidence and azimuth spread (AS), respectively, $D_t(p,q) = 2\pi\frac{d_t(p,q)}{\lambda}$, where $d(p,q)$ is the distance between the p-th and q-th transmit antenna elements and λ is the wavelength. $D_r(m,n) = 2\pi\frac{d_r(m,n)}{\lambda}$ is the corresponding normalized distance between the m-th and n-th receive antenna elements. Due to the rich scattering at the SU, only $\boldsymbol{R_{Rx}} = \boldsymbol{I}$. The overall channel is determined completely by the correlation between the impinging waves observed by the BS in this environment. Therefore Eq. (2.7) can be rewritten as

$$\boldsymbol{H} \backsim \boldsymbol{H_w}\boldsymbol{R_{Tx}}^{1/2}. \tag{2.33}$$

This type of channel is usually referred as a semi-correlated channel and has been validated by empirical measurements in urban environments [38].

2.2 Orthogonal Space-Time Block Coding

Orthogonal space-time block codes (OSTBC) was first proposed by Alamouti [3] and then generalized in [67]. We will focus on linear orthogonal design for complex-valued signals since the linearity ensures simple code construction and current communication systems tend to employ complex-valued constellations due to their higher spectral efficiencies. The designed codes have the following generalized form

$$\boldsymbol{C} = \begin{pmatrix} c_1^1 & c_2^1 & \dots & c_{T_b}^1 \\ \vdots & \vdots & \ddots & \vdots \\ c_1^{N_t} & c_2^{N_t} & \dots & c_{T_b}^{N_t} \end{pmatrix}.$$

Each element c_t^i is a linear combination of data symbols $x_1, x_2, \ldots, x_k$. This code has the following properties:

1. All the columns are orthogonal to one another such that $\boldsymbol{C}^{\dagger}\boldsymbol{C} = \left[\left(\sum_{k=1}^{N_t} |x_k|^2\right)\right] I_{N_t}$.
2. The code rate is $r_c = \frac{k}{T_b}$.

It is shown that the rate-one linear orthogonal space-time block code only exists when $N_t = 2$ [67], which is the Alamouti space-time block code.

2.2.1 Maximum-Likelihood Decoding with Perfect Channel State Information

Assume the channel is constant at least for the entire coded block T_b, and the receiver obtains perfect CSI. The signal received at the j-th receive antenna from a transmitter with uniform power allocation at time t is given by

$$r_t^j = \frac{\rho}{N_t} \sum_{i=1}^{N_t} h_{i,j} c_t^i + n_t^j, \tag{2.34}$$

where the noise n_t^i is a complex Gaussian variable with zero mean and unit-variance, and ρ is the transmit signal power. The optimal maximum-likelihood (ML) decoding problem takes the following formulation form [68]:

$$\begin{aligned}&(\hat{c}_1^1 \hat{c}_2^1 \ldots \hat{c}_{T_b}^1 \hat{c}_1^2 \hat{c}_2^2 \ldots \hat{c}_{T_b}^2 \ldots\ldots \hat{c}_1^{N_t} \hat{c}_2^{N_t} \ldots \hat{c}_{T_b}^{N_t}) \\ &= arg\ min_{c_1^1 c_2^1 \ldots c_{T_b}^1 c_1^2 c_2^2 \ldots c_{T_b}^2 \ldots\ldots c_1^{N_t} c_2^{N_t} \ldots c_{T_b}^{N_t}} \sum_{t=1}^{T_b} \sum_{j=1}^{N_r} \left| r_t^j - \frac{\rho}{N_t} \sum_{i=1}^{N_t} h_{i,j} c_t^i \right|^2 .\end{aligned} \tag{2.35}$$

2.2.2 Performance Analysis with Perfect CSI

From [60, 67] the effective signal model induced by orthogonal space-time block codes for complex-value constellations is

$$\bar{y} = \sqrt{\frac{\rho}{N_t}} \|\boldsymbol{H}\|_F^2 \bar{x} + \overline{w}, \tag{2.36}$$

where $\bar{y}$ is a $k \times 1$ vector after OSTBC decoding of the received $N_r \times T_b$ matrix $\boldsymbol{Y}$, $\bar{x}$ is a $k \times 1$ vector of the complex symbols from the transmitter with power $\frac{T_b}{2k}$ per dimension, $||\boldsymbol{H}||_F^2$ denotes the squared Frobenius norm of channel matrix, and $\overline{w}$ is the noise vector after OSTBC decoding. It can be shown that the elements in $\overline{w}$ are i.i.d complex Gaussian random variables with zero mean and variance $\frac{\|\boldsymbol{H}\|_F^2}{2}$ per dimension.

For a 2-by-2 MIMO system with Alamouti space-time block code, Eq. (2.36) becomes

$$\begin{pmatrix} y_{11} \\ y_{21}^* \\ y_{12} \\ y_{22}^* \end{pmatrix} = \frac{\rho}{2} \underbrace{\begin{pmatrix} h_{11} & h_{21} \\ h_{21}^* & -h_{11}^* \\ h_{12} & h_{22} \\ h_{22}^* & -h_{12}^* \end{pmatrix}}_{\boldsymbol{H_{new}}} \begin{pmatrix} x_1 \\ x_2 \end{pmatrix} + \begin{pmatrix} w_{11} \\ w_{21}^* \\ w_{12} \\ w_{22}^* \end{pmatrix}. \tag{2.37}$$

The new $(N_t T) \times k$ channel matrix $\boldsymbol{H_{new}}$ has following property

$$\boldsymbol{H_{new}}^\dagger \boldsymbol{H_{new}} = ||\boldsymbol{H}||_F^2 I_k. \tag{2.38}$$

The above illustration shows that OSTBC decouples the MIMO system into k SISO channels, each with instantaneous effective signal-to-noise ratio

$$SNR_{effective} = \frac{\rho}{N_t r_c} \|\boldsymbol{H}\|_F^2. \tag{2.39}$$

The capacity of the OSTBC coded MIMO system is the summation of k SISO channels, which is

$$C_s = r_c \log_2 \left(1 + SNR_{effective}\right). \tag{2.40}$$

When the instantaneous capacity in Eq. (2.40) falls below the transmission rate the system is said to be in outage, and the outage probability is

$$\begin{aligned} p_{out}(C_{outage}) &= \mathbb{P}(C_s < C_{outage}) \\ &= \mathbb{P}\left(\frac{T - N_t T_{\tau/N_t}}{T} \log_2\left(1 + \frac{\rho}{2\sigma_n^2}\right) < C_{outage}\right). \end{aligned} \tag{2.41}$$

The average effective SNR and ergodic capacity are, respectively,

$$\overline{SNR}_{effective} = E\left[\frac{\rho}{N_t\ r_c}\|\boldsymbol{H}\|_F^2\right], \tag{2.42}$$

$$\overline{C}_s = E\left[r_c \log_2\left(1 + SNR_{effective}\right)\right]. \tag{2.43}$$

2.3 MIMO-OFDM Wireless Communication Systems

Wide-band wireless communications can further increase the data rate. However as bandwidth of the signal increases, the channel is more likely to experience frequency-selective fading. This type of channel has been discussed in Section 2.1.2. The major challenge for this type of wireless communication system is the inter-symbol interference (ISI). Conventional techniques to mitigate this destructive effect is through channel equalization [55], which increases the system complexity significantly. Orthogonal frequency division multiplexing (OFDM) using a cyclic-prefix (CP) with length L_{CP} is able to convert a frequency-selective channel into parallel frequency-flat channels if L_{CP} is greater than the length of the discrete-time channel impulse response L, therefore avoiding channel equalization. The channel decoupling is shown in greater detail in Section 2.3.1. By combining OFDM with MIMO, a high-data rate and lower-complexity wireless communication system can be attained. MIMO-OFDM systems can be efficiently implemented using inverse DFT (IDFT) as a modulator, and DFT as a demodulator. The signals before the IDFT and after the DFT are in the frequency-domain, while the signals between the IDFT and DFT

are in the time-domain. Consider a MIMO-OFDM system with $N + L_{CP}$ subcarriers. Let $\ddot{\boldsymbol{T}}_{\boldsymbol{i}}[n] = \{\ddot{t}_i[n,0], \ddot{t}_i[n,1], \ldots, \ddot{t}_i[n,N-1]\}$ denote the length-N frequency-domain data symbol block through transmit branch i at time n. The IDFT of the data block gives the time-domain signal $\boldsymbol{T}_{\boldsymbol{i}}[n] = \{t_i[n,0], t_i[n,1], \ldots, t_i[n,N-1]\}$, then

$$t_i[n,k] = IDFT_N\{\ddot{\boldsymbol{T}}_{\boldsymbol{i}}[n]\}[k]. \tag{2.44}$$

A CP is then appended to the time-domain signal $\boldsymbol{T}_{\boldsymbol{i}}[n]$. The system scheme is illustrated in Fig. 2.4.

The post-FFT signal at the k-th subcarrier from the j-th receive branch for each time instant n within the block length T can be expressed as

$$\ddot{r}_i[n,k] = \frac{\rho}{N_t} \sum_{i=1}^{N_t} \ddot{h}_{i,j}[k]\ddot{t}_i[n,k] + \ddot{w}_j[n,k], \tag{2.45}$$

where $h_{i,j}[k]$ denotes the channel frequency response from the i-th transmit branch to the j-th receive branch at the subcarrier k, $w_j[n,k]$ denotes the additive Gaussian noise at the

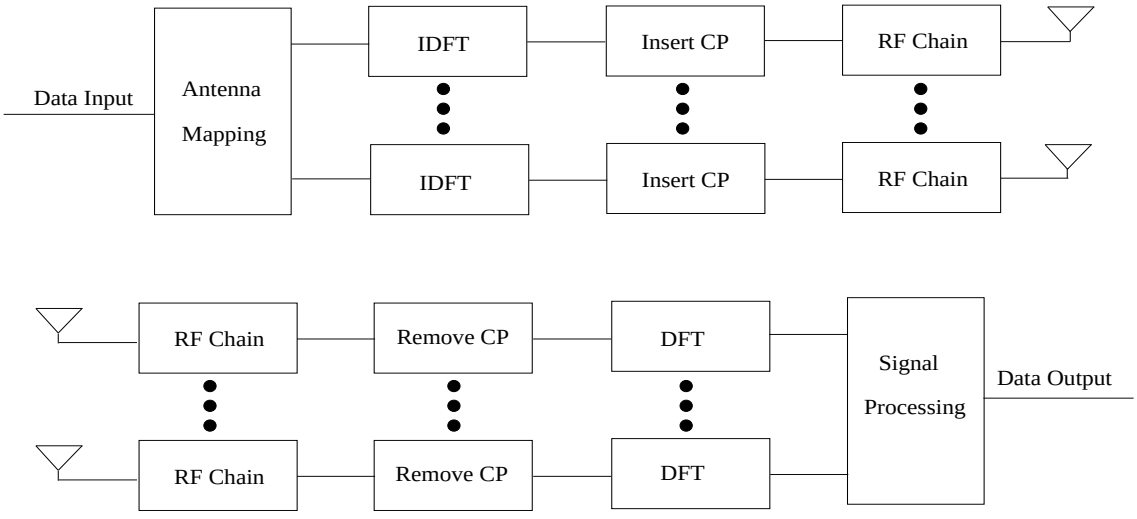

Figure 2.4: MIMO-OFDM System

j-th receive branch at the k-th subcarrier and each element is a Gaussian random variable with unit variance, and ρ is the transmit power at the k-th subcarrier. All the subcarriers at all the transmit antennas are assumed to have identical power. Uniform power allocation among the subcarriers is a natural choice for transmitters without CSI. The received signal at the k-th subcarrier can also be expressed in vector form as

$$\overline{\bar{r}}[n,k] = \frac{\rho}{N_t}\boldsymbol{H}[\boldsymbol{k}]\overline{\bar{t}}[n,k] + \overline{\bar{w}}[n,k], \tag{2.46}$$

where

$$\ddot{\boldsymbol{H}}[\boldsymbol{k}] = \begin{pmatrix} \ddot{h}_{1,1}[k] & \ddot{h}_{2,1}[k] \\ \ddot{h}_{1,2}[k] & \ddot{h}_{2,2}[k] \end{pmatrix}, \bar{\bar{t}}[n,k] = \begin{pmatrix} \ddot{t}_1[n,k] \\ \ddot{t}_2[n,k] \end{pmatrix}, \overline{\bar{w}}[n,k] = \begin{pmatrix} \ddot{w}_1[n,k] \\ \ddot{w}_2[n,k] \end{pmatrix},$$

and $\overline{\bar{w}}[k]$ satisfies

$$E\{\overline{\bar{w}}[n,k]\overline{\bar{w}}^{\dagger}[n,k]\} = \boldsymbol{I}_{N_r}.$$

Therefore we can see the frequency-selective MIMO fading channel decouples into parallel frequency-flat MIMO fading channels. A similar expression can be seen in [43] for a four-by-N_r configuration. This result can only be obtained when the length of the cyclic prefix L_{CP} is greater than the maximum delay of the channel. In practice, it is recommended that L_{CP} should be about two to four times the root-mean-square (RMS) value of the delay spread L [20]. In summary, the OFDM-MIMO system can be treated as N narrow-band MIMO wireless systems, each operating at a distinct carrier frequency.

2.3.1 Channel Statistics

In the previous section, we have shown that a properly designed MIMO-OFDM system can decouple a frequency-selective wide band channel into parallel frequency-flat channels. However the characteristics of each decoupled channel have not been described. It has been mathematically verified in [8] that all the effective frequency-domain channels

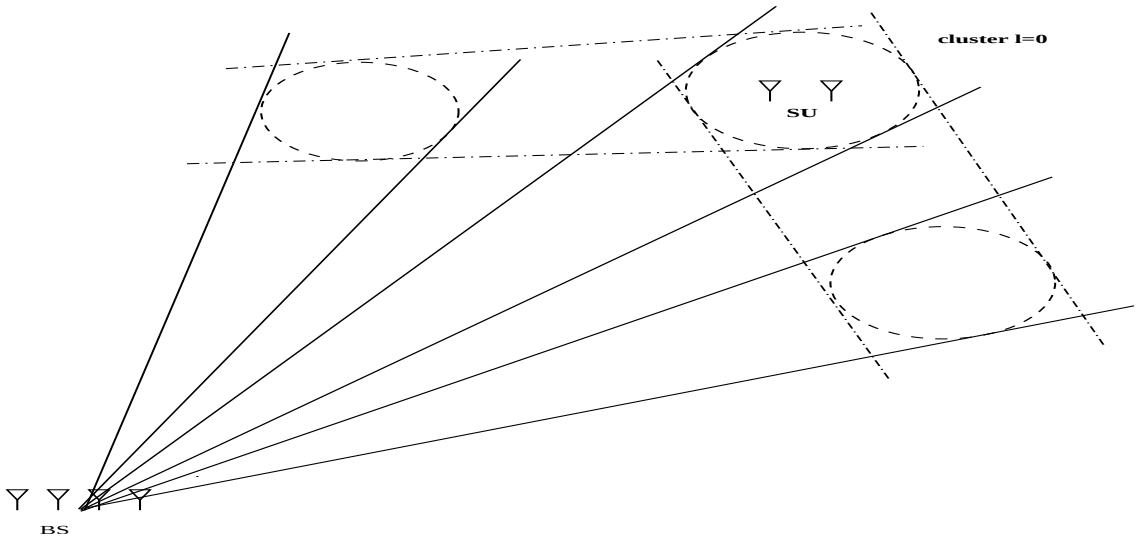

Figure 2.5: Illustration of MIMO delay spread channel consisting of multiple clusters.

observed at each subcarrier, $\ddot{\boldsymbol{H}}[\boldsymbol{k}]$ for $k = 0 \ldots N-1$, are identically distributed for a semi-correlated channel as described in Section 2.1.6. We will verify that it is also true for more general channels that are spatially correlated at both the transmitter and receiver. We consider a wireless channel with L significant delay paths, each from a different scattering cluster. A geometric interpretation of the model is illustrated in Fig. 2.5. The l^{th} delayed channel is defined by an $N_r \times N_t$ complex random matrix $\boldsymbol{H^l}$. The elements of the individual $\boldsymbol{H^l}$ are complex Gaussian random variables under a spatially correlated Rayleigh fading assumption. As we can see from Fig. 2.5, most paths experience double scattering as described in [21, 63]. The channel matrices for those paths can be written as

$$\boldsymbol{H^l} = \sqrt{A^l}\frac{1}{\sqrt{s}}\boldsymbol{R_{Rx}^l}^{1/2}\boldsymbol{H_{w,1}^l}\boldsymbol{R_S^l}^{1/2}\boldsymbol{H_{w,2}^l}\boldsymbol{R_{Tx}^l}^{1/2} \qquad l = 0 \ldots L-1, \tag{2.47}$$

where $\boldsymbol{H_{w,1}^l} \backsim N_c(\boldsymbol{0}, A^l \boldsymbol{I}_{N_r} \otimes \boldsymbol{I}_s)$, $\boldsymbol{H_{w,2}^l} \backsim N_c(\boldsymbol{0}, \boldsymbol{I}_s \otimes \boldsymbol{I}_{N_t})$, A^l is the power associated with the l-th path, s is number of scatters (usually large) in the cluster, $\boldsymbol{R_{Tx}^l}$, $\boldsymbol{R_s^l}$ and $\boldsymbol{R_{Rx}^l}$ are the transmit, scatterer, and receive correlation matrices, respectively. In this thesis, we assume that the system does not experience a pinhole channel. In particular we let $\boldsymbol{R_s^l} = \boldsymbol{I}_s$ [21].

After applying central-limit theorem and performing some manipulations, the channel at the l-th path becomes

$$\boldsymbol{H^l} = \boldsymbol{R_{Rx}^l}^{1/2} \boldsymbol{H_w^l} \boldsymbol{R_{Tx}^l}^{1/2}, \tag{2.48}$$

where $\boldsymbol{H_w} \backsim N_c(\boldsymbol{0}, \boldsymbol{I}_{N_r \times N_t})$. The expression in Eq. (2.48) is identical to the narrow-band MIMO case with additional path energy factor absorbed into $\boldsymbol{H_w^l}$. The channels from different clusters are assumed to be uncorrelated, i.e.,

$$E[\boldsymbol{h^l} \boldsymbol{h^{l'}}^{\dagger}] = \boldsymbol{0}_{NrNt} \text{ where } l \neq l'.$$

We first consider the general case with arbitrary cluster locations, where a scattering cluster might not be around the subscriber unit and basestation. In this case, the signal observed at both the transmitter and receiver are correlated. The covariance matrix of each $\boldsymbol{H^l}$ is defined as

$$\begin{aligned} \boldsymbol{R^l} &= E[\boldsymbol{h^l} \boldsymbol{h^l}^{\dagger}] \\ &= \boldsymbol{R_{Rx}^l} \otimes \boldsymbol{R_{Tx}^l}. \end{aligned} \tag{2.49}$$

This relationship between transmit and receive correlations is experimentally verified in [77]. Then $\boldsymbol{h^l}$ has the equivalent distribution given as

$$\begin{aligned} \boldsymbol{h^l} &\backsim \left(\boldsymbol{R_{Rx}^l} \otimes \boldsymbol{R_{Tx}^l} \right)^{1/2} \boldsymbol{h_w^l} \\ &\backsim \left(\boldsymbol{R_{Rx}^l}^{1/2} \otimes \boldsymbol{R_{Tx}^l}^{1/2} \right) \boldsymbol{h_w^l}, \end{aligned} \tag{2.50}$$

where $\boldsymbol{h_w^l}$ is zero-mean Gaussian vector with covariance defined as

$$E[\boldsymbol{h_w^l} \boldsymbol{h_w^l}^{\dagger}] = \boldsymbol{I}_{N_t N_r}. \tag{2.51}$$

The MIMO channel of the k-th subcarrier can be expressed as

$$\ddot{\boldsymbol{H}}[k] = \sum_{l=0}^{L-1} \boldsymbol{H^l} \omega_{N+L_{CP}}^{kl}, \tag{2.52}$$

where

$$\omega_{N+L_{CP}}^{kl} = e^{\left(-j2\pi\frac{kl}{N+L_{CP}}\right)}. \tag{2.53}$$

Since $\boldsymbol{H^l}$ for $l = 0 \ldots L-1$ are independent Gaussian matrices, $\ddot{\boldsymbol{H}}[\boldsymbol{k}]$ for $k = 1 \ldots N$ are also Gaussian matrices. After substituting Eq. (2.50) into Eq. (2.52) and converting it into vector representation, we have

$$\begin{aligned}\ddot{\boldsymbol{h}}[\boldsymbol{k}] &= \sum_{l=0}^{L-1} \boldsymbol{h^l}\omega_{N+LCP^{kl}} \\ &\backsim \sum_{l=0}^{L-1} \left(\boldsymbol{R_{Rx}^l}^{1/2} \otimes \boldsymbol{R_{Tx}^l}^{1/2}\right) \boldsymbol{h_w^l}\boldsymbol{\omega}_{N+L_{CP}}^{kl},\end{aligned}$$

then the covariance of $\boldsymbol{H}[\boldsymbol{k}]$ is given as

$$\begin{aligned}&E\{\ddot{\boldsymbol{h}}[\boldsymbol{k}]\ddot{\boldsymbol{h}}[\boldsymbol{k}]^{\dagger}\} \\ &= E\left[\sum_{l=0}^{L-1} \left(\boldsymbol{R_{Rx}^l}^{1/2} \otimes \boldsymbol{R_{Tx^l}}^{1/2}\right) \boldsymbol{h_w^l}\boldsymbol{\omega}_{N+L_{CP}}^{kl} \sum_{l=0}^{L-1} \boldsymbol{h_w^l}^{\dagger} (\boldsymbol{R_{Tx}^l}^{1/2} \otimes \boldsymbol{R_{Rx}^l}^{1/2})\boldsymbol{\omega}_{N+L_{CP}}^{-kl}\right] \\ &= \left[\sum_{l=0}^{L-1} \left(\boldsymbol{R_{Rx}^l} \otimes \boldsymbol{R_{Tx}^l}\right)\right]. \end{aligned} \tag{2.54}$$

Eq. (2.54) shows that the channel covariance is identical for all the subcarriers, since the expression is independent of k. Hence it follows that

$$\begin{aligned}\ddot{\boldsymbol{h}}[\boldsymbol{k}] &\backsim \left[\sum_{l=0}^{L-1} (\boldsymbol{R_{Rx}^l} \otimes \boldsymbol{R_{Tx}^l})\right]^{1/2} \boldsymbol{h_w} \\ &\backsim \sum_{l=0}^{L-1} (\boldsymbol{R_{Rx}^l}^{1/2} \otimes \boldsymbol{R_{Tx}^l}^{1/2})\boldsymbol{h_w^l} \\ \ddot{\boldsymbol{H}}[\boldsymbol{k}] &\backsim \sum_{l=0}^{L-1} (\boldsymbol{R_{Tx}^l}^{1/2}\boldsymbol{H_w^l}\boldsymbol{R_{Rx}^l}^{1/2}) \qquad \text{by property (A.5),}\end{aligned} \tag{2.55}$$

where

$$\boldsymbol{h_w} = \sum_{l=0}^{L-1} \boldsymbol{h_w^l}. \tag{2.56}$$

Since $\boldsymbol{h_w^l}$ are independent zero-mean Gaussian vectors, $\boldsymbol{h_w}$ also a zero-mean Gaussian vector with covariance matrix $A_l\boldsymbol{I}_{N_tN_r}$. If a cluster is present around the SU, the channels at the

SU can be considered to be mutually independent so $\boldsymbol{R}_{\boldsymbol{Rx}}^{\boldsymbol{l}} = \boldsymbol{I}_{N_r}$. Then Eq. (2.55) can be expressed as

$$\ddot{\boldsymbol{H}}[\boldsymbol{k}] \backsim \boldsymbol{H}_{\boldsymbol{w}} \left[\sum_{l=0}^{L-1} \boldsymbol{R}_{\boldsymbol{Tx}}^{\boldsymbol{l}} \right]^{1/2}. \tag{2.57}$$

The $\boldsymbol{H}_{\boldsymbol{w}}$ is outside of the summation because $\boldsymbol{h}^{\boldsymbol{l}}$ are Gaussian and assumed to be independent between different paths. For data transmission from SU to BS under the identical environment, $\boldsymbol{R}_{\boldsymbol{Tx}}^{\boldsymbol{l}} = \boldsymbol{I}_{N_t}$. The expression becomes

$$\ddot{\boldsymbol{H}}[\boldsymbol{k}] \backsim \left[\sum_{l=0}^{L-1} \boldsymbol{R}_{\boldsymbol{Rx}}^{\boldsymbol{l}} \right]^{1/2} \boldsymbol{H}_{\boldsymbol{w}}. \tag{2.58}$$

The expression for downlink transmission is identical to the result from [8].

2.4 Antenna Selection

MIMO wireless systems promise high data rate communications. However transmitting through multiple antennas requires an equivalent number of RF chains that consist of amplifiers, A/D converters, and mixers, etc. Those components are generally very expensive. Also the system complexity increases as the size of the antenna array increases. Therefore there are strong incentives for developing low-cost and low-demodulation-complexity MIMO systems. Antenna selection is one of most efficient techniques developed to achieve that goal. In antenna selection, RF switches along with a smaller number of RF chains (N_{RF}) are deployed at transmitter and/or receiver, instead of having a number of RF chains equal to the number of antennas ($N_t > N_{RF}$). A subset of the transmitter and/or receiver antennas in the array is selected for data transmission and reception, based on a selection criterion.

For uncoded MIMO systems, the antenna selection for maximizing instantaneous capacity is proposed in [23] where it is shown that capacity of the selected system can be

greater than a system without antenna selection under low-rank channels. A selection algorithm for the system applying a water-pouring method at the transmitter is developed in [59]. The antenna selection technique based on a capacity bound is proposed in [49]. A selection technique based on minimum error rate is presented in [28]. However since all of the above selection methods use exhaustive search to perform selection, the complexity becomes unaffordable for large antenna arrays. Efforts to reduce complexity for antenna selection techniques are presented in [10, 25, 32, 56, 80]. Receive and transmit antenna selection have many similarities. Therefore almost all of the techniques discussed in the prior literature can be applied to both types of selection. The main difference is that feedback is required for transmit antenna selection. Different types of feedback information have been proposed including CSI, channel correlation, and selection-decision. The selection-decision type of feedback seems to be most attractive because only the information on which transmit antennas are selected is transmitted from the receiver through a feedback channel. The performance of most selection techniques is evaluated by assuming perfect CSI is available except in [52]. In [52], it is shown that the ergodic capacity for systems with imperfect CSI is comparable to that of a system with perfect CSI. However neither the effect of training overhead nor the channel estimation method is considered in the literature.

For orthogonal space-time block coded systems, antenna selection based on instantaneous SNR is studied in [24]. The performance of such a system against different degrees of channel correlation is analyzed in [79]. Again perfect CSI is assumed in those studies. The selection criterion for maximizing instantaneous SNR and capacity of such systems is to select the transmitter antennas that results in largest channel squared Frobenius norm.

Antenna selection for MIMO-OFDM has been proposed in [18]. A maximum instantaneous SNR, averaged over all subcarriers, is developed as the selection technique in [4]. However like in the MIMO systems, perfect CSI is assumed. For MIMO-OFDM systems,

the antenna selection is conceptually similar to that for MIMO, given that all the subcarriers use the identical antenna subset after antenna selection. The antenna selection algorithm would need to select the transmit antenna that yields the largest instantaneous effective SNR or capacity.

2.4.1 Performance Enhancement due to Antenna Selection

To obtain a rough idea of how antenna selection improves the system performance, we look at an Alamouti space-time block coded MIMO systems with N_t transmit antennas and two receive antennas. Perfect CSI is assumed. The antenna selection criterion is

$$\max_{\boldsymbol{H_s} \in columns\ of\ \boldsymbol{H}} \|\boldsymbol{H_s}\|_F^2. \tag{2.59}$$

Now define T_m, $m = 1 \ldots N_t$ as the squared Frobenius norm of each of the N_t columns of the channel matrix $\boldsymbol{H}$. That is

$$\begin{aligned} T_m &= \sum_{i=1}^{N_r} |h_{i,m}|^2 \\ &= \sum_{i=1}^{N_r} |x_{i,m} + jy_{i,m}|^2 \\ &= \sum_{i=1}^{N_r} x_{i,m}^2 + y_{i,m}^2 \\ &= \sum_{i=1}^{2N_r} z_{i,m}^2 \qquad \text{since x y are i.i.d,} \end{aligned}$$

where i.i.d. denotes "independent and identically distributed". For independent Rayleigh fading, $\boldsymbol{h} \backsim N_c(\boldsymbol{0}, \boldsymbol{I})$. The p.d.f. of T_m can be expressed as [55]

$$P(t_m) = \frac{1}{\Gamma(N_r) t_m} t_m^{N_r - 1} e^{-t_m},$$

which is Gamma distributed with shape parameter N_r, scalar parameter 1, and location parameter 0. The mean values of the order statistics of T_m have been summarized in [27].

The expected squared Frobenius norms of the selected two-by-two channel matrices, $\boldsymbol{H_s}$, for different numbers of available transmit antennas are summarized in Table 2.1. The instantaneous effective SNR after antenna selection can be expressed as

$$SNR_{effective} = \frac{\rho}{N_t\ r_c} \|\boldsymbol{H_s}\|_F^2. \tag{2.60}$$

The average effective SNR is given as

$$\overline{SNR}_{effective} = \frac{\rho}{N_t\ r_c} E\left[\|\boldsymbol{H_s}\|_F^2\right]. \tag{2.61}$$

From Table 2.1, we notice that the average effective SNR increases logarithmically with the number of available transmit antennas.

2.5 Channel Estimation

CSI is required in OSTBC coded systems with antenna selection for decoding at a receiver with antenna selection. The accuracy of initial channel estimation is essential for a system with antenna selection. In this section, we provide an overview of various channel estimation techniques for both MIMO and MIMO-OFDM systems. In most communication standards, the initial channel estimation is performed within a dedicated interval. Such a signal frame is illustrated in Fig. 2.6. A transmission frame of T symbols is divided into training and data phases, occupiing T_τ and T_d symbols, respectively. The training phase needs to be larger than N_t symbols in order for the receiver to obtain a meaningful channel estimate.

Figure 2.6: Signal frame structure of a training-based wireless communication system

Number of Transmit Antennas(N_t)	$E[\|\|\boldsymbol{H_s}\|\|_F^2]$
2	4.0000
4	5.7575
6	6.7604
8	7.4647
10	8.0074
12	8.4483
14	8.9044
16	9.1399
18	9.4215
20	9.6728
22	9.8995
24	10.106
26	10.296
28	10.471

Table 2.1: Expected value of squared Frobenius norm for the selected channel matrix

2.5.1 MIMO Channel Estimation

Here we introduce the two most commonly used channel estimation techniques, namely linear minimum-mean-square error (LMMSE) and maximum-likelihood (ML). Let us define $\boldsymbol{H}$, $\widehat{\boldsymbol{H}}$ and $\widetilde{\boldsymbol{H}}$ be the true channel, channel estimate and estimation error, respectively. The corresponding vector representations are $\boldsymbol{h}$, $\widehat{\boldsymbol{h}}$ and $\widetilde{\boldsymbol{h}}$. A general relation between them is

$$\boldsymbol{H} = \widehat{\boldsymbol{H}} + \widetilde{\boldsymbol{H}}.$$

MIMO LMMSE channel estimation assumes the channel is a realization of a random vector. The channel estimate is obtained as [6, 33]

$$\begin{aligned}\widehat{\boldsymbol{h}} &= E\left(\boldsymbol{h}|\boldsymbol{y}_\tau\right) \\ &= \sqrt{\frac{N_t}{\rho}}\left(\frac{N_t}{\rho}\boldsymbol{R}_{\boldsymbol{hh}}^{-\boldsymbol{1}} + \boldsymbol{X}^\dagger\boldsymbol{X}\right)^{-1}\boldsymbol{X}^\dagger\boldsymbol{y}_\tau.\end{aligned}$$

The ML channel estimation assumes the channel is a deterministic but unknown constant. The channel estimate [37, 48] is given as

$$\widehat{\boldsymbol{H}} = \sqrt{\frac{N_t}{\rho}}\boldsymbol{Y}\boldsymbol{S}_\tau^\dagger(\boldsymbol{S}_\tau\boldsymbol{S}_\tau^\dagger)^{-1}.$$

2.5.2 MIMO-OFDM Channel Estimation

In this section, we present three channel estimation approaches for MIMO-OFDM, namely frequency-domain, time-domain, and enhanced time-domain estimation. Training sequences are transmitted through all the subcarriers during the training phase as described in the 802.11n proposal [26]. The frame structure is shown in Fig. 2.7.

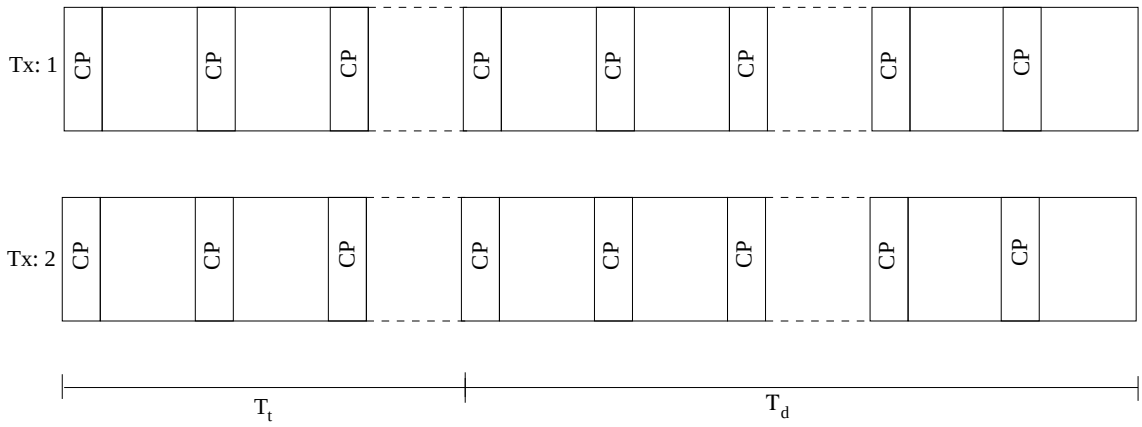

Figure 2.7: Training-based MIMO-OFDM Frame Structure

2.5.2.1 Frequency-Domain Channel Estimation

MIMO-OFDM can be represented as multiple MIMO systems operating at different frequencies. The most intuitive way to perform channel estimation is by deploying MIMO channel estimation on each subcarrier at the receiver. The ML and LMMSE channel estimation methods described in Section 2.5.1 can be used on each subcarrier. Since the channel on each subcarrier is identically distributed, the statistical properties for channel estimation on all subcarriers are also identical. Although the total number of channel parameters is larger than for a single-carrier MIMO system, the overall training time to achieve equal estimation quality remains the same, given that the power on each subcarrier is identical to that of the single-carrier MIMO system.

2.5.2.2 Time-Domain Channel Estimation

As shown in Section 2.3.1, all the $\ddot{\boldsymbol{H}}[\boldsymbol{k}]$ are functions of $\boldsymbol{H}^{\boldsymbol{l}}$. Therefore the receiver can estimate the time-domain channel $\boldsymbol{H}^{\boldsymbol{l}}$ at each delayed path. This estimation method is studied in [5, 43, 44, 53]. The time-domain channel estimation method allows the receiver to estimate the channel with fewer observations because there are only $N_t \times N_r \times L$ parameters, which is usually less than the number of parameters in the frequency domain, e.g., $N_t \times N_r \times N$. One of the major applications of this technique is on channel estimation refining or tracking techniques based on pilot insertion. The time-domain channel estimation offers additional spectral efficiency gain since pilot symbols need not to appear on each subcarrier. However this approach has a limited applicability to antenna selection systems. If the system does not acquire accurate channel estimates, the resulting system might result in sending information-bearing symbols through unfavorable transmit antennas. The loss in performance is not recoverable by techniques that refine the channel estimates during the data phase of transmission, since they can only be applied to the selected channel.

Decision-feedback or pilot-symbol-aided channel estimation are examples of such techniques.

One challenge for channel estimation is that the temporal length of the channel's delay profile is an environmentally dependent variable, therefore is generally unknown. In practice, a rule of thumb is to assume a length of two to four times the RMS-value of the delay spread as is suggested for CP length [20]. Having extended length is important since the performance degradation is large when the system fails to capture energy in most signal paths [44]. However merely performing channel estimation in the time domain should not improve the quality of channel estimation in the frequency domain since it only transforms the problem onto a lower dimensional space. The corresponding channel estimation quality in the frequency domain is directly related to system performance.

2.5.2.3 Enhanced Channel Estimation

The real benefit of time-domain channel estimation comes from exploiting the temporal correlation within the channel delay profile. As empirical data shows, the delay profile has exponential decay characteristics [77]. By exploiting temporal correlation within the channel delay profile, the accuracy of frequency-domain estimates can be improved. This technique is first presented in [45] and then summarized in [65]. The time-domain estimate can be obtained by projecting the channel estimate obtained in the frequency-domain by the channel estimation method described in Section 2.5.2.1. Herein

$$\begin{aligned} \widehat{\boldsymbol{H}} &= (\Omega^{\dagger}\Omega)^{-1}\Omega^{\dagger}\widehat{\ddot{\boldsymbol{H}}} \\ &= \boldsymbol{H} + \widetilde{\boldsymbol{H}}, \end{aligned} \tag{2.62}$$

where the FFT matrix is defined as

$$\Omega = \frac{1}{N+N_{CP}} \begin{pmatrix} 1 & 1 & \dots & 1 \\ 1 & e^{-j2\pi 1/(N+N_{CP})} & \dots & e^{-j2\pi(L-1)/(N+N_{CP})} \\ 1 & e^{-j2\pi 2/(N+N_{CP})} & \dots & e^{-j2\pi 2(L-1)/(N+N_{CP})} \\ \vdots & \vdots & \vdots & \vdots \\ 1 & e^{-j2\pi(N-1)/(N+N_{CP})} & \dots & e^{-j2\pi(N-1)(L-1)/(N+N_{CP})} \end{pmatrix}, \quad (2.63)$$

where N_{CP} is the number of subcarriers that is occupied by CP. The frequency-domain estimate can be improved by computing

$$\widehat{\ddot{\boldsymbol{H}}}_{\boldsymbol{i,j}}[k] = \sum_{l=0}^{L-1} \alpha_{i,j}^{l} \widehat{\boldsymbol{H}}_{\boldsymbol{i,j}}^{\boldsymbol{l}} \Omega_{N+N_C P}^{kl}. \quad (2.64)$$

It has been proven [45] that the optimal weight factors α_l are

$$\alpha_{i,j}^{l} = \frac{\frac{\sigma_l^2}{\sigma_l^2+\sigma_{\tilde{h}_{i,j}^{l}}^2}}{\sum_{l'=0}^{L-1} \frac{\sigma_l'^4}{\sigma_l'^2+\sigma_{\tilde{h}_{i,j}^{l}}^2}}, \quad (2.65)$$

where σ_l^2 is the power of the l-th delay path, and $\sigma_{\tilde{h}_{i,j}^{l}}^2$ is the equivalent time-domain error power of the i, j-th element of $\boldsymbol{H}^{\boldsymbol{l}}$. The estimation error for each channel element in the frequency domain is given by

$$\sigma'_{\tilde{\tilde{h}}_{i,j}}[k]^2 = \sigma_{\tilde{\tilde{h}}_{i,j}}^2 \frac{\sum_{l=0}^{L-1} \frac{\sigma_l^2}{\sigma_l^2+\sigma_{\tilde{\tilde{h}}_{i,j}}^2}}{\sum_{l=0}^{L-1} \frac{\sigma_l^4}{\sigma_l^2+\sigma_{\tilde{\tilde{h}}_{i,j}}^2}} \quad (2.66)$$

$$= \beta_{i,j} \sigma_{\tilde{\tilde{h}}_{i,j}}^2. \quad (2.67)$$

where $\beta_{i,j}$ is defined as the improvement factor that depends on the actual channel delay profile. The exact power distribution within the delay profile needs to be estimated in practice. Since the channels corresponding to different antenna pairs should have approximately identical delay profiles, σ_l^2 can be estimated via

$$\sigma_l^2 = \frac{1}{N_t N_r} \sum_{i=1}^{N_t} \sum_{j=1}^{N_r} |\widehat{\boldsymbol{H}}_{\boldsymbol{i,j}}^{\boldsymbol{l}}|^2. \quad (2.68)$$

2.6 Objectives

All the MIMO signal processing techniques mentioned in the previous sections require CSI at the receiver. When transmit antenna selection is deployed in orthogonal space-time block coded MIMO systems, the system's average effective SNR increases as the number of available antennas increases. In the majority of existing studies it is usually assumed that the CSI is perfectly known at the receiver and CSI estimation does not consume system resources. Based on this assumption, the system capacity would monotonically increase with the number of transmit antennas. However the most common way to obtain the CSI at the receiver is through transmitting training symbols, which reduces capacity. The length of training is directly proportional to the number of transmit antennas. So in training-based MIMO systems the increase in capacity due to additional transmit antennas is offset by the increased amount of required training [6]. Prior studies on effects of imperfect CSI on antenna selection systems exclude the degradation of capacity due to training. In this thesis, we redesign the antenna selection algorithms to accommodate both LMMSE and ML channel estimators and provide a more realistic perspective of the system performance. Also this thesis intends to reveal insights into system design by determining the performance of OSTBC coded MIMO/MIMO-OFDM systems with antenna selection under both spatially uncorrelated and semi-correlated channels.

Chapter 3

Training-Based MIMO Antenna Selection with Orthogonal Space-Time Block Coding

3.1 Introduction

Wireless communications systems can significantly enhance the data rate by having multiple antennas at transmitters and receivers given rich scattering environments [19, 69]. However multiple-antenna deployment requires multiple RF chains, including amplifiers, A/D converters and mixers. Those RF components are generally very expensive. The complexity of signal processing also becomes extremely high as the number of antennas increases. Therefore there are strong incentives to develop a low-cost and low–complexity multiple-input multiple-output (MIMO) system. Antenna selection is one of the most efficient techniques that has drawn significant attention [23, 28, 49, 59]. The cost of antenna elements is much less than that of other RF components. By making more antenna elements available at both transmitter and receiver without additional RF chains, the system can exploit additional spatial dimensions while maintaining the cost and signal processing complexity at a reasonable level. In [22], it is shown that a system with antenna selection

can achieve the same diversity order as a full MIMO system. If channel state information (CSI) is assumed to be perfect, as in many instances in the literature, diversity order can increase without any tradeoff. However in a real system, the most common way to estimate the CSI is by transmitting known symbols from the transmitter to receiver. This type of system is referred to as a training-based system in this thesis. The influence of the channel estimation error on both ergodic and outage capacity for an uncoded antenna selection system with maximum-ratio transmission/combining has been studied in [50,51]. It is claimed that the channel estimation errors do not decrease the capacity significantly if the signal-to-noise ratio (SNR) during the training is comparable to or larger than the SNR during the data transmission. It is shown that both the ergodic and outage capacity are non-decreasing functions of the number of antennas. However [50, 51] neither considers the capacity degradation due to training overhead nor specifies the channel estimator.

In wireless communications, a subscriber unit (SU) usually has limited space for antenna allocation. A large number of antennas at the SU are unlikely. Therefore it is more reasonable to perform antenna selection at a basestation (BS). In this chapter, we study a downlink wireless communication with the BS acting as the transmitter and the SU acting as the receiver. One of the challenges for the downlink communication of this setup is that the BS requires additional information in order to select an optimal antenna subset. Instantaneous channel matrix, channel covariance matrix, and selection decision have been proposed as feedback information. In most of the literature, instantaneous channel and channel covariance matrices are referred to as short-term and long-term CSI, respectively. It is usually undesirable for the transmitter to obtain the CSI through a feedback channel. For a system employing antenna selection at the BS, the situation is generally worse since there are fewer antenna elements at the SU. The amount of information per antenna at the

SU could be potentially large, which implies that it would take longer for the SU to reliably transmit this information back to the BS under bandlimited channels. Therefore the feedback information rate should be minimized through techniques such as quantization or other transformation into an alternative representation. Depending on the type of transformation, limited or explicit feedback are used, in contrast to implicit feedback, where the receiver-estimated CSI is transmitted without modification. Selection-based decision is an effective solution since only one bit of information per antenna is required for the feedback as discussed in Section 2.4. For a frequency division duplex (FDD) system, this feedback is mandatory to perform transmit antenna selection. However for a time division duplex (TDD) system, it is more convenient for the transmitter to obtain the explicit CSI by taking advantage of reciprocity between uplink and downlink channels. A TDD system, like the one described in the IEEE 802.11n proposal [26], can also optionally operate in the implicit feedback mode.

One of the advantages in using an orthogonal space-time block code (OSTBC) is that it allows the system to achieve full transmit diversity even when the transmitter does not have explicit CSI without sacrificing significant data rate [3]. It is superior over conventional repetition coding in terms of data rate and coding gain while achieving identical diversity order [70]. On the other hand, OSTBC can achieve the same diversity order as a system with transmit beamforming without CSI at the transmitter while imposing a 3dB loss in coding gain [37]. Those properties are very attractive to wireless systems with multiple transmit antennas. It is worth noting that OSTBC is already a part of the 3G standard [17]. Combining antenna selection and OSTBC under spatially uncorrelated Rayleigh fading has been studied in [22, 24, 76, 79]. All of these studies assume that perfect CSI is available, and show that the SNR or BER improves with the number of total available antennas.

In this chapter, we study a training-based OSTBC MIMO downlink wireless communication medium with N_t antennas at the BS and two antennas at the SU. Directed by the selection decision feedback from the receiver, the transmitter uses two out of its N_t antennas for data transmission. The following discussion will focus on the following aspects of the problem. The length of the required training increases as the number of transmit antennas increase. So the capacity is offset by two major competitors:

- increased capacity resulting from an increase of N_t.
- decreased capacity resulting from the increase in training overhead for larger N_t.

In this chapter, we will analyze the tradeoff between those two effects in order to provide some insights to the following questions:

- 1) How many transmit antennas are worth deploying?
- 2) How does spatial correlation affect the capacity?

This chapter is organized as follow: First we describe the system and channel model in Section 3.2. In Section 3.3, we introduce the channel estimation errors and relate them to the training overhead. Then we use the results to evaluate the performance of the OSTBC coded MIMO system without antenna selection in Section 3.4. In Section 3.5, we present the antenna selection algorithms for the system under study.

A note on the notation is in order. Vectors and matrices are represented in lowercase and uppercase **boldface**, respectively. The superscript T represents transpose, † denotes hermitian and $*$ represents complex conjugation. The operator E denotes statistical expectation. $\boldsymbol{C}^{\boldsymbol{M}\times\boldsymbol{N}}$ represents the $M \times N$ complex domain. $\boldsymbol{I_N}$ is the identity matrix of dimension $N \times N$ and $\boldsymbol{0_{M\times N}}$ is the $M \times N$ matrix of zeros. M and N are omitted whenever referring to arbitrary dimension or no confusion can occur. $N_c(\overline{\boldsymbol{\mu}}, \boldsymbol{R})$ represents a circular symmetric

complex Gaussian random variable with mean $\overline{\boldsymbol{\mu}}$ and covariance matrix $\boldsymbol{R}$. $x \backsim y$ denotes the statistical distributions of x and y are equal. Tr denotes trace of a matrix. i.i.d. denotes "independent and identically distributed".

3.2 System and Channel Model

The system under consideration is illustrated in Fig. 3.1, which is an Alamouti space-time block coded single-carrier MIMO system with transmit antenna selection in a single-user scenario. The transmitter is equipped with N_t antennas with two RF chains, and the receiver has two antennas and RF chains. Downlink communication is considered. In this study, we assume N_t is a multiple of two. The selection is performed at the receiver, and the transmitter obtains the decisions through a feedback channel that has negligible error. The feedback delay, T_f, is defined as the time between when the CSI is estimated at the receiver and when the feedback is actually used by the transmitter in the downlink transmission. In order to use the feedback information in a meaningful way, the feedback needs to arrive at the transmitter within the channel coherence time, T_c. Both the downlink transmission and

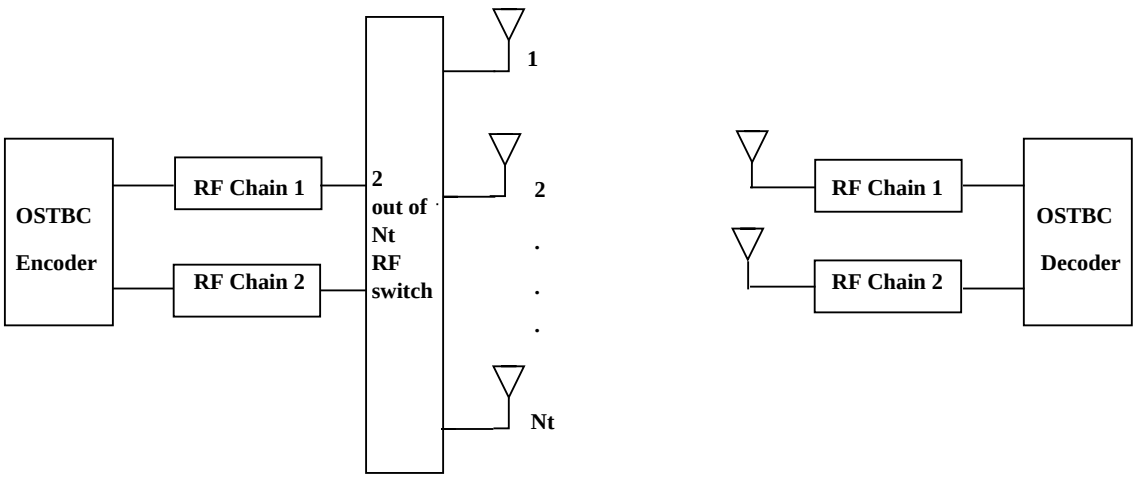

Figure 3.1: Transmit Antenna Selection with Orthogonal Space-Time Block Code

feedback must be accomplished within T_c. The relationship between timing is

$$T_c = T + T_f, \tag{3.1}$$

where T is the transmission block length. Both spatially uncorrelated ($\boldsymbol{R_{Tx}} = \boldsymbol{R_{Rx}} = \boldsymbol{I}$) and semi-correlated MIMO channels (only $\boldsymbol{R_{Rx}} = \boldsymbol{I}$) described in Section 2.1.6 are considered. The geometric interpretation of the semi-correlated MIMO channels is shown in Fig. 2.3. We assume that the antennas at the BS and SU have identical spacing so $D_t(p,q) = D_r(m,n) = 2\pi\frac{d}{\lambda}$, where d is the distance between antenna elements, and λ is the wavelength. Since the line-of-sight signal component is likely to be blocked by the rich scattering around the SU and the single-carrier MIMO system is considered to operate in a narrow band, we assume a frequency-flat Rayleigh block-fading MIMO channel, where the single-tap channel is constant for some discrete time interval of T_c symbols, and then changes independently to another value over another time interval of T_c symbols. Also we assume both SNR and spatial correlation are constant during the entire transmission. This assumption is valid in a fixed or low mobility wireless environment. In the study for semi-correlated channels, we assume the power azimuth spectrum (PAS) observed at the SU obeys a Laplacian distribution described in Section 2.1.4.3. This PAS distribution shows a good fit with empirical measurements [54]. The antenna elements are considered to be omnidirectional. Therefore the PAS is not truncated.

The statistical model for the Rayleigh fading MIMO channel employed in this thesis is given as [54, 61]

$$\boldsymbol{H} = \boldsymbol{R_{Rx}}^{1/2} \boldsymbol{H_w} \boldsymbol{R_{Tx}}^{1/2},$$

where $\boldsymbol{H_w} \backsim N_c(\boldsymbol{0_{2\times N_t}}, \boldsymbol{I_{N_t\times 2}})$. The received signal of a general MIMO system with N_t

transmit antennas and two receive antennas under frequency-flat fading channel is represented as

$$\boldsymbol{Y} = \sqrt{\frac{\rho}{N_t}}\boldsymbol{H}\boldsymbol{S} + \boldsymbol{W}, \tag{3.2}$$

where $\boldsymbol{Y} \in \boldsymbol{C}^{2\times T}$ is the received signal matrix. $\boldsymbol{S} \in \boldsymbol{C}^{N_t \times T}$ is the transmitted signal with unit average power on each of the antenna elements, $\boldsymbol{W} \backsim N_c(\boldsymbol{0}_{\boldsymbol{N_r}\times \boldsymbol{T}}, \boldsymbol{I}_{\boldsymbol{N_r}\times \boldsymbol{T}})$ is an additive noise matrix, $\boldsymbol{H} \in \boldsymbol{C}^{\boldsymbol{2}\times \boldsymbol{N_t}}$ is the channel matrix within each block of T, and ρ is the channel SNR at each receive antenna.

3.2.1 Training-Based MIMO

The described system requires the CSI at the receiver to perform coherence detection and antenna selection. For a training-based MIMO system, each transmission frame is divided into two time segments, a training phase and a data phrase. The duration of a transmission frame is therefore

$$T = T_\tau + T_d, \tag{3.3}$$

where T_τ is the duration of the training phase and T_d is the duration of the data phase. The channel estimation is performed at the end of the training phase, and the resulting channel estimate is then used as the true channel for antenna selection and OSTBC decoding. The details of the transmission scheme is described in the subsequent sections.

3.2.1.1 Training Phase

For a MIMO system with transmit antenna selection, there are fewer RF chains than the number of transmit antennas. So instead of transmitting training symbols through all of the antennas simultaneously, we let the system transmit the training symbols from two antennas at a time and then scan through all the transmit antennas. The idea is illustrated

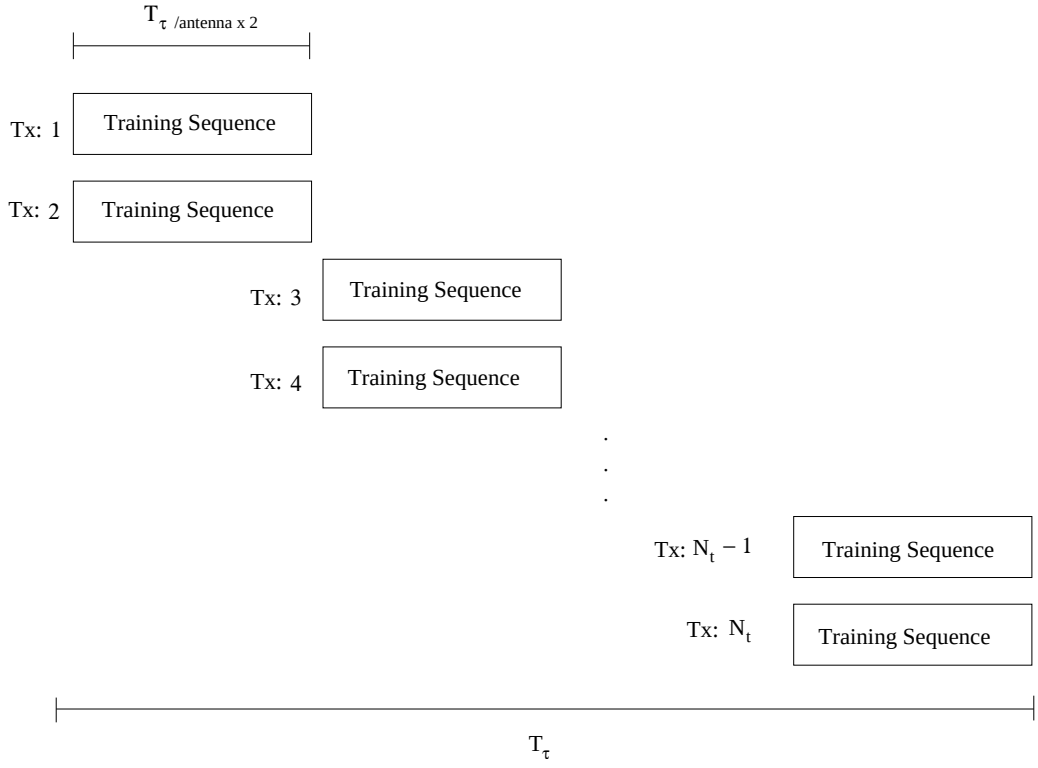

Figure 3.2: Illustration of Training Phase.

in Fig. 3.2. At the end of the training phase, the received signal can be expressed as

$$\boldsymbol{Y}_\tau = \sqrt{\frac{\rho}{N_t}}\boldsymbol{H}\boldsymbol{S}_\tau + \boldsymbol{W}_\tau, \quad \boldsymbol{S}_\tau \in \boldsymbol{C}^{\boldsymbol{N_t}\times\boldsymbol{T_\tau}}, \quad Tr(\boldsymbol{S}_\tau\boldsymbol{S}_\tau^\dagger) = N_t \times T_\tau, \tag{3.4}$$

where $\boldsymbol{S}_\tau$ is the training symbol, which is known to the receiver, within duration T_τ, and $\boldsymbol{Y}_\tau \in \boldsymbol{C}^{N_t\times T_\tau}$ is the received signal. A total of $T_\tau \geqslant N_t$ training symbols are transmitted in order to have meaningful channel estimation at the receiver. Let the training symbols from any two paired transmit antennas be $\boldsymbol{X}_\tau$, then

$$\boldsymbol{S}_\tau = \begin{pmatrix} \boldsymbol{X}_\tau & & & \\ & \boldsymbol{X}_\tau & & \\ & & \ddots & \\ & & & \boldsymbol{X}_\tau \end{pmatrix}. \tag{3.5}$$

The off-diagonal terms in the above matrix are zero. The details on the channel estimation method are discussed in Section 3.3.

3.2.1.2 Data Phase

During the data phase, the Alamouti OSTBC coded data are transmitted through the two selected antennas. Within each coded block, two symbols, x_1 and x_2, are encoded in space and time. Table 3.1 shows this encoding map. The signal model can be expressed as

$$\boldsymbol{Y_d} = \sqrt{\frac{\rho}{N_t}}\boldsymbol{H}\boldsymbol{S_d} + \boldsymbol{W_d}, \quad \boldsymbol{S_d} \in \boldsymbol{C^{2\times T_d}}, \quad E[Tr(\boldsymbol{S_d}\boldsymbol{S_d^{\dagger}})] = 2 \times T_d, \tag{3.6}$$

where $\boldsymbol{S_d}$ is the data symbol with duration T_d, and $\boldsymbol{Y_d} \in \boldsymbol{C^{2\times T_d}}$ is the received signal. Since the data is random and unknown to the receiver, the signal power in Eq. (3.6) has expectation.

	Antenna 1	Antenna 2
t	x_1	$-x_2^*$
$t+1$	x_2	x_1^*

Table 3.1: The encoding for Alamouti space-time block code

3.3 MIMO Channel Estimation

After receiving the entire $N_t \times T_\tau$ training block, the receiver performs the channel estimation for the $2 \times N_t$ channel matrix $\boldsymbol{H}$. The CSI at the receiver can be obtained by the following channel estimation techniques, namely linear minimum-mean-square error (LMMSE) and maximum-likelihood (ML). LMMSE channel estimation is a classical approach that assumes the channel is a realization of random variable, while the ML channel estimation assumes the channel is a deterministic but unknown constant. LMMSE channel estimation requires knowledge of SNR and channel spatial correlation, while ML channel estimation does not. Since we assume a fixed or low mobility wireless environment, both SNR and

spatial correlation can be obtained with high accuracy. In this section, we will examine the statistical properties of both channel estimation techniques under block-fading channels. Quality of SNR estimation tends to decrease as true SNR increases [33]. However it can be shown in the following discussions, the statistical properties of the ML channel estimation converges to that of the LMMSE channel estimation in a high SNR environment. Therefore a receiver with ML channel estimator should be implemented to avoid using inaccurate SNR knowledge when designing a system that is only expected to operate in high SNR environments.

Let us define $\boldsymbol{h}$, $\widehat{\boldsymbol{h}}$, and $\widetilde{\boldsymbol{h}}$ as the vector representations of true channel $\boldsymbol{H}$, channel estimate $\widehat{\boldsymbol{H}}$, and channel estimation error matrices $\widetilde{\boldsymbol{H}}$, respectively. Therefore

$$\widetilde{\boldsymbol{h}} = \boldsymbol{h} - \widehat{\boldsymbol{h}}. \tag{3.7}$$

3.3.1 LMMSE Channel Estimation and Optimal Training Sequence

In order to derive the properties of LMMSE MIMO channel estimation, we rewrite the signal model in Eq. (3.4) into vector form.

$$\boldsymbol{y}_\tau = \underbrace{\left(\boldsymbol{S}_\tau^{\boldsymbol{T}} \otimes \boldsymbol{I_2}\right)}_{\boldsymbol{X}} \sqrt{\frac{\rho}{N_t}}\boldsymbol{h} + \boldsymbol{w}_\tau, \tag{3.8}$$

where $\boldsymbol{h}$ and $\boldsymbol{y}_\tau$ are jointly Gaussian. The joint Gaussianity can be verified by the following. Let $\boldsymbol{z} = [\boldsymbol{h}^T \boldsymbol{y}^T]^T$, so that from Eq. (3.8) we have

$$\begin{aligned} \boldsymbol{z} &= \begin{bmatrix} \boldsymbol{X}\sqrt{\frac{\rho}{N_t}}\boldsymbol{h} + \boldsymbol{w}_\tau \\ \boldsymbol{h} \end{bmatrix} \\ &= \begin{bmatrix} \boldsymbol{X}\sqrt{\frac{\rho}{N_t}} & \boldsymbol{I} \\ \boldsymbol{I} & \boldsymbol{0} \end{bmatrix} \begin{bmatrix} \boldsymbol{h} \\ \boldsymbol{w}_\tau \end{bmatrix}, \end{aligned} \tag{3.9}$$

where the identity matrix at the upper right is of dimension $N_t \times N_t$, and $T_\tau \times T_\tau$, is the dimension of the one at the lower left, and $\boldsymbol{0}$ is an $T_\tau \times N_t$ matrix of zeros. Because $\boldsymbol{h}$ and

$\boldsymbol{w}_\tau$ are independent of each other and are both Gaussian, they are jointly Gaussian. Because $\boldsymbol{z}$ is an affine transformation of a Gaussian vector, it is also a Gaussian vector itself. So this verifies that $\boldsymbol{h}$ and $\boldsymbol{y}_\tau$ are jointly Gaussian.

We use the well known equation from [33], where the LMMSE channel estimator is given as

$$\begin{aligned}\widehat{\boldsymbol{h}} &= E\left(\boldsymbol{h}|\boldsymbol{y}_\tau\right) \\ &= \sqrt{\frac{N_t}{\rho}}\left[\frac{N_t}{\rho}\boldsymbol{R}_{\boldsymbol{hh}}^{-\boldsymbol{1}} + \boldsymbol{S}_\tau{}^\dagger\boldsymbol{S}_\tau\right]^{-1}\boldsymbol{S}_\tau{}^\dagger\boldsymbol{y}_\tau. \end{aligned} \tag{3.10}$$

As indicated by Eq. (3.10), the LMMSE estimator requires the knowledge of SNR and spatial correlation of the channel. The covariance of the channel estimation errors is given as [33]

$$\boldsymbol{R}_{\widetilde{\boldsymbol{hh}}} = \left[\boldsymbol{R}_{\boldsymbol{hh}}^{-\boldsymbol{1}} + \frac{\rho}{N_t}\boldsymbol{S}_\tau\boldsymbol{S}_\tau^\dagger \otimes \boldsymbol{I}_{\boldsymbol{2}}\right]^{-1}, \tag{3.11}$$

and the mean-square error (MSE) is

$$\varepsilon = Tr\left[\boldsymbol{R}_{\boldsymbol{hh}}^{-\boldsymbol{1}} + \frac{\rho}{N_t}\boldsymbol{S}_\tau\boldsymbol{S}_\tau{}^\dagger \otimes \boldsymbol{I}_{\boldsymbol{2}}\right]^{-1}. \tag{3.12}$$

For independent Rayleigh fading, $\boldsymbol{R}_{\boldsymbol{hh}} = \boldsymbol{I}_{\boldsymbol{N_t\times 2}}$, so we can rewrite Eq. (3.12) as

$$\varepsilon = Tr\left(\boldsymbol{I}_{\boldsymbol{N_t}} + \frac{\rho}{N_t}\boldsymbol{S}_\tau\boldsymbol{S}_\tau{}^\dagger\right)^{-1} \otimes \boldsymbol{I}_{\boldsymbol{2}}.$$

The optimal training sequences would be those that minimize the MSE by solving

$$\begin{aligned}&\min_{\boldsymbol{S}_\tau,\ Tr\left(\boldsymbol{S}_\tau\boldsymbol{S}_\tau{}^\dagger\right)=N_tT_\tau} \varepsilon \\ =&\min_{\lambda_1,\ldots,\lambda_{N_t};\ \sum\lambda_m\leqslant N_tT_\tau}\sum_{m=1}^{N_t}\frac{1}{1+\frac{\rho}{N_t}\lambda_m},\end{aligned} \tag{3.13}$$

which is solved by letting $\lambda_1 = \ldots = \lambda_{N_t} = T_\tau$. Therefore the optimal training sequences are in the forms of an orthogonal matrix such that

$$\boldsymbol{S}_\tau\boldsymbol{S}_\tau{}^\dagger = T_\tau\boldsymbol{I}_{\boldsymbol{N_t}}. \tag{3.14}$$

For correlated Rayleigh fading, the orthogonal matrix is only suboptimal [7]. The optimal training sequence when the CSI is known at the transmitter under the correlated fading is presented in [35]. However the orthogonal training sequences are a natural choice for transmitters that cannot acquire the CSI.

3.3.1.1 Properties of LMMSE Channel Estimation with Orthogonal Training Sequences

With orthogonal training sequences, the covariance matrix of channel estimation errors in Eq. (3.11) becomes

$$\boldsymbol{R}_{\widetilde{\boldsymbol{h}}\widetilde{\boldsymbol{h}}} = \left[\boldsymbol{R}_{\boldsymbol{hh}}^{-\boldsymbol{1}} + \frac{\rho T_\tau}{N_t}\boldsymbol{I}_{N_t\times \boldsymbol{2}}\right]^{-1}. \tag{3.15}$$

The mean value of the estimation errors is

$$\begin{aligned} E_{\boldsymbol{h},\boldsymbol{y}_\tau}(\widetilde{\boldsymbol{h}}) &= E_{\boldsymbol{h},\boldsymbol{y}_\tau}\{\boldsymbol{h} - E[\boldsymbol{h} - E(\boldsymbol{h}|\boldsymbol{y}_\tau)]\} \\ &= E_{\boldsymbol{y}_\tau}[E_{\boldsymbol{h}|\boldsymbol{y}_\tau}(\boldsymbol{h}) - E_{\boldsymbol{h}|\boldsymbol{y}_\tau}(\boldsymbol{h}|\boldsymbol{y}_\tau)] \\ &= E_{\boldsymbol{y}}[E(\boldsymbol{h}|\boldsymbol{y}_\tau) - E(\boldsymbol{h}|\boldsymbol{y}_\tau)] = \boldsymbol{0}. \end{aligned} \tag{3.16}$$

Therefore the error is on average zero. By the orthogonality principle for LMMSE estimations, the channel estimate and estimation error are independent. From Eq. (3.7), the vector form of the estimation error can be represented as

$$\widetilde{\boldsymbol{h}} = \boldsymbol{h} - \sqrt{\frac{N_t}{\rho}}\left[\frac{N_t}{\rho}\boldsymbol{R}_{\boldsymbol{hh}}^{-\boldsymbol{1}} + \boldsymbol{S}_\tau^\dagger \boldsymbol{S}_\tau\right]^{-1}\boldsymbol{S}^\dagger \boldsymbol{y}_\tau. \tag{3.17}$$

From Eq. (3.17), we can see that the channel estimation error is a linear transformation of $\boldsymbol{H}$, $\boldsymbol{Y}$, which themselves are jointly Gaussian. Hence the estimation error is also Gaussian and has the following distribution

$$\widetilde{\boldsymbol{h}} \backsim N_c\left(\boldsymbol{0}, \left[\boldsymbol{R}_{\boldsymbol{hh}}^{-\boldsymbol{1}} + \frac{\rho T_\tau}{N_t}\boldsymbol{I}_{N_t\times \boldsymbol{2}}\right]^{-1}\right). \tag{3.18}$$

From the orthogonality principle for LMMSE estimates and Eq. (3.7), the following relation holds.

$$\boldsymbol{R}_{\boldsymbol{hh}} = \boldsymbol{R}_{\widehat{\boldsymbol{hh}}} + \boldsymbol{R}_{\widetilde{\boldsymbol{hh}}}, \tag{3.19}$$

$$E[\boldsymbol{h}] = E[\widehat{\boldsymbol{h}}] + E[\widetilde{\boldsymbol{h}}]. \tag{3.20}$$

Since $\widehat{\boldsymbol{h}}$ is a linear transformation of a Gaussian matrix, it is also Gaussian. Therefore the distribution is given as

$$\widehat{\boldsymbol{h}} \backsim N_c \left(\boldsymbol{0}_{N_t \times 2}, \boldsymbol{R}_{\boldsymbol{hh}} - \left[\boldsymbol{R}_{\boldsymbol{hh}}^{-1} + \frac{\rho T_\tau}{N_t} \boldsymbol{I}_{N_t \times 2} \right]^{-1} \right). \tag{3.21}$$

Fig. 3.3 shows the MSE of a four-by-two MIMO with LMMSE channel estimation method under spatially uncorrelated and correlated channels. It is interesting to see that the quality of LMMSE channel estimation is significantly improved when the channel is highly

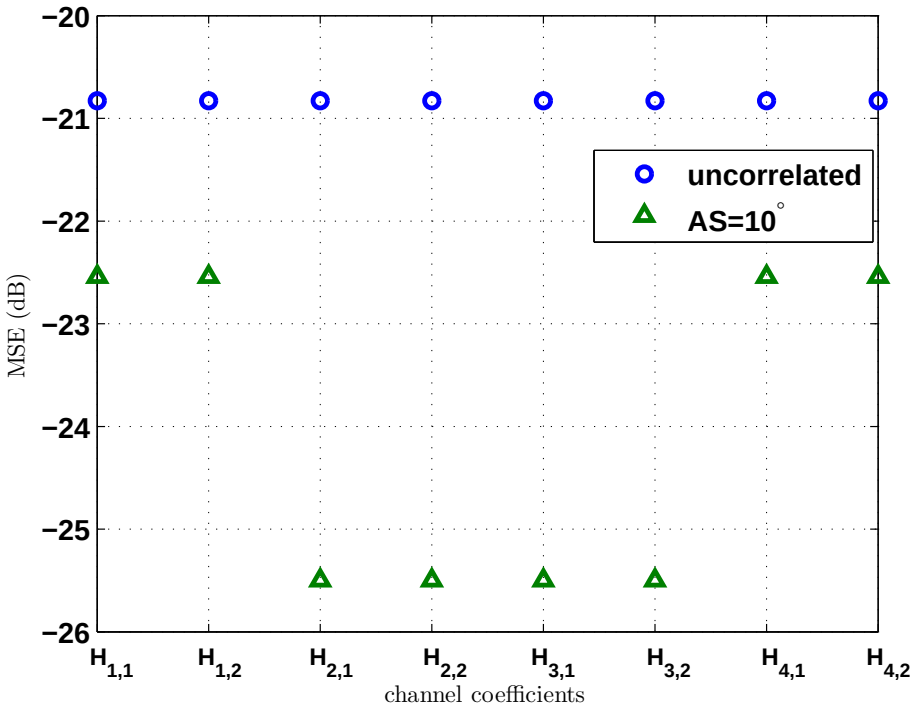

Figure 3.3: The MSE of each channel coefficient of a four-by-two MIMO system with LMMSE channel estimation under different channel spatial correlation. SNR= 10 dB

spatially correlated. The corresponding $\boldsymbol{R_{Tx}}$ for AS$=10^\circ$ is shown in Appendix C.1.

3.3.2 ML Channel Estimation and Optimal Training Sequence

The ML MIMO channel estimator [37, 48] is given as

$$\begin{aligned}\widehat{\boldsymbol{H}} &= \boldsymbol{Y}\boldsymbol{S}_\tau^\dagger(\boldsymbol{S}_\tau\boldsymbol{S}_\tau^\dagger)^{-1} \\ &= \boldsymbol{H}+\boldsymbol{W}_\tau\boldsymbol{S}_\tau^\dagger(\boldsymbol{S}_\tau\boldsymbol{S}_\tau^\dagger)^{-1} \\ &= \boldsymbol{H}+\widetilde{\boldsymbol{H}}.\end{aligned} \tag{3.22}$$

As we can see from Eq. (3.22), ML channel estimation does not require knowledge of SNR and spatial correlation of the channels. For some simple systems, the ML channel estimator is attractive since the SNR and spatial correlation of the channel is not required at the receiver. Without the above prior information, the LMMSE estimator is identical to the ML estimator [33]. Since

$$E[\boldsymbol{w}_\tau{\boldsymbol{w}_\tau}^\dagger] = \boldsymbol{I_{2\times T_\tau}},$$

and using the properties in Appendix A, the covariance of the estimation errors is

$$\begin{aligned}\boldsymbol{R}_{\widetilde{\boldsymbol{h}}\widetilde{\boldsymbol{h}}} &\triangleq E[\widetilde{\boldsymbol{h}}\widetilde{\boldsymbol{h}}^\dagger] \\ &= \left(\frac{N_t}{\rho}\right)\{[\boldsymbol{S}_\tau^\dagger(\boldsymbol{S}_\tau\boldsymbol{S}_\tau^\dagger)^{-\boldsymbol{I}}]^T\otimes\boldsymbol{I_2}\}E[\boldsymbol{w}_\tau\boldsymbol{w}_\tau^\dagger]\{[\boldsymbol{S}_\tau^\dagger(\boldsymbol{S}_\tau\boldsymbol{S}_\tau^\dagger)^{-\boldsymbol{I}}]^T\otimes\boldsymbol{I_2}\}^\dagger \\ &= \left(\frac{N_t}{\rho}\right)\{[\boldsymbol{S}_\tau^\dagger(\boldsymbol{S}_\tau\boldsymbol{S}_\tau^\dagger)^{-\boldsymbol{I}}]^T\otimes\boldsymbol{I_2}\}\{[\boldsymbol{S}_\tau^\dagger(\boldsymbol{S}_\tau\boldsymbol{S}_\tau^\dagger)^{-\boldsymbol{I}}]^*\otimes\boldsymbol{I_2}\} \\ &= \left(\frac{N_t}{\rho}\right)(\boldsymbol{S}_\tau\boldsymbol{S}_\tau^\dagger)^{-T}(\boldsymbol{S}_\tau{\boldsymbol{S}_\tau}^\dagger)^T[(\boldsymbol{S}_\tau(\boldsymbol{S}_\tau^\dagger)^{-1})*\otimes\boldsymbol{I_2}] \qquad \text{by (A.2)} \\ &= \left(\frac{N_t}{\rho}\right)[(\boldsymbol{S}_\tau\boldsymbol{S}_\tau^\dagger)^{-T}\otimes\boldsymbol{I_2}].\end{aligned} \tag{3.23}$$

The $\sqrt{\frac{N_t}{\rho}}$ in Eq. (3.23) is a normalization factor to invert the scaling effect due ML estimation. It is done merely for the analytical convenience and has no effect on the system

performance. The MSE is given as

$$\varepsilon = Tr\left[\left(\frac{N_t}{\rho}\right)\left[(\boldsymbol{S}_\tau \boldsymbol{S}_\tau^\dagger)^{-T} \otimes \boldsymbol{I_2}\right]\right]. \tag{3.24}$$

The optimal training sequence would need to minimize the MSE subject to energy constraint $Tr(\boldsymbol{S}_\tau \boldsymbol{S}_\tau^\dagger) = N_t \times T_\tau$ stated in Eq. (3.4). To achieve that, we first represent $\boldsymbol{S}_\tau$ according to its SVD, $\boldsymbol{S}_\tau = \boldsymbol{\Phi V \Psi}$,where $\boldsymbol{\Phi}$ is $N_t \times N_t$ with orthogonal columns, $\boldsymbol{\Psi}$ is $N_t \times T_\tau$ unitary, and V is an $N_t \times N_t$ diagonal matrix. Then the MSE equals.

$$\begin{aligned}\varepsilon &= Tr\left[\left(\frac{N_t}{\rho}\right)(\boldsymbol{S}_\tau \boldsymbol{S}_\tau^\dagger)^{-T} \otimes \boldsymbol{I_2}\right] \\ &= 2\left(\frac{N_t}{\rho}\right) Tr\left[(\boldsymbol{S}_\tau \boldsymbol{S}_\tau^\dagger)^{-1}\right] \\ &= 2\left(\frac{N_t}{\rho}\right) Tr(\boldsymbol{\Phi V^{-2} \Phi}^\dagger).\end{aligned} \tag{3.25}$$

The MSE is proportional to $\sum_{m=1}^{N_t} v_{mm}^{-2}$. Subject to energy constraint, $\sum_{m=1}^{N_t} v_{mm}^2 = N_t \times T_\tau$, Eq. (3.25) is minimized when all the singular values are equal, that is $v_m = \sqrt{T_\tau}$. Then the training symbol $\boldsymbol{S}_\tau = \sqrt{T_\tau}\,\boldsymbol{\Phi \Psi}^\dagger$. Therefore the optimal training sequences are in the form of an orthogonal matrix. It is important to notice that the orthogonal training sequence is optimal regardless of the channel spatial correlation.

3.3.2.1 Properties of ML Channel Estimation with Orthogonal Training Sequence

With optimal training sequences, the resulting error covariance and MSE are

$$\boldsymbol{R}_{\widetilde{\boldsymbol{h}}\widetilde{\boldsymbol{h}}} = \left(\frac{N_t}{\rho T_\tau}\right)\boldsymbol{I}_{\boldsymbol{N_t \times 2}}, \tag{3.26}$$

$$\varepsilon = \frac{N_t 2}{\rho T_\tau}. \tag{3.27}$$

The white Gaussian noise matrix $\boldsymbol{W}_\tau$ is independent of $\boldsymbol{H}$ and $E[\boldsymbol{W}_\tau] = \boldsymbol{0}$. Therefore from Eq. (3.22)

$$E_{\boldsymbol{H},\boldsymbol{Y}_\tau}[\widetilde{\boldsymbol{H}}] = \boldsymbol{0}. \tag{3.28}$$

So the distribution of the channel estimation error is

$$\widetilde{\boldsymbol{H}} \backsim N_c \left(\boldsymbol{0}_{2\times N_t}, \frac{N_t}{\rho T_\tau} \boldsymbol{I}_{N_t \times 2} \right), \tag{3.29}$$

which is consistent with the result from [48]. It can be observed that Eq. (3.27) is unbounded as SNR decreases. At low SNR, ML channel estimation deteriorates due to noise amplification. Since the $\boldsymbol{H}$ and $\widetilde{\boldsymbol{H}}$ are independent of each other using Eq. (3.7),

$$\boldsymbol{R}_{\widehat{h}\widehat{h}} = \boldsymbol{R}_{hh} + \boldsymbol{R}_{\widetilde{h}\widetilde{h}} \tag{3.30}$$

$$E[\widehat{\boldsymbol{h}}] = E[\boldsymbol{h}] + E[\widetilde{\boldsymbol{h}}]. \tag{3.31}$$

The channel estimate $\widehat{\boldsymbol{H}}$ is a Gaussian matrix, since both $\boldsymbol{H}$ and $\widetilde{\boldsymbol{H}}$ are Gaussian matrices and independent of each other. Then the distribution of the channel estimate is also Gaussian and is given as

$$\widehat{\boldsymbol{h}} \backsim N_c \left(\boldsymbol{0}_{N_t \times 2},\, \boldsymbol{R}_{hh} + \frac{\boldsymbol{N_t}}{\rho \boldsymbol{T}_\tau} \boldsymbol{I}_{N_t \times 2} \right). \tag{3.32}$$

Now let consider the correlation between $\widehat{\boldsymbol{h}}$ and $\widetilde{\boldsymbol{h}}$.

$$\begin{aligned} E\left[\widehat{\boldsymbol{h}}\widetilde{\boldsymbol{h}}^{\dagger}\right] &= E\left[\left(\boldsymbol{h}+\widetilde{\boldsymbol{h}}\right)\widetilde{\boldsymbol{h}}^{\dagger}\right] \\ &= E\left[\widetilde{\boldsymbol{h}}\widetilde{\boldsymbol{h}}^{\dagger}\right] \\ &= \left(\frac{N_t}{\rho T_\tau}\right) \boldsymbol{I}_{2\times N_t}. \end{aligned} \tag{3.33}$$

As it can be observed, $\widehat{\boldsymbol{H}}$ and $\widetilde{\boldsymbol{H}}$ both are Gaussian random matrices, and can be assumed to be independent as the channel SNR gets large.

3.4 Detection of Training-based Alamouti OSTBC

In this section, we present the signal detection under the channel estimation error. A two-by-two Alamouti OSTBC coded MIMO system is considered. Since the receiver treats the

estimated channel as the true channel, we may rewrite the signal model as

$$\boldsymbol{Y_d} = \sqrt{\frac{\rho}{N_t}}\widehat{\boldsymbol{H}}\boldsymbol{S_d} + \sqrt{\frac{\rho}{N_t}}\widetilde{\boldsymbol{H}}\boldsymbol{S_d} + \boldsymbol{W_d}. \tag{3.34}$$

The detection rule is

$$\begin{pmatrix} \widehat{\boldsymbol{x}}_1 \\ \widehat{\boldsymbol{x}}_2 \end{pmatrix} = arg\min_{\boldsymbol{x_1},\boldsymbol{x_2}} \|\boldsymbol{Y_d} - \widehat{\boldsymbol{H}}\boldsymbol{S_d}\|_F^2. \tag{3.35}$$

This detection rule is only suboptimal and $\|\boldsymbol{Y_d} - \widehat{\boldsymbol{H}}\boldsymbol{S_d}\|_F^2$ is usually referred to as a mismatched metric. However the properties of simple decoding and diversity gain of OSTBC are preserved, while an optimal decoder requires a Viterbi algorithm [66]. As we can see from the previous section, the channel estimation errors resulting from LMMSE channel estimation are spatially colored Gaussian. Therefore in order to use a decoder designed for i.i.d noise, whitening the noise is necessary [37]. Rewrite Eq. (3.34) into vector form as

$$\boldsymbol{y_d} = \sqrt{\rho}N_t(\boldsymbol{I_2} \otimes \widehat{\boldsymbol{H}})\boldsymbol{s_d} + \sqrt{\rho}N_t(\boldsymbol{I_2} \otimes \widetilde{\boldsymbol{H}})\boldsymbol{s_d} + \boldsymbol{w_d}. \tag{3.36}$$

The received signals are multiplied by a whitening matrix $\boldsymbol{Q}$ so that the overall noise resulting from the ML and LMMSE channel estimation methods are spatially whitened with unity power for each channel coefficient. That is

$$\begin{aligned} \boldsymbol{z_d} &= \boldsymbol{Q}\boldsymbol{y_d} \\ &= \sqrt{\frac{\rho}{N_t}}(\boldsymbol{I_2} \otimes \widehat{\boldsymbol{H}}')\boldsymbol{s_d} + \boldsymbol{n_d}, \end{aligned} \tag{3.37}$$

where

$$\widehat{\boldsymbol{H}}' = \boldsymbol{Q}\widehat{\boldsymbol{H}}, \tag{3.38}$$

$$\boldsymbol{n_d} = \boldsymbol{Q}\left[\sqrt{\frac{\rho}{N_t}}(\boldsymbol{I_2} \otimes \widetilde{H})\boldsymbol{s_d} + \boldsymbol{w_d}\right]. \tag{3.39}$$

It can be shown that the whitening matrix is

$$\boldsymbol{Q} = \left(\frac{\rho}{N_t}\boldsymbol{I_2} \otimes E[\widetilde{H}\widetilde{H}^{\dagger}] + \boldsymbol{I_{N_t \times N_r}}\right)^{-1/2}, \tag{3.40}$$

where $E[\widetilde{H}\widetilde{H}^{\dagger}]$ can be calculated from Eqs. (3.18) and (3.29) for LMMSE and ML channel estimations, respectively. The resulting noise has the following distribution:

$$\boldsymbol{N_d} \backsim N_c(\boldsymbol{0},\boldsymbol{I}).$$

The noise whitening is not necessary in practice for a system with the ML channel estimator since the estimation error is already spatially white (see Eq. (3.29)).

Now let $z_d^{j,t}$ and $n_d^{j,t}$ be the received data signal and white noise from the j-th receiving antenna at time t, respectively. The time index for the channel matrix is dropped due to the block-fading channel. After taking the channel estimation error into account and reorganizing the equation, the received signals at the j-th receive antenna at time t are

$$\begin{aligned} z_d^{j,1} &= \sqrt{\frac{\rho}{N_t}}\left(\widehat{h}'_{j,1}x_1 + \widehat{h}'_{j,2}x_2\right) + n_d^{j,1} \\ z_d^{j,2} &= \sqrt{\frac{\rho}{N_t}}\left(-\widehat{h}'_{j,1}x_2^* + \widehat{h}'_{j,2}x_1^*\right) + n_d^{j,2}. \end{aligned} \tag{3.41}$$

The channel estimation error is treated as part of the noise term because the receiver uses the estimated channel for signal demodulation. It can be shown that the combined noise terms are temporally uncorrelated. The estimates of the data signal from the ML decoder are

$$\widehat{x}_1 = \frac{\sum_{j=1}^{N_r=2}\left[z_d^{j,1}\widehat{h}'^{*}_{j,1} + z_d^{j,2*}\widehat{h}'_{j,2}\right]}{\|\widehat{\boldsymbol{H}}'\|_F^2} \tag{3.42}$$

$$\widehat{x}_2 = \frac{\sum_{j=1}^{N_r=2}\left[z_d^{j,1}\widehat{h}'^{*}_{j,2} - z_d^{j,2*}\widehat{h}'_{j,1}\right]}{\|\widehat{\boldsymbol{H}}'\|_F^2}. \tag{3.43}$$

Substituting Eq. (3.41) into Eq. (3.42) and after some manipulation the estimate $\widehat{\boldsymbol{x}}$ has components

$$\widehat{x}_1 = \sqrt{\frac{\rho}{N_t}}x_1 + \underbrace{\frac{\sum_{j=1}^{N_r=2}[n_d^{j,1}\widehat{h}'_{j,1} + n_d^{j,2}\widehat{h}'_{j,2}]}{\|\widehat{\boldsymbol{H}}'\|_F^2}}_{n'_1}$$

$$\widehat{x_2} = \sqrt{\frac{\rho}{N_t}} x_2 + \underbrace{\frac{\sum_{j=1}^{N_r=2} [n_d^{j,1} \widehat{h}'_{j,2} - n_d^{j,2} \widehat{h}'_{j,1}]}{\|\widehat{\boldsymbol{H}}'\|_F^2}}_{n'_2}, \tag{3.44}$$

where n'_1 and n'_2 are the effective noise terms. For the ML estimation at high SNR and LMMSE estimation, the channel estimation error $\widetilde{\boldsymbol{H}}$ and channel estimate $\widehat{\boldsymbol{H}}$ are independent. The general expression for instantaneous effective noise power in each frame is given as

$$\begin{aligned} \sigma_n^2 &= \sigma_{n'_1}^2 = \sigma_{n'_2}^2 \\ &= \frac{1}{\|\widehat{\boldsymbol{H}}'\|_F^2}. \end{aligned} \tag{3.45}$$

$$\tag{3.46}$$

The equivalent instantaneous effective SNR is

$$SNR_{effective} = \frac{\rho}{2\sigma_n^2} \ . \tag{3.47}$$

It can be shown that the effective noise components n'_1 and n'_2 are uncorrelated, and independent of the data signal x_1, x_2. This claim is generally not true for systems with the ML estimator, since the noise term is highly correlated with the data signal at low SNR (see Eq. (3.33)). For the system with an ML or LMMSE channel estimator operating at appropriate SNR regions, where the uncorrelated assumption holds, the effective instantaneous capacity is

$$\begin{aligned} C_s &\geq \frac{T - N_t T_{\tau/N_t}}{T} \log_2 \left(1 + SNR_{effective}\right) \\ &= \frac{T - N_t T_{\tau/N_t}}{T} \log_2 \left(1 + \frac{\rho}{2\sigma_n^2}\right), \end{aligned} \tag{3.48}$$

where T_{τ/N_t} is the number of training symbols per transmit antenna and it must be real valued such that T_τ is an integer. We can observe that the effective noise terms in Eq. (3.44) are not Gaussian. Therefore the capacity expression in Eq. (3.48) is a lower bound since Gaussian noise provides worst-case performance (see appendix B).

3.5 Antenna Selection Algorithm

From Eq. (3.47) and Eq. (3.48), the antenna selection algorithms would choose the antenna subset that results in minimum instantaneous effective noise power. This method maximizes instantaneous SNR and capacity. It is obvious that an antenna selection method should select the transmit antennas that results in largest $\|\widehat{\boldsymbol{H}}'\|_F^2$, which maximizes both instantaneous effective SNR and instantaneous capacity. From a signal processing point of view, it is equivalent to selecting the two columns of $\widehat{\boldsymbol{H}}'$ with largest squared Frobenius norm. This antenna selection method for OSTBC systems is in a similar form to the one developed in [24]. This selection method is optimal for both ML and LMMSE channel estimation. However the novelty of this proposed method is the fact that the selection algorithm exploits knowledge of both $\widehat{\boldsymbol{H}}$ and $\boldsymbol{R_{hh}}$. Letting $\widehat{\boldsymbol{H}}_s$ be the selected sub-matrix from $\widehat{\boldsymbol{H}}$, the mathematical representation of the transmit selection method is given as

$$\begin{aligned} &\min_{\widehat{\boldsymbol{H}}_s \in \text{ columns of } \widehat{\boldsymbol{H}}} \sigma_n^2 \\ &= \max_{\widehat{\boldsymbol{H}}_s \in \widehat{\boldsymbol{H}}} \|\widehat{\boldsymbol{H}}_s\|_F^2. \end{aligned} \tag{3.49}$$

The average effective SNR after selection is

$$\overline{SNR}_{effective} = \frac{\rho}{2E_{\widehat{\boldsymbol{H}}_s}[\sigma_n^2]}. \tag{3.50}$$

3.6 Performance Criterion

We treat the space-time block code as an inner code while an outer code operates across the effective channel resulting from OSTBC decoding. As shown in the previous section, the effective channel is equivalent to two parallel single-input signal-output (SISO) channels as shown in Eq. (3.44). In designing a system, a delay constraint on how frequently a receiver can decode the encoded messages to usable outputs is needed. The appropriate

value depends on the nature of service. For low-delay real-time application, such as voice, the delay constraint is generally small, while a data transmission service could tolerate longer delays. For a long duration non-real-time applications, the delay could be as long as the entire transmission. In this section, we study the different achievable rates under two extreme delay constraints, namely infinite delay and one-block delay.

3.6.1 No Delay Constraints

When there are no delay constrains, the outer code could ideally span an infinite number of fading blocks. The channel is information stable and capacity coincides with the maximum expected instantaneous capacity [71], which is called the ergodic capacity. After taking the training overhead into account the achievable rate is expressed as

$$\overline{C_s} \geq \frac{T - N_t T_{\tau/N_t}}{T} E_{\widehat{\boldsymbol{H}}_s} \left[\log_2 (1 + SNR_{effective}) \right]. \tag{3.51}$$

3.6.2 One-Block Delay Constraint

When the outer code only spans one fading block, the channel is not information stable and capacity cannot be represented by the maximum expected instantaneous capacity. Due to the nature of the fading channel, the instantaneous capacity of each block is a random variable. Therefore the error probability cannot be made arbitrarily small for any transmission rate. When the instantaneous capacity falls below the transmission rate the system is said to be in outage, and the outage probability is

$$\begin{aligned} p_{out}(C_{outage}) &= \mathbb{P}(C_s < C_{outage}) \\ &= \mathbb{P}\left(\frac{T - N_t T_{\tau/N_t}}{T} \log_2 \left(1 + SNR_{effective}\right) < R \right). \end{aligned} \tag{3.52}$$

The outage probability is defined for block length $T \to \infty$. In practice, a value of T of about 100 coded symbols is sufficient to represent frame-error rate (FER) [36]. The corresponding ε-outage capacity is the largest rate C_{outage} that such that

$$p_{out}(C_{outage}) \leq \varepsilon. \tag{3.53}$$

For a system with a bit rate R, the FER is lower bounded as follows:

$$FER \geq p_{out}(C_{outage}). \tag{3.54}$$

3.6.3 Performance Enhancement

Let $C^M_{outage}(N_t)$ and $\overline{C}^M_s(N_t)$ be the outage capacity and ergodic capacity, respectively, for the MIMO antenna selection system with N_t transmit antenna. The marginal ergodic and outage capacity gains expressed as percentage due to an additional pair of transmit antennas is defined as

$$G^M_s(N_t) = \frac{\overline{C}^M_s(N_t) - \overline{C}^M_s(N_t-2)}{\overline{C}_s(N_t)} \times 100\%, \tag{3.55}$$

$$G^M_{outage}(N_t) = \frac{C^M_{outage}(N_t) - C^M_{outage}(N_t-2)}{C^M_{outage}(N_t)} \times 100\%. \tag{3.56}$$

where

$$\overline{C}^M_s(N_t) - \overline{C}^M_s(N_t-2), \tag{3.57}$$

$$C^M_{outage}(N_t) - C^M_{outage}(N_t-2), \tag{3.58}$$

are referred to as marginal ergodic and marginal outage capacity gain, respectively, in the future discussions.

3.7 Extension to OSTBC MIMO-OFDM System with Antenna Selection

MIMO-OFDM wireless communication systems are designed to further increase data rates. However MIMO-OFDM inherits the disadvantages from MIMO systems. The system cost and signal processing complexity increases dramatically with the spatial dimension of the signal. To remedy the problem, antenna selection for MIMO-OFDM has been proposed [4, 18]. However antenna selection for MIMO and MIMO-OFDM are typically discussed as two separate entities. In this chapter, performance enhancement due to an additional pair of transmit antennas for an OSTBC MIMO-OFDM system with transmit antenna selection is discussed by using the signal processing method developed in Chapter 3 and the results in Chapter 4.

3.7.1 System and Channel Model

For a system without channel knowledge at the transmitter, OSTBC can be applied to a MIMO-OFDM system to achieve higher diversity. In the system proposed in [40], each subcarrier is independently encoded with an orthogonal space-time block code. The orthogonal space-time block coded MIMO-OFDM system with antenna selection under consideration is depicted in Fig. 3.4, where N_t antennas are located at the transmitter and N_r antennas are located at the receiver. The system uses N subcarriers for data transmission. From Section 2.3.1, we recall that the channel at each subcarrier has identical spatial correlation.

At each time instant, blocks of signal $t_i[n,k]$ for $i = 1 \ldots T_b$ and $k = 1 \ldots N$ are mapped onto the two OFDM branches. On the subcarrier k, $t_i[n,k]$ for $n = 1 \ldots T_b$ forms an OSTBC block. At each OFDM branch, an $(N \times 1)$ vector is transformed by an N-point IFFT, F_N^H.

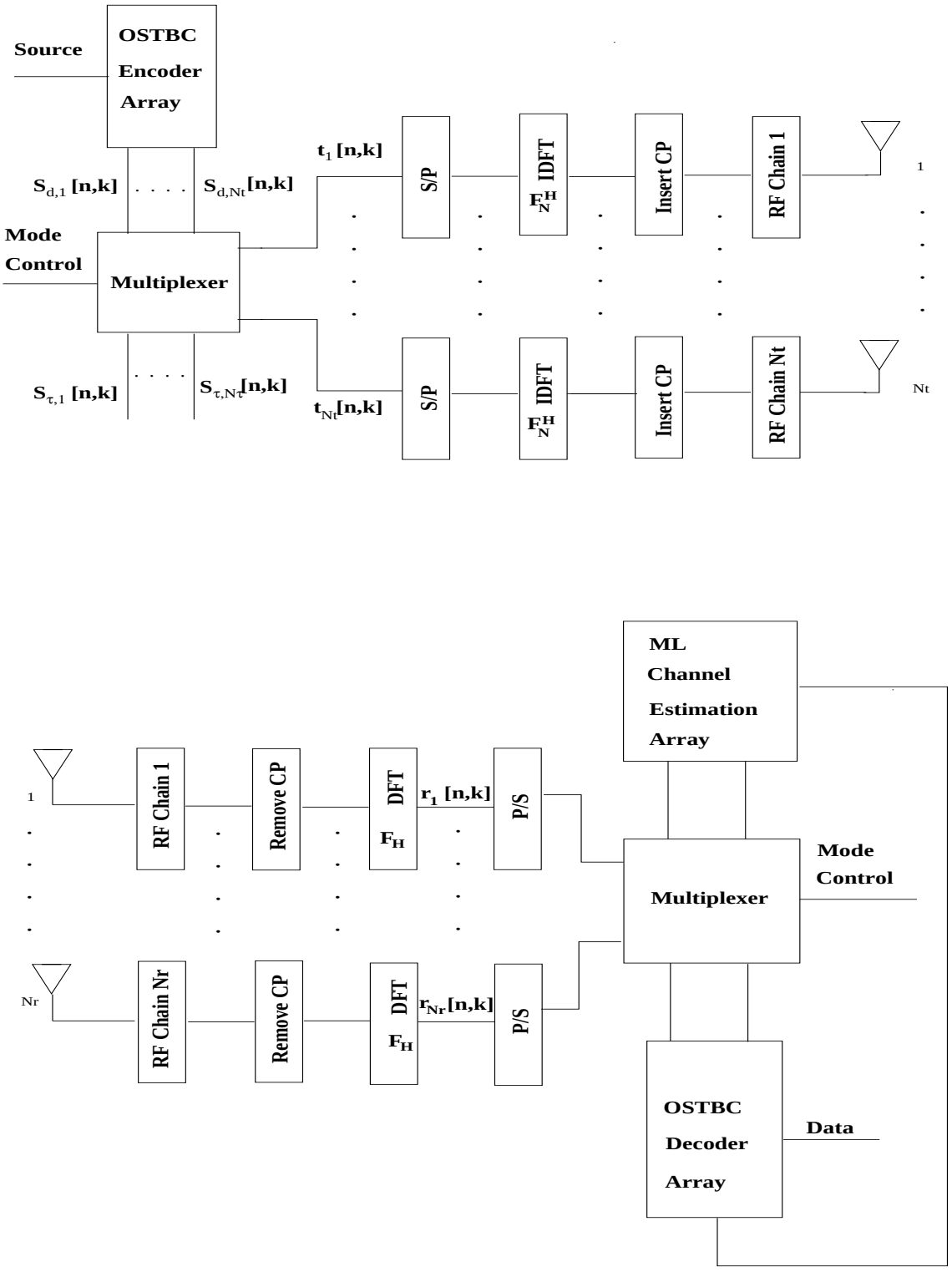

Figure 3.4: Illustration of orthogonal space-time block coded MIMO-OFDM system

Before transmission, an $N \times 1$ vector is appended with a CP of length L_{CP} to construct an OFDM symbol. The CP-prefix is removed at each receiver branch, and then the received signal is transformed into the frequency domain by an N-point FFT, F_N. The output signals after FFT transformation are blocks of $r_j[n,k]$ for $j = 1 \ldots 2$ and $k = 1 \ldots N$.

3.7.2 Performance Analysis

Since each subcarrier can be seen as an independent space-time coded MIMO system, the instantaneous effective SNR becomes

$$SNR_{effective} = \frac{1}{N} \sum_{k=0}^{N-1} \frac{\rho}{N_t \, r} \|\boldsymbol{H}\|_F^2. \tag{3.59}$$

The capacity of the OSTBC coded MIMO-OFDM system is the summation of N OSTBC coded MIMO systems, shown in Eq. (2.40). By taking the CP and training overhead into account, the instantaneous capacity is

$$C_s = \frac{T - (N_t T_{\tau/N_t} + L_{CP})}{T} r_c \sum_{k=0}^{N-1} \log_2 \left(1 + SNR_{effective}\right), \tag{3.60}$$

where T is the total transmission time. The average SNR and ergodic capacity are

$$\overline{SNR}_{effective} = \frac{1}{N} E \left[\sum_{k=0}^{N-1} \frac{\rho}{N_t \, r} \|\boldsymbol{H}\|_F^2 \right], \tag{3.61}$$

$$\overline{C}_s = \frac{T - (N_t T_{\tau/N_t} + L_{CP})}{T} r_c E \left[\sum_{k=0}^{N-1} \log_2 \left(1 + SNR_{effective}\right) \right]. \tag{3.62}$$

The channel at each subcarrier has identical spatial correlation. After using the channel estimation scheme defined in Section 2.5.2.1, which views each subcarrier as a MIMO system, the channel estimates and estimation errors are identical to the ones described in Section 3.3. Let us define $\widehat{\ddot{\boldsymbol{H}}}[\boldsymbol{k}]$ the channel estimate at subcarrier k. The antenna selection algorithm would need to select the transmit antenna that yields the largest instantaneous

effective SNR which is

$$\max_{\substack{\widehat{\ddot{\boldsymbol{H}}}_s[\boldsymbol{k}] \in columns\ of\ \widehat{\ddot{\boldsymbol{H}}}[\boldsymbol{k}]\ k=0...N-1; \\ all\ \widehat{\ddot{\boldsymbol{H}}}_s[\boldsymbol{k}]\ are\ from\ the\ same\ antenna\ subset}} \sum_{k=0}^{N-1} \|\widehat{\ddot{\boldsymbol{H}}}_s[\boldsymbol{k}]\|_F^2, \tag{3.63}$$

where $\widehat{\ddot{\boldsymbol{H}}}_s[\boldsymbol{k}]$ is the selected channel matrix at subcarrier k and all $\widehat{\ddot{\boldsymbol{H}}}_s[\boldsymbol{k}]$ for $k = 0 \ldots N-1$ are from an identical antenna subset. It is equivalent to select the two slices with largest squared Frobenius norm. Similar to the MIMO case, the optimality in terms of instantaneous capacity is also achieved by this selection method. The resulting two-by-two system is then used for data transmission. The instantaneous SNR after antenna selection is

$$SNR_{effective} = \frac{1}{N} \sum_{k=0}^{N-1} \frac{\rho}{N_t\ r_c} \|\widehat{\ddot{\boldsymbol{H}}}_s[\boldsymbol{k}]\|_F^2. \tag{3.64}$$

The average effective SNR is

$$\overline{SNR}_{effective} = \frac{1}{N} \sum_{k=0}^{N-1} \frac{\rho}{N_t\ r_c} E\left[\|\widehat{\ddot{\boldsymbol{H}}}_s[\boldsymbol{k}]\|_F^2\right]. \tag{3.65}$$

The corresponding instantaneous and ergodic capacities

$$C_s = \frac{T - (N_t T_{\tau/N_t} + L_{CP})}{T} \sum_{k=0}^{N-1} log_2\left(1 + SNR_{effective}\right), \tag{3.66}$$

and

$$\overline{C}_s = \frac{T - (N_t T_{\tau/N_t} + L_{CP})}{T} \sum_{k=0}^{N-1} E_{\widehat{\ddot{\boldsymbol{H}}}_s[\boldsymbol{k}]} log_2\left(1 + SNR_{effective}\right). \tag{3.67}$$

Even though $\widehat{\ddot{\boldsymbol{H}}}[\boldsymbol{k}]$ has the same statistics for all k, it is very complicated to further simplify Eq. (3.67) due to the properties of the order statistics.

3.7.3 Upper Bound on Performance Enhancement

As we can see from Eq. (3.63), the antenna selection for the MIMO-OFDM system chooses the antennas that yields the largest squared Frobenius norm summing over all the subcarriers. All the channels seen at each subcarrier are statistically identical as shown in Section

2.3.1. Therefore the resulting channel after antenna selection is not always optimal at each subcarrier.

Let $C_{outage}^{MO[k]}(N_t)$ and $\overline{C}_s^{MO[k]}(N_t)$ be the outage capacity and ergodic capacity, respectively, for the MIMO-OFDM antenna selection system at subcarrier k for $k = 0 \ldots N-1$ with N_t transmit antennas. If the channel of the MIMO-OFDM system at each subcarrier and the channel of the MIMO system have identical statistics, then

$$C_{outage}^{MO[k]}(N_t) \leq C_{outage}^{M}(N_t), \tag{3.68}$$

and

$$\overline{C}_s^{MO[k]}(N_t) \leq \overline{C}_s^{M}(N_t). \tag{3.69}$$

Eq. (3.68) and Eq. (3.69) hold because the antenna selection in MIMO-OFDM does not guarantee the optimality at each subcarrier. Now let us look at the performance enhancement due to additional transmit antennas. For the MIMO-OFDM system, the enhancement in outage capacity becomes

$$G_{outage}^{MO}(N_t) = \frac{1}{N}\sum_{k=1}^{N-1} \frac{C_{outage}^{MO}(N_t) - C_{outage}^{MO}(N_t-2)}{C_{outage}^{MO}(N_t)} \times 100\%. \tag{3.70}$$

By Eq. (3.68),

$$G_{outage}^{MO}(N_t) \leq G_{outage}^{M}(N_t). \tag{3.71}$$

For the MIMO-OFDM system, the enhancement in outage capacity becomes

$$G_s^{MO}(N_t) = \frac{1}{N}\sum_{k=1}^{N-1} \frac{\overline{C}_s^{MO}(N_t) - \overline{C}_s^{MO}(N_t-2)}{\overline{C}_s^{MO}(N_t)} \times 100\%. \tag{3.72}$$

By Eq. (3.69),

$$G_s^{MO}(N_t) \leq G_s^{M}(N_t). \tag{3.73}$$

From Eq. (3.73) and Eq. (3.71) we can conclude that the performance gain in both ergodic and outage capacity due to additional transmit antennas of a OSTBC coded MIMO-OFDM

antenna selection system is upper bounded by the performance of a OSTBC MIMO antenna selection system for a given value of channel spatial correlation. Therefore the results on marginal capacity gain in Chapter 4 can be used as an upper bound for a OSTBC MIMO-OFDM with transmit antenna selection. This bound is tight when the correlation between the channels at subcarriers are high. It is expected to become looser when the channels at subcarriers are uncorrelated.

3.8 Chapter Summary and Discussions

In this chapter, we have defined the training-based Alamouti space-time coded MIMO system with transmit antenna selection under study and developed the antenna selection method. We also have defined the training-based Alamouti space-time coded MIMO-OFDM with transmit antenna selection under study. The mathematical expressions for both the resulting outage and ergodic capacities are derived. The extension to OSTBC MIMO-OFDM systems with antenna selection is discussed, and an upper bound of performance enhancement on the system is determined. The mathematical expressions for both the resulting outage and ergodic capacities are derived. Although Eq. (3.51) and Eq. (3.52) provide closed-form expressions for ergodic capacity and outage capacity, respectively, it is still difficulty to numerically evaluate the performance due the order statistics resulting from antenna selection.

Therefore we make the following observations concerning Eq. (3.51) and Eq. (3.52). After taking the training overhead into consideration, the ergodic capacity upper bound based on Jensen's inequality is given as

$$\overline{C_s} \leq \frac{T - N_t T_{\tau/N_t}}{T} r_c \; log_2 \left(1 + E\left[SNR_{effective}\right]\right). \tag{3.74}$$

The ergodic capacity upper bound based on Jensen's inequality is shown to be tight for

semi-correlated MIMO channels [34, 35, 46] under perfect CSI assumption. The tightness of Eq. (3.74) is not verified previously but it still reveals more insight into performance. From the above upper bound, we can see that as the number of transmit antennas increases, the increase in capacity due to increasing $\overline{SNR}_{effective}$ is offset by training overhead. As the training length T_{τ/N_t} increases, the $\overline{SNR}_{effective}$ also increases. However $\overline{SNR}_{effective}$ only increases logarithmically with N_t, as demonstrated in Section 2.4.1. Also, Eq. (3.74) is a logarithmical function of $\overline{SNR}_{effective}$ and decreases linearly with increasing T_{τ/N_t}. From the aforementioned reasons, the capacity should be a concave function of both T_{τ/N_t} and N_t.

The LMMSE channel estimation uses knowledge of channel spatial correlation. As demonstrated in Section 3.3.1.1, the LMMSE channel estimation quality of spatially correlated channels is better than that of spatially uncorrelated channels. Therefore a system under a spatially correlated channel might outperform a system under a spatially uncorrelated channel, in terms of capacity, in some regions of operation. The aforementioned observations will later be confirmed by the Monte Carlo analysis in the next chapter.

Chapter 4

Numerical Results and Discussions

4.1 Monte Carlo Analysis Description

Downlink wireless communication is considered. In this section, we study the system performance under both spatially uncorrelated and correlated Rayleigh channels. Capacity with delay constraints specified in Section 3.6 are considered. Since 1%-outage capacity is considered throughout, the terms 1%-outage capacity and outage capacity are used interchangeably in the following discussions. Although we have obtained the closed-form expressions for both the ergodic capacity in Eq. (3.51) and outage capacity in Eq. (3.52), it is still difficult to analytically evaluate both expressions due to the order statistics resulting from the antenna selection. Therefore Monte Carlo analysis with 10^5 realizations are used to evaluate performance. The worst-case 99.9% confidence interval for ergodic capacity and 1%-outage capacity, in $bits/sec/Hz$, are ± 0.014 and ± 0.080, respectively. The one-ring channel model in Fig. 2.3 is deployed by placing a cluster at the receiver of the SU. Therefore $\boldsymbol{R_{Rx}} = \boldsymbol{I}$. Different channel correlations are achieved by adjusting the angle spread at the BS transmitter. It is shown in [61] that angle spreads below 60° are typically observed in many environments. Therefore angle spreads between 10° to 60° in increments

of 10° are chosen in the analysis. The corresponding $\boldsymbol{R_{Tx}}$ for each AS is shown in Appendix C. SNR ranging from 0 dB to 30 dB with an increment of 2 dB is chosen. We assume that the antenna arrays at the transmitter and receiver are parallel to each other. Block lengths ranging T from 100 to 800 symbols are used to consider different coherence times T_c. The feedback time T_f is assumed to be negligible. Only the LMMSE MIMO channel estimator is considered, since it has been shown that the ML estimator converges to the LMMSE estimator at high SNR. Therefore the results of the LMMSE estimator implicitly indicate the performance for the ML estimator in a high SNR environment. Knowledge of SNR and channel spatial correlation are assumed to be perfect at the receiver due to a low mobility wireless environment.

The parameters for the Monte Carlo analysis are tabulated in Section 4.1.1. Realizations of the channel are randomly generated under both spatially uncorrelated and semi-correlated Rayleigh fading channels. The spatially semi-correlated Rayleigh fading are simulated based on Tables 4.1, 4.2, and 4.3. Eqs. (3.51) and (3.52) are evaluated by generating $\widehat{\boldsymbol{H}}$ according to Eq. (3.21), and evaluating Eq. (3.38) and (3.47), followed by antenna selection. The results and discussion are presented in Section 4.2.

4.1.1 Parameters

The parameters for the Monte Carlo Analysis are stated below.

Parameter	Range	Increment
N_t	$2 \sim 20$	2
N_r	2	–
T	$100, 800$ symbols	2 symbols
$T_{\tau_{per/antenna}}$	$1 \sim \frac{T}{N_t}$ symbols	$1/2$ symbol

Table 4.1: Transmitter Parameters for MIMO Physical Layer

Parameter	Value(s)
SNR	$0, 2, \ldots, 28, 30\,\text{dB}$
Channel realizations	10^5
Antenna spacing $\left(\frac{d}{\lambda}\right)$	$1/2$
Power azimuth spectrum	Laplacian
Number of clusters	1 around the SU
Angle of incident ϕ_0	0°
Azimuth Spread σ	$10^\circ, 20^\circ, \ldots, 60^\circ$
PAS Distribution Boundary	180°

Table 4.2: Channel Parameters for MIMO Physical Layer

Parameter	Value
Channel estimation	LMMSE
OSTBC decoder	(3.35)
Antenna selection criterion	(3.49)
RF impairment	None

Table 4.3: Receiver Parameters for MIMO Physical Layer

4.2 Results and Discussions

We now present and discuss the results of the Monte Carlo analysis with the parameters stated in the previous section. All the results are expressed in terms of capacity under different delay constraints described in Section 3.6. Various spatial channel correlations, block lengths and training strategies are considered. For the system with an optimal training strategy, the optimal training length and number of transmit antennas are found by a two-dimensional exhaustive search. We will not state the optimal training length because no

general relation is observed. Since not all the systems can intelligently adjust the training length, we also present the simulation results on the number of available transmit antennas with minimum training length ($T_\tau = N_t$). In this scenario, the optimal number of transmit antennas are found through exhaustive search.

4.2.1 System with Minimum Training Length

Fig. 4.1 shows the achievable ergodic capacity under spatially uncorrelated Rayleigh fading as a function of the number of available transmit antennas N_t, SNR, and block lengths, $T = 100, 200, 400, 800$, for selecting two transmit antennas using the antenna selection

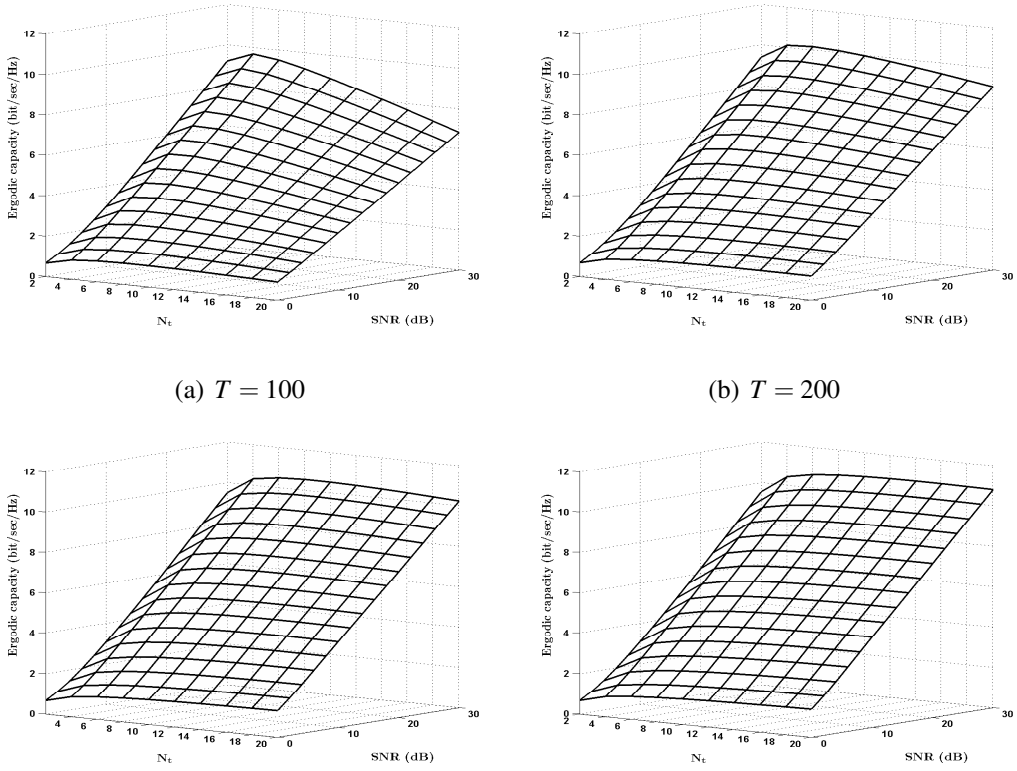

(a) $T = 100$ (b) $T = 200$

(c) $T = 400$ (d) $T = 800$

Figure 4.1: Achievable ergodic capacity for the minimum-trained system as a function of N_t, SNR under spatially uncorrelated Rayleigh fading.

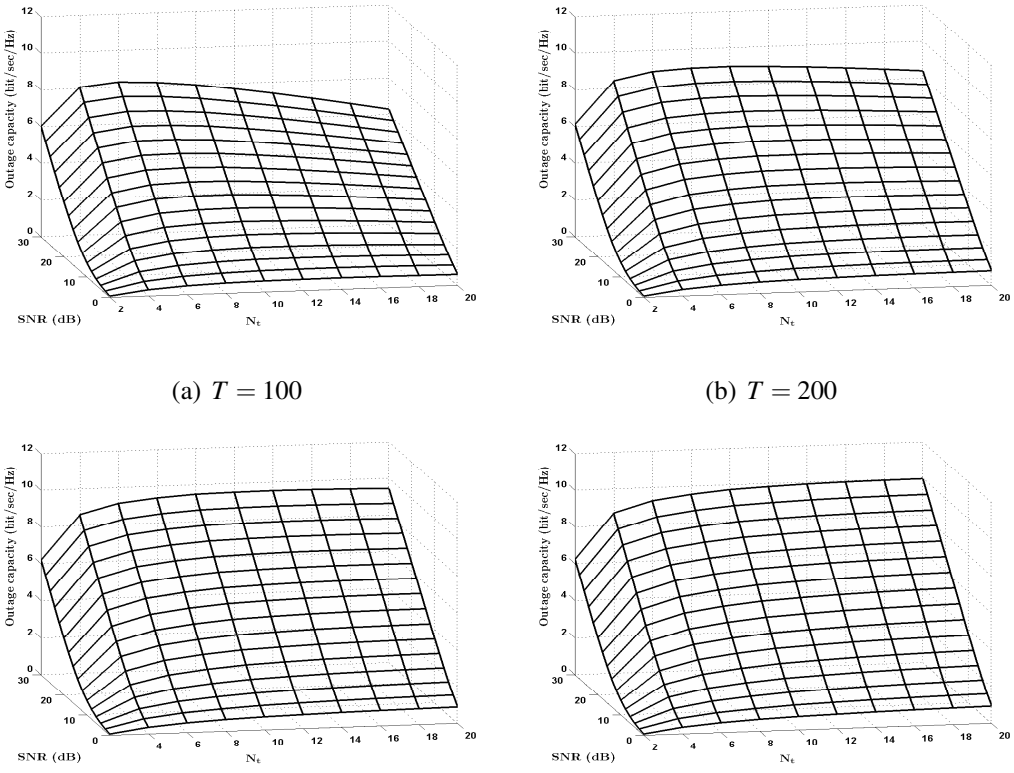

(a) $T = 100$ (b) $T = 200$

(c) $T = 400$ (d) $T = 800$

Figure 4.2: Achievable outage capacity for the minimum-trained system as a function of N_t, and SNR under spatially uncorrelated Rayleigh fading.

algorithm discussed in Section 3.5. Fig. 4.2 shows the corresponding achievable outage capacity. As we can see, the capacity is an increasing function of the block length. From Fig. 4.1 and Fig. 4.2 we observe that the achievable outage capacity is generally a concave function of N_t and becomes a strictly concave function of N_t as the block length decreases. The achievable outage capacity has lower values as expected. The concavity relation is more obvious in Fig. 4.3 and Fig. 4.4, which shows the corresponding marginal gains in ergodic capacity and outage capacity, respectively. As indicated by the area masked by the zero-reference plane, the optimal N_t increases as T increases. However very little gain or even a loss in capacity is observed for $N_t > 4$, except when the block length is large ($T = 800$) and SNR is extremely low (SNR $= 0$ dB).

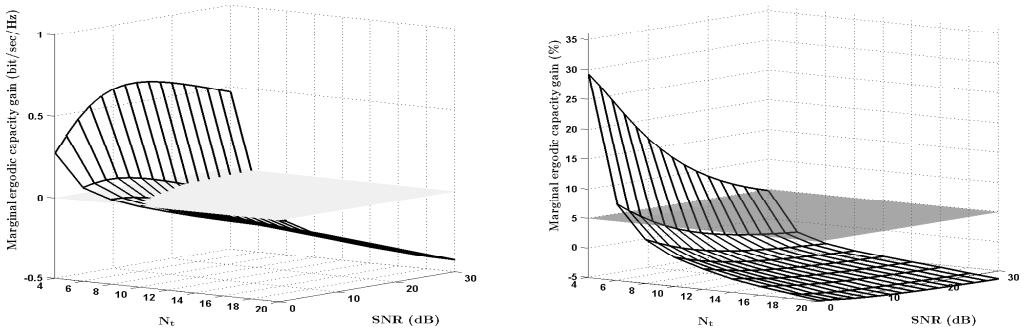

(a) $T = 100$

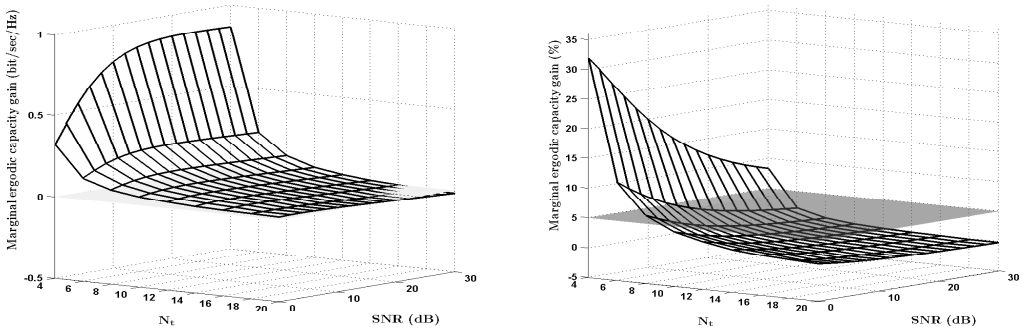

(b) $T = 800$

Figure 4.3: Marginal achievable ergodic capacity gain for the minimum-trained system as a function of N_t, SNR under spatially uncorrelated Rayleigh fading. The nontransparent plane represents the numerical value, zero, and the transparent plane indicates the numerical value, five.

Despite the fact that marginal capacity gain is smaller in low SNR regions, it is more significant in terms of percentage improvement. About 30% improvement in ergodic capacity is attained at SNR $= 0$ dB as N_t increases from two to four, while there is less than 10% improvement at SNR $= 30$ dB. Similar to the ergodic capacity, the marginal gain in outage capacity is smaller in low SNR regions and is more significant in terms of percentage improvement. About 80% improvement in outage capacity is attained at SNR$= 0$ dB as N_t increases from two to four, while the improvement is about 30% at SNR $= 30$ dB. From the figures we can see that both the ergodic capacity and outage capacity exhibit either very little gain or even a loss when $N_t > 4$. The decrease in marginal gain in outage capacity due

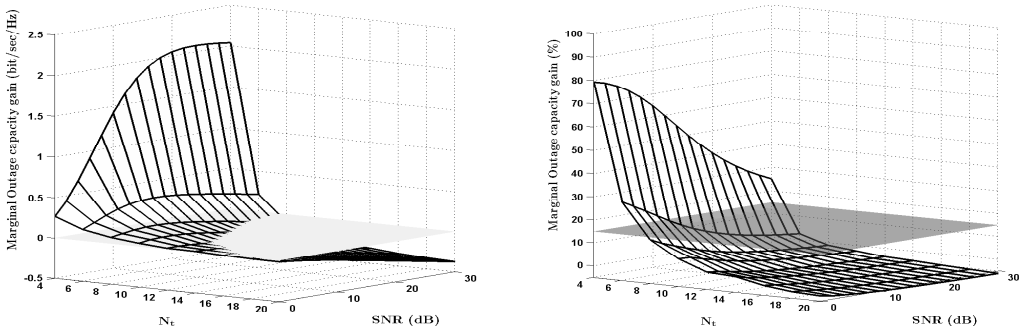

(a) $T = 100$

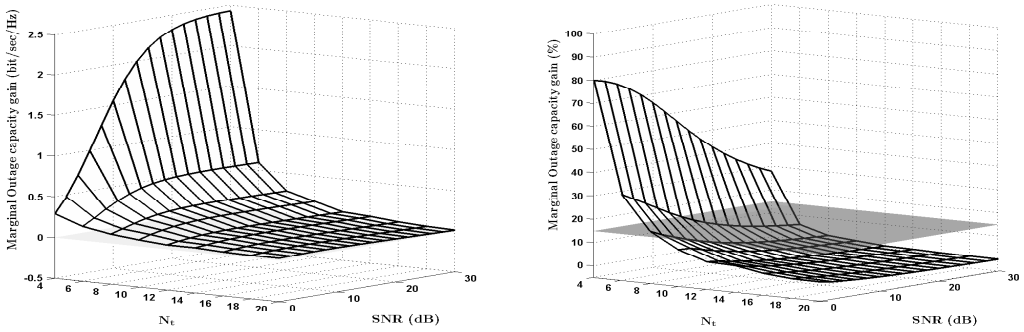

(b) $T = 800$

Figure 4.4: Marginal achievable outage capacity gain for the minimum-trained system as a function of N_t, and SNR under spatially uncorrelated Rayleigh fading. The nontransparent plane represents the numerical value, zero, and the transparent plane indicates the numerical value, 15.

to additional antenna is more significant, compared to that of the ergodic capacity.

4.2.2 Effects of Spatial Correlation on a System with Minimum Training Length

Now let us shift the focus onto spatially correlated channels. Fig. 4.5 shows the marginal gain in achievable ergodic capacity for AS $= 10^\circ$, and 30°. Fig. 4.6 shows the corresponding marginal gain in achievable outage capacity. All the curves exhibit similar trends to the uncorrelated case where either very little gain or even a loss in ergodic capacity is observed

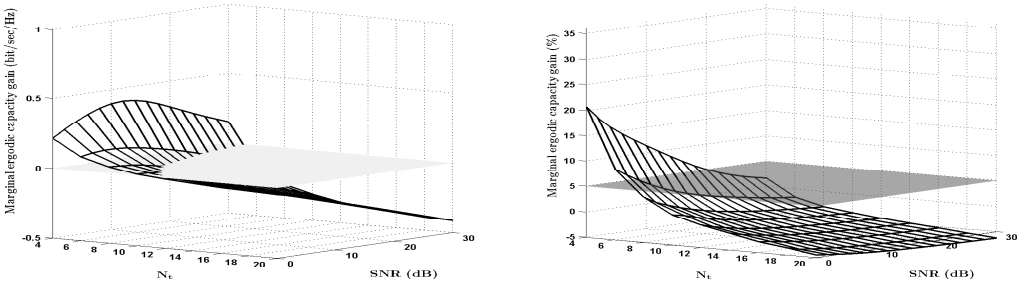

(a) $AS = 10^{\circ}$, $T = 100$

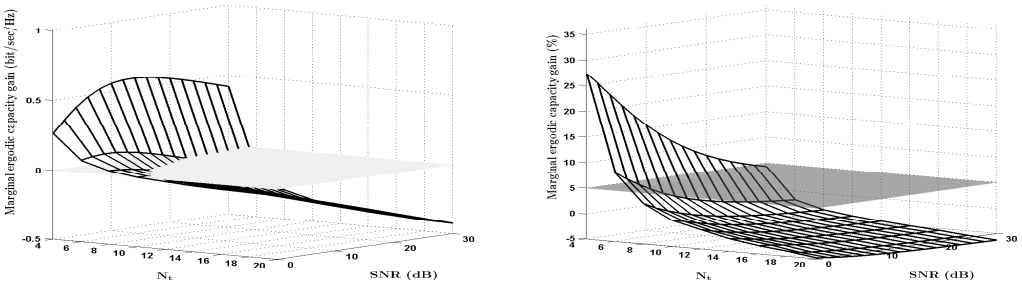

(b) $AS = 30^{\circ}$, $T = 100$

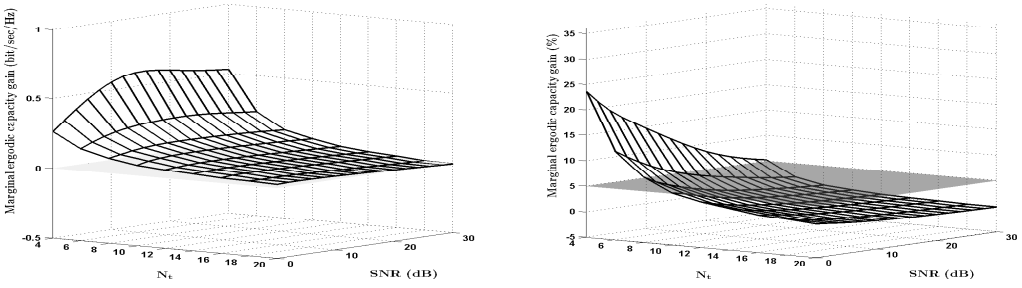

(c) $AS = 10^{\circ}$, $T = 800$

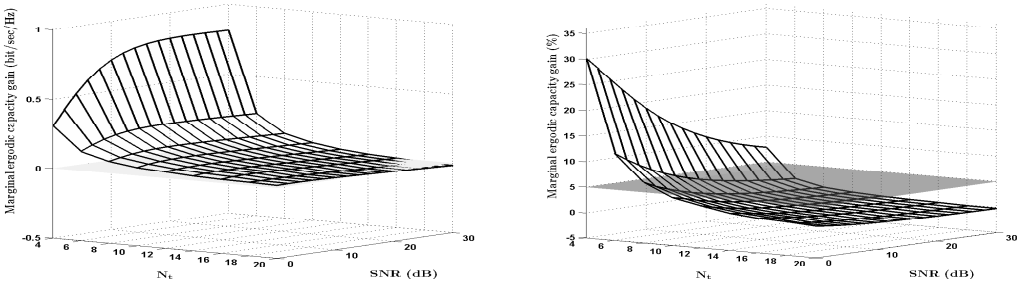

(d) $AS = 30^{\circ}$, $T = 800$

Figure 4.5: Marginal achievable ergodic capacity gain for the minimum-trained system as a function of N_t, and SNR under spatially correlated Rayleigh fading. The nontransparent planes represent the numerical value, zero, and the transparent planes indicate the numerical value, five.

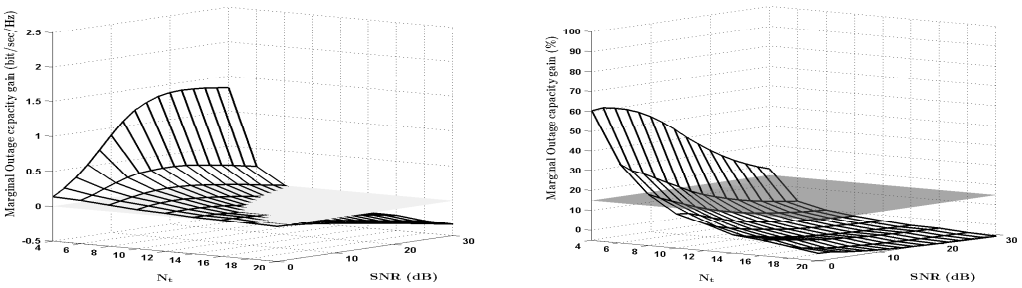

(a) $AS = 10^{\circ}$, $T = 100$

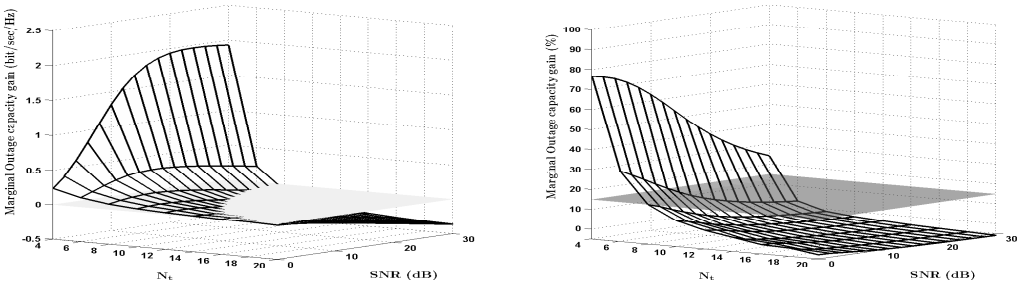

(b) $AS = 30^{\circ}$, $T = 100$

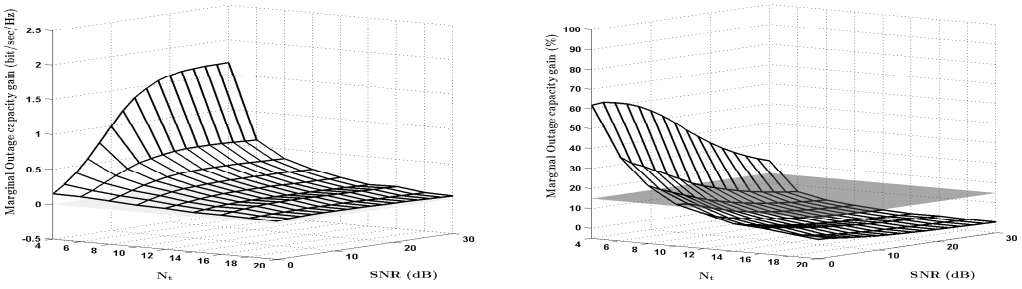

(c) $AS = 10^{\circ}$, $T = 800$

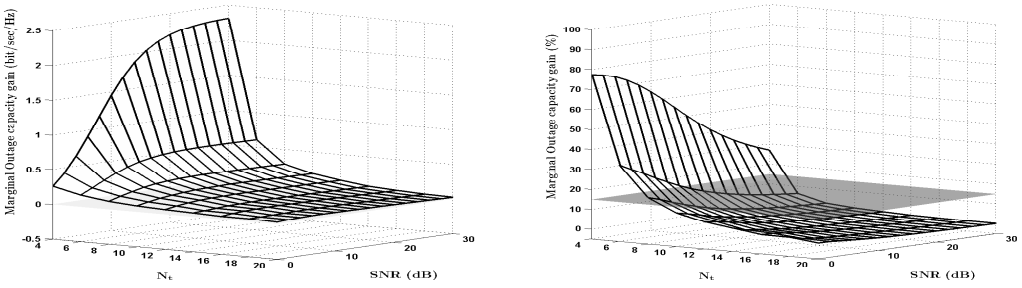

(d) $AS = 30^{\circ}$, $T = 800$

Figure 4.6: Marginal achievable outage capacity gain for the minimum-trained system as a function of N_t, SNR under spatially correlated Rayleigh fading. The nontransparent plane represents the numerical value, zero, and the transparent plane indicates the numerical value, 15.

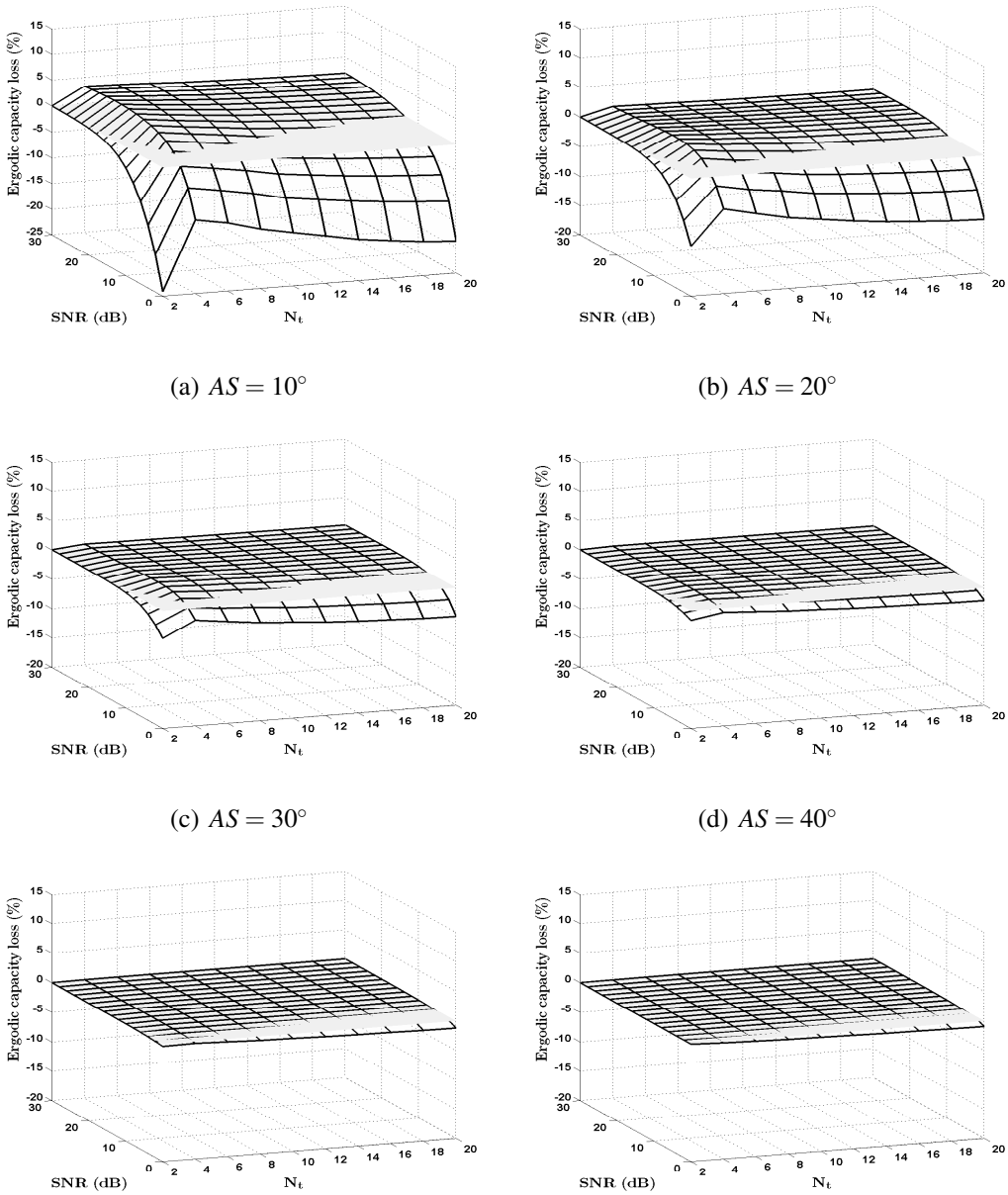

(a) $AS = 10^\circ$ (b) $AS = 20^\circ$

(c) $AS = 30^\circ$ (d) $AS = 40^\circ$

(e) $AS = 50^\circ$ (f) $AS = 60^\circ$

Figure 4.7: Change in achievable ergodic capacity due to channel spatial correlation for the minimum-trained system as a function of N_t, SNR under spatially correlated Rayleigh fading. The nontransparent planes represent the numerical value, zero.

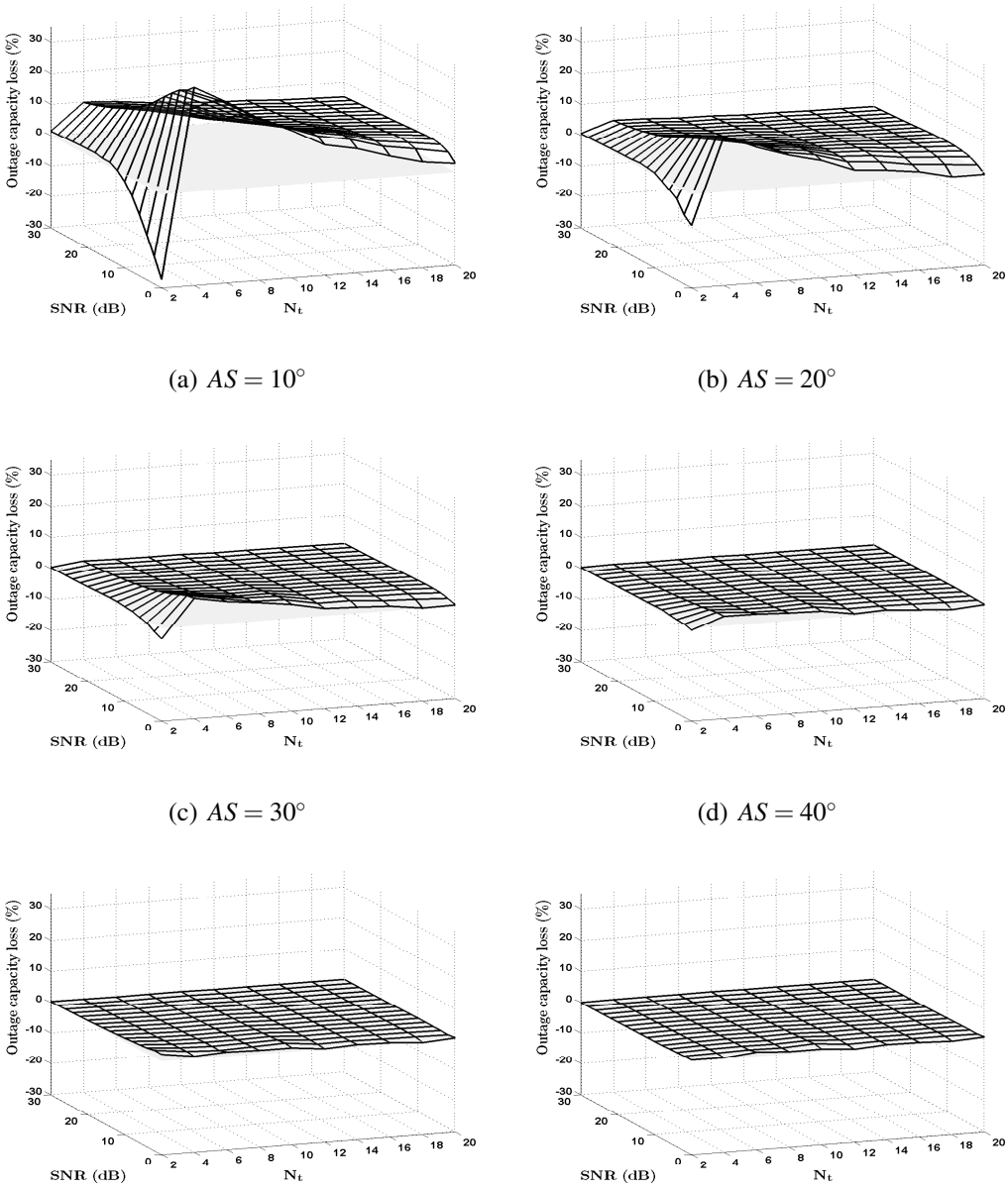

(a) $AS = 10^\circ$

(b) $AS = 20^\circ$

(c) $AS = 30^\circ$

(d) $AS = 40^\circ$

(e) $AS = 50^\circ$

(f) $AS = 60^\circ$

Figure 4.8: Change in achievable outage capacity due to channel spatial correlation for the minimum-trained system as a function of N_t, SNR under spatially correlated Rayleigh fading. The nontransparent plane represents the numerical value, zero

when $N_t > 4$. One exception is that when the block length is large (T=800) and SNR is extremely low (SNR $= 0$ dB). Also, the marginal gains for spatially correlated channels are smaller than that of spatially uncorrelated channels. A $4 \sim 8\%$ loss in marginal ergodic capacity and a 15% loss in outage capacity are observed for $T = 100, 800$ when AS changes from 30° to 10°. Thus, as the channel becomes more spatially correlated, the advantage of using antenna selection decreases. Therefore, the OSTBC MIMO antenna selection system with minimum training length under spatially correlated Rayleigh fading channels does not benefit significantly from having a number of transmit antennas larger than four.

Fig. 4.7 compares the ergodic capacity resulting from different degrees of spatially correlated Rayleigh fading. There is no need to discuss various T here since T_τ is independent of T and channel spatial correlation due to the minimum training length. It is interesting to notice that the ergodic capacity can actually increase with increasing spatial correlation as indicated by the regions below the 0%-reference plane. Also the spatial correlation does not significantly reduce the ergodic capacity in the region above the 0%-reference plane. The capacity loss due to spatial correlation is generally quite small and is at most about 5% when $AS = 10^\circ$, when comparing to the uncorrelated case. The region of ergodic capacity gain due to spatial correlation expands toward the lower SNR region as the channel becomes less spatially correlated and does not completely vanish at AS $= 60^\circ$.

Fig. 4.8 compares the outage capacity resulting from different degrees of spatially uncorrelated Rayleigh fading. As compared to ergodic capacity, we can observe that channel spatial correlation has more negative effects on outage capacity. For outage capacity, the region of capacity gain due to the spatial correlation only occurs for the system without antenna selection and at extremely high spatial correlation (AS $= 10^\circ, 20^\circ$) at relatively lower SNR.

4.2.3 System with Optimal Training Length

In this section, we assume the system has the ability to adjust the training length according to channel conditions such as SNR, spatial correlation and block length. Fig. 4.9 shows the achievable ergodic capacity under the spatially uncorrelated Rayleigh fading as a function of the number of available transmit antennas N_t, and the SNR, block lengths, $T = 100, 200, 400, 800$, for selecting two transmit antennas using the algorithm discussed in Section 3.5. Fig. 4.10 shows the corresponding achievable outage capacity. The curves exhibit similar trends as in the minimum-training-length case in Section 4.2.1. The performance improvement due to optimal training length is not noticeable due to the resolution

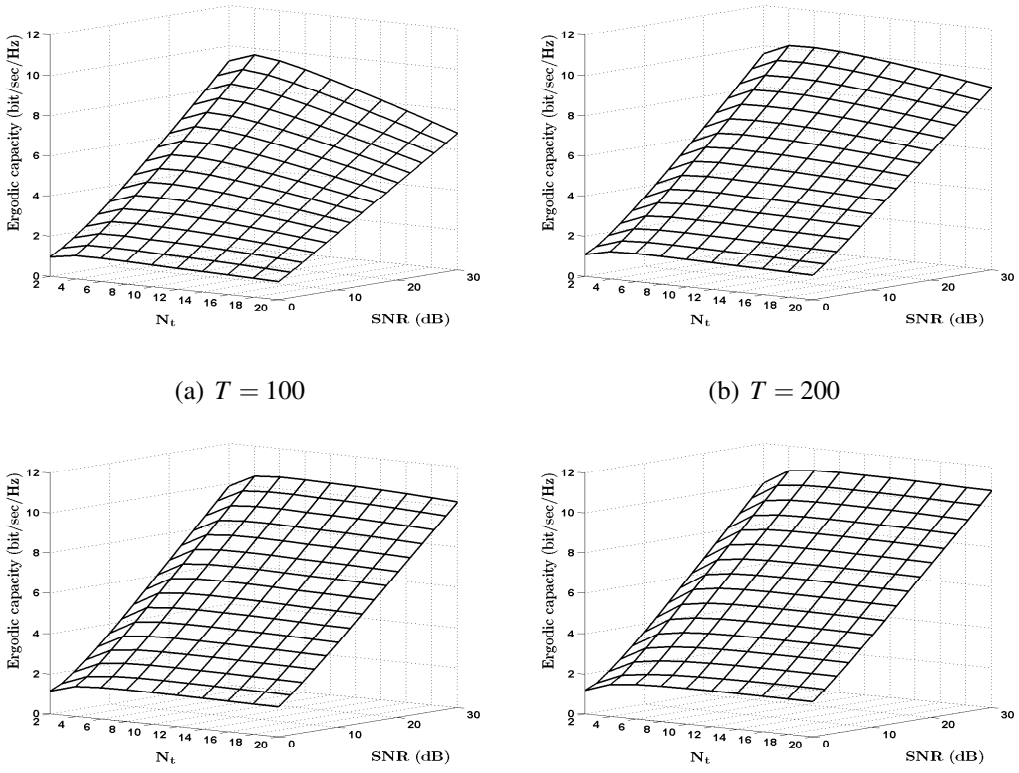

(a) $T = 100$ (b) $T = 200$

(c) $T = 400$ (d) $T = 800$

Figure 4.9: Achievable ergodic capacity for the optimally-trained system as a function of N_t, SNR under spatially uncorrelated Rayleigh fading.

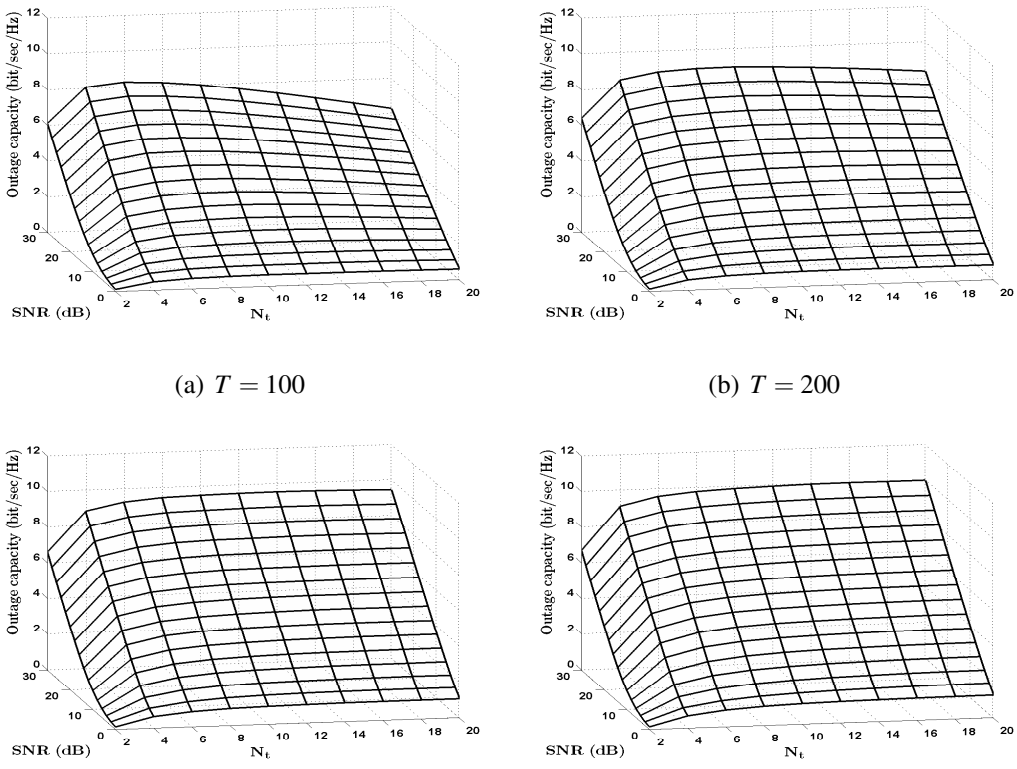

(a) $T = 100$ (b) $T = 200$

(c) $T = 400$ (d) $T = 800$

Figure 4.10: Achievable outage capacity for the optimally-trained system as a function of N_t, SNR under spatially uncorrelated Rayleigh fading.

of the figures. However it will be quantified in Section 4.2.5.

Fig. 4.11 shows the marginal ergodic capacity gain under spatially uncorrelated Rayleigh fading for various block lengths T. Fig. 4.12 shows the corresponding marginal outage capacity gain. Again when $N_t > 4$, depending on the frame length, there is no significant gain and even a loss in capacity. The optimal N_t, indicated by the nontransparent zero-reference plane, is generally less than that of the minimum-training-length case. The marginal gain in direction of N_t also increases more as T increases, compared to the minimum-training-length case (see Fig. 4.3 and Fig. 4.4). Also the capacity gain at $N_t = 4$ is much larger than that of the minimum-training cases. From Fig. 4.11 and Fig. 4.12, we can see that both the ergodic capacity and outage capacity exhibit either very little gain or even a loss when

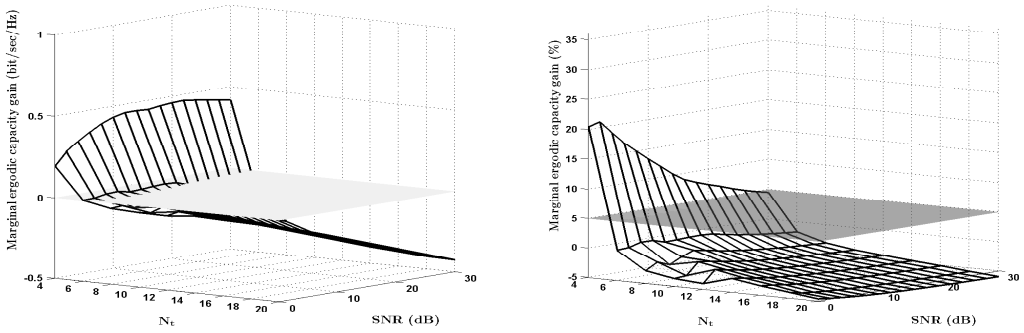

(a) $T = 100$

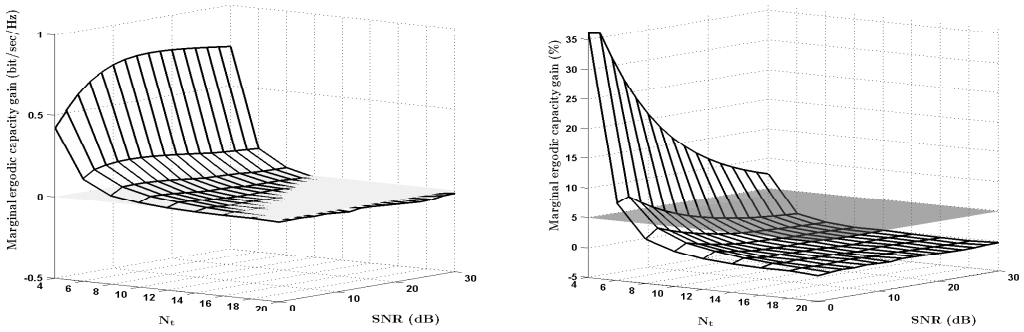

(b) $T = 800$

Figure 4.11: Marginal achievable ergodic capacity gain for the optimally-trained system as a function of N_t, SNR under spatially uncorrelated Rayleigh fading. The nontransparent plane represents the numerical value, zero, and the transparent plane indicates the numerical value, five.

$N_t > 4$. The decrease in marginal gain in outage capacity due to additional antenna is more significant, compared to that of the ergodic capacity.

4.2.4 Effects of Spatial Correlation on a System with Optimal Training Length

Fig. 4.13 shows the marginal gain in achievable ergodic capacity. Fig. 4.14 shows the corresponding marginal gain in achievable outage capacity. All the curves exhibit a similar trend as the uncorrelated case. From Fig. 4.11, 4.12, 4.13, 4.14, we observe that when

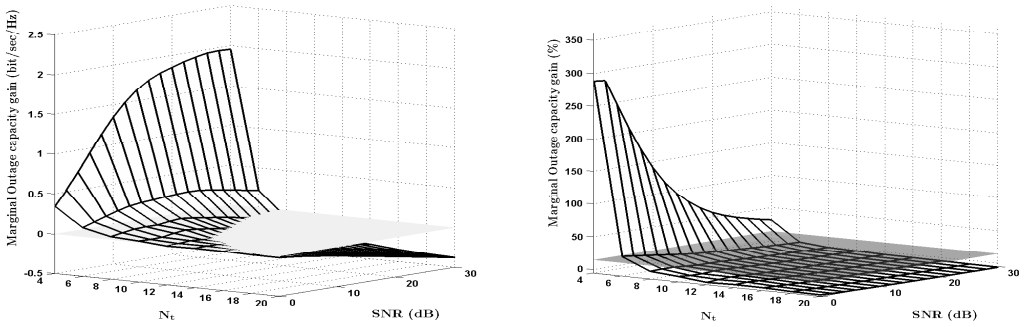

(a) $T = 100$

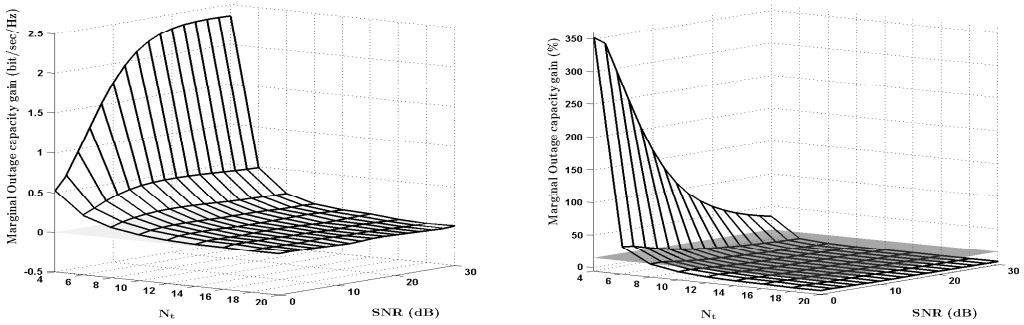

(b) $T = 800$

Figure 4.12: Marginal achievable outage capacity gain for the optimally-trained system as a function of N_t, and SNR under spatially uncorrelated Rayleigh fading. The nontransparent plane represents the numerical value, zero, and the transparent plane indicates the numerical value, 15.

the channel becomes more spatially correlated, the marginal capacity gain lowers. Therefore, the attraction of using antenna selection in an optimally-trained system decreases as the channel becomes more spatially correlated. The marginal capacity gain at $N_t = 4$ is generally lower than that of the minimum-training case. Again we observe that in terms of capacity, the number of transmit antenna should not be larger than four for the OSTBC MIMO antenna selection system with optimal training length under spatially correlated Rayleigh fading channels.

Fig. 4.15 and Fig. 4.16 are plots of the ergodic capacity loss under various degrees of spatial channel correlation for different T. Fig. 4.17 and Fig. 4.18 show the corresponding

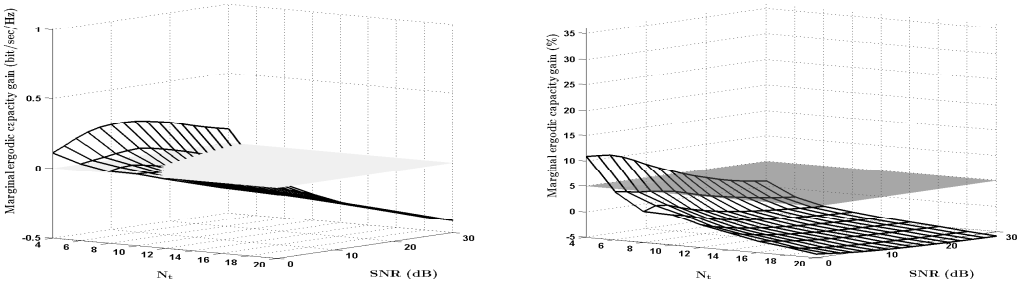

(a) $AS = 10^\circ$, $T = 100$

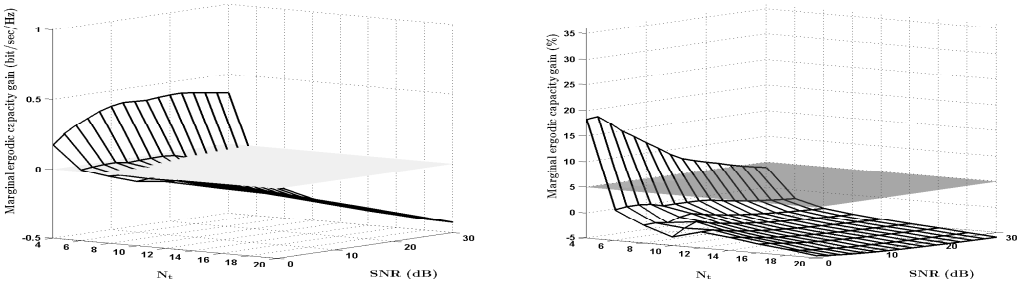

(b) $AS = 30^\circ$, $T = 100$

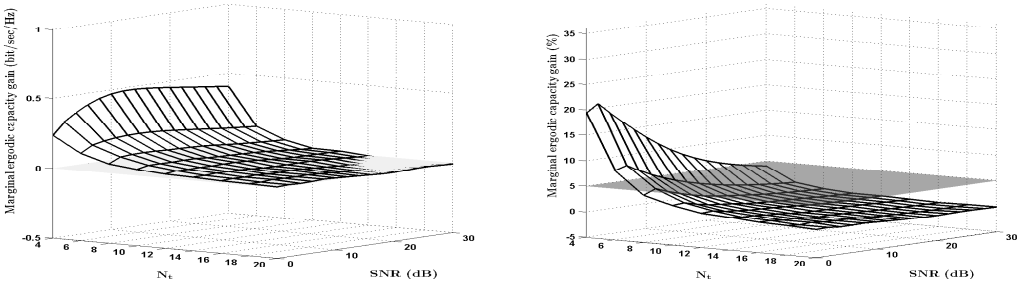

(c) $AS = 10^\circ$, $T = 800$

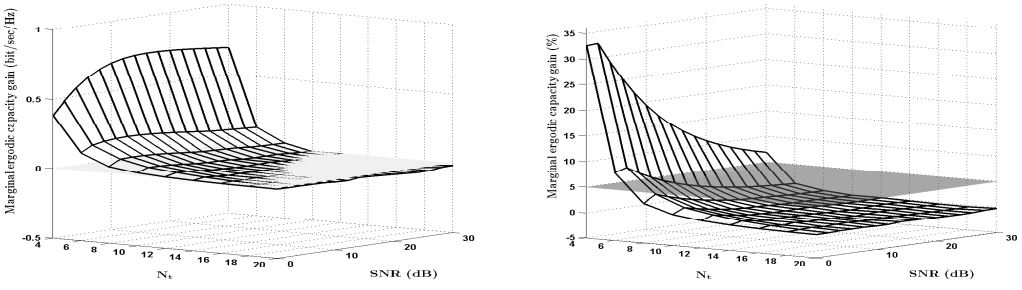

(d) $AS = 30^\circ$, $T = 800$

Figure 4.13: Marginal achievable ergodic capacity gain for the optimally-trained system as a function of available transmit antenna, N_t, and SNR under spatially correlated Rayleigh fading. The nontransparent planes represent the numerical value, zero, and the transparent planes indicate the numerical value, five.

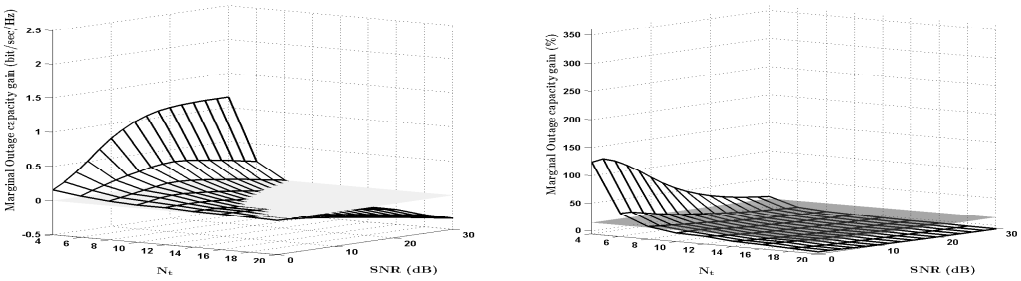

(a) $AS = 10^\circ$, $T = 100$

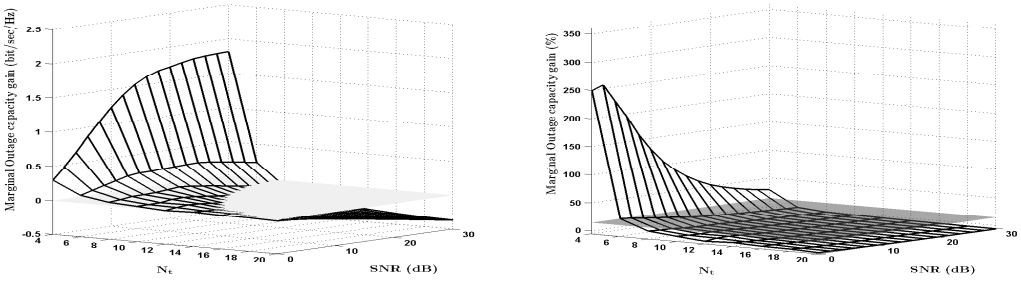

(b) $AS = 30^\circ$, $T = 100$

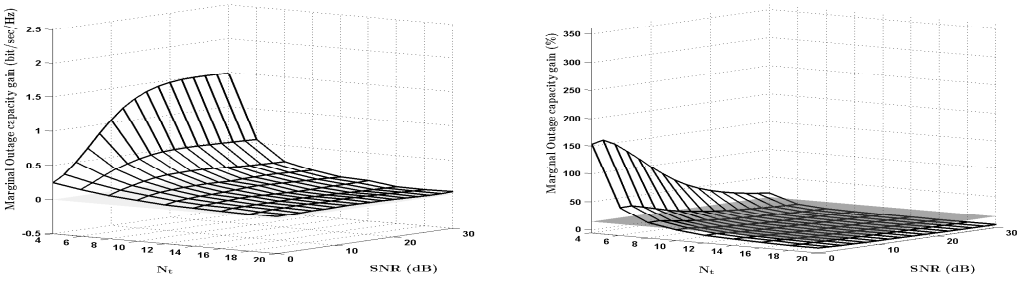

(c) $AS = 10^\circ$, $T = 800$

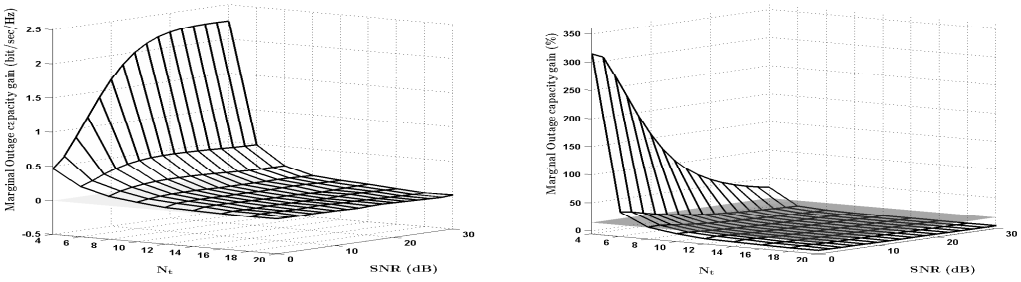

(d) $AS = 30^\circ$, $T = 800$

Figure 4.14: Marginal achievable outage capacity gain for the optimally-trained system as a function of N_t, and SNR under spatially correlated Rayleigh fading. The nontransparent plane represents the numerical value, zero, and the transparent plane indicates the numerical value, 15.

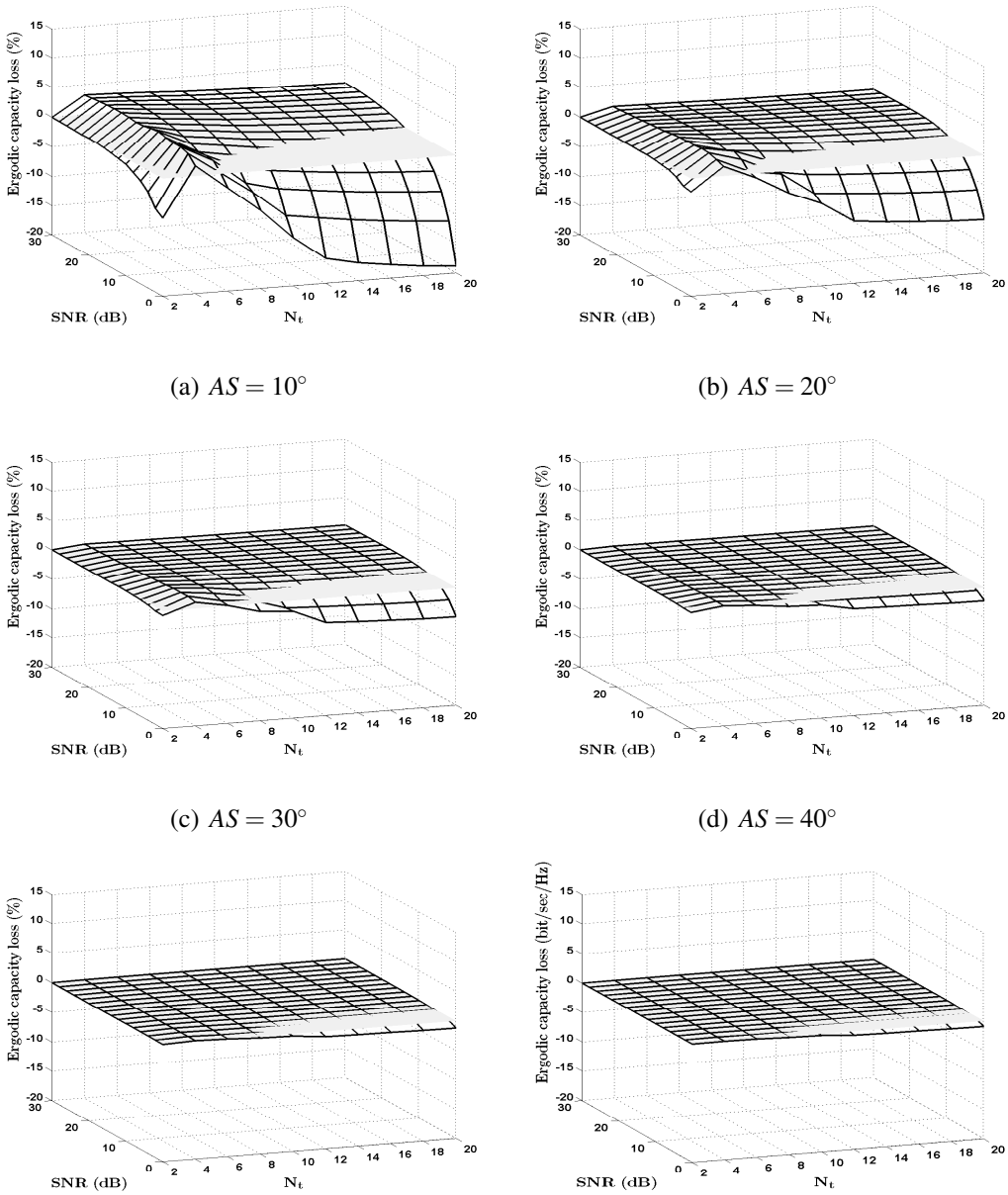

(a) $AS = 10^\circ$ (b) $AS = 20^\circ$

(c) $AS = 30^\circ$ (d) $AS = 40^\circ$

(e) $AS = 50^\circ$ (f) $AS = 60^\circ$

Figure 4.15: Change in achievable ergodic capacity for the optimally-trained system as a function of N_t, SNR and $T = 100$ under spatially correlated Rayleigh fading. The nontransparent planes represent the numerical value, zero.

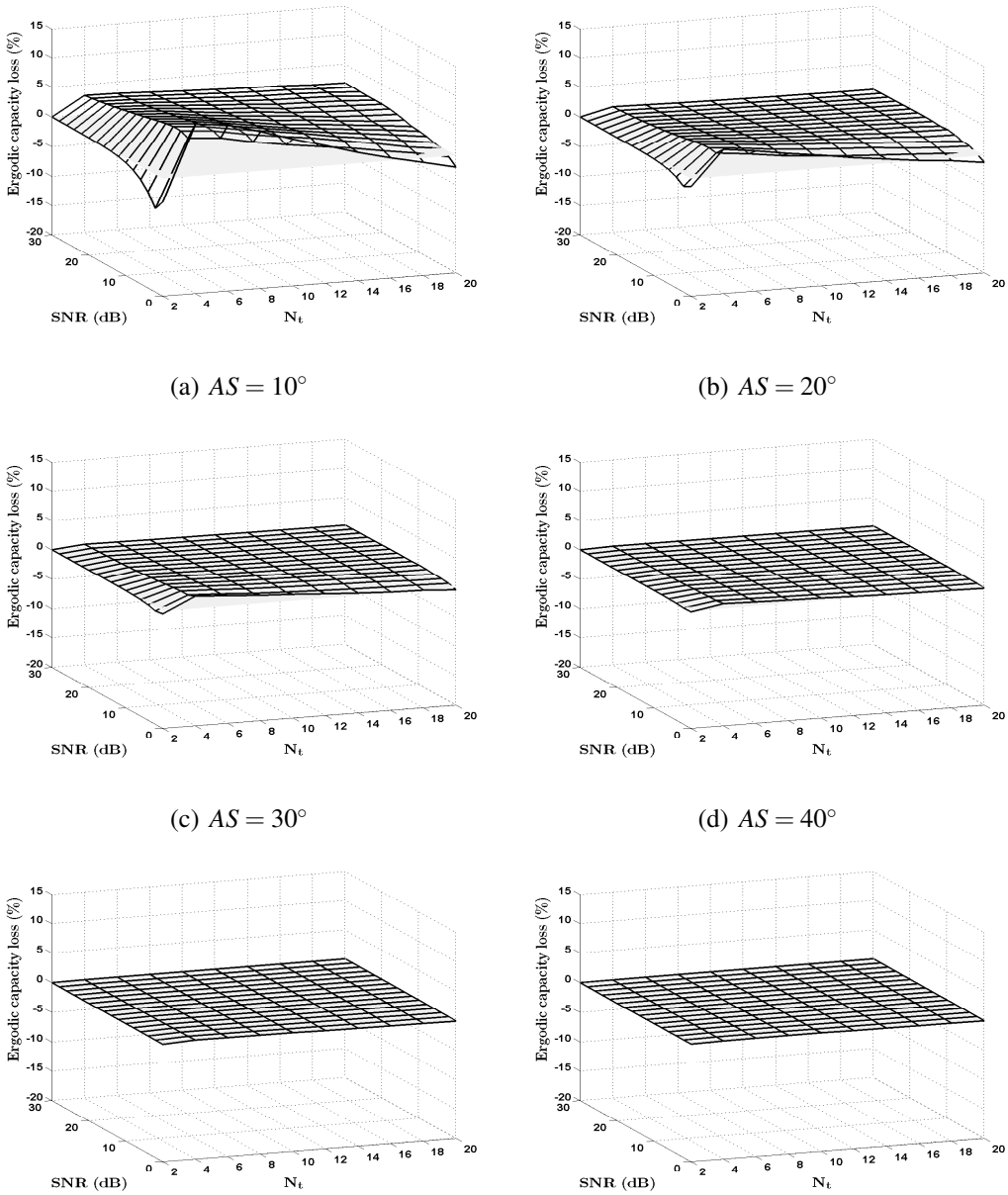

(a) $AS = 10^\circ$ (b) $AS = 20^\circ$

(c) $AS = 30^\circ$ (d) $AS = 40^\circ$

(e) $AS = 50^\circ$ (f) $AS = 60^\circ$

Figure 4.16: Change in achievable ergodic capacity for the optimally-trained system as a function of N_t, SNR and $T = 800$ under spatially correlated Rayleigh fading. The nontransparent planes represent the numerical value, zero, and the transparent planes indicate the numerical value, five.

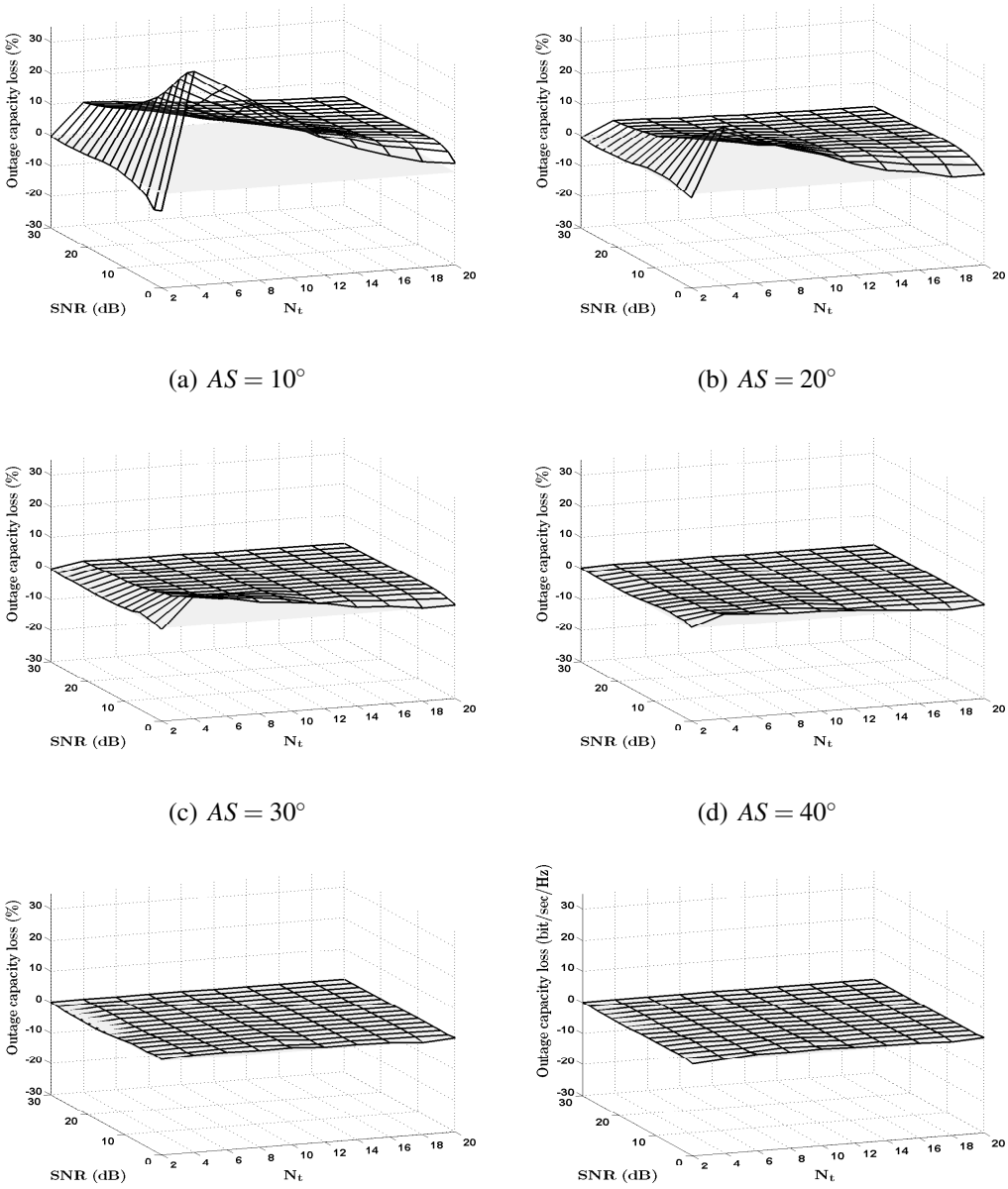

(a) $AS = 10^\circ$

(b) $AS = 20^\circ$

(c) $AS = 30^\circ$

(d) $AS = 40^\circ$

(e) $AS = 50^\circ$

(f) $AS = 60^\circ$

Figure 4.17: Change in achievable outage capacity for the optimally-trained system as a function of N_t, SNR and $T = 100$ under spatially correlated Rayleigh fading. The nontransparent plane represents the numerical value, zero.

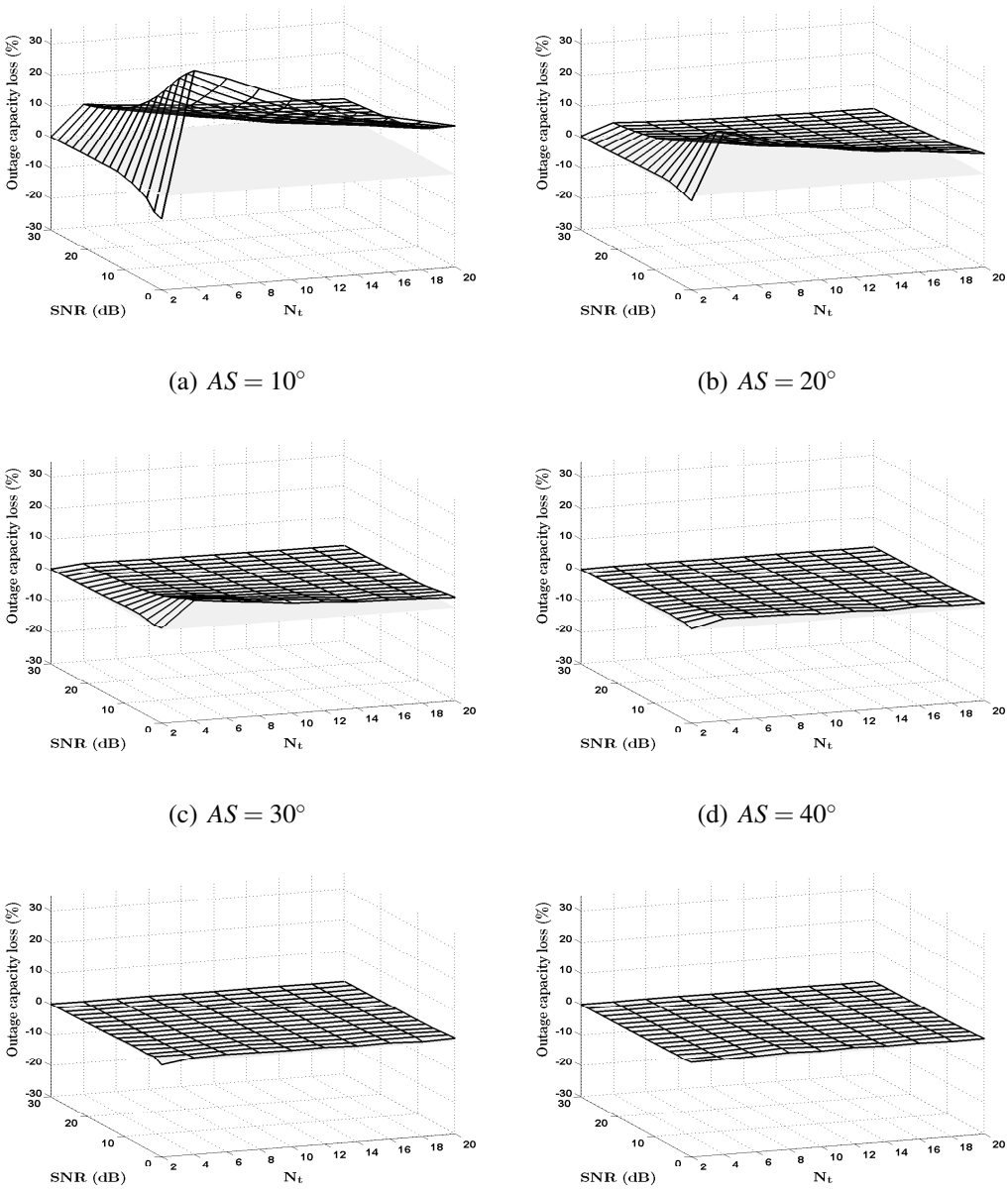

(a) $AS = 10^\circ$ (b) $AS = 20^\circ$

(c) $AS = 30^\circ$ (d) $AS = 40^\circ$

(e) $AS = 50^\circ$ (f) $AS = 60^\circ$

Figure 4.18: Change in achievable outage capacity for the optimally-trained system as a function of N_t, SNR and $T = 800$ under spatially correlated Rayleigh fading. The nontransparent plane represents the numerical value, zero.

outage capacity loss. Similar to the minimum-training-length case (see Fig. 4.8) , the capacity can be higher for spatially correlated channels. By observing Fig. 4.15 and Fig. 4.16, we can see that the system with antenna selection ($N_t > 4$) does not benefit from the channel correlation as T increases. Also the region of capacity gain due to spatial correlation shrinks and eventually disappears as T increases .

4.2.5 Capacity Gain Resulting from Optimal Training Length

Fig. 4.19 shows the ergodic capacity gain for using optimal training length while Fig. 4.20 shows the outage capacity gain for using optimal training length. We can observe that the improvement due to optimal training length is more significant when:

- transmission block length is large.
- channel spatial correlation is small.
- SNR is low.

We also notice that the curves are never masked by the zero-reference plane, so minimum training length ($T_\tau = N_t$) is never optimal within the range of parameters chosen.

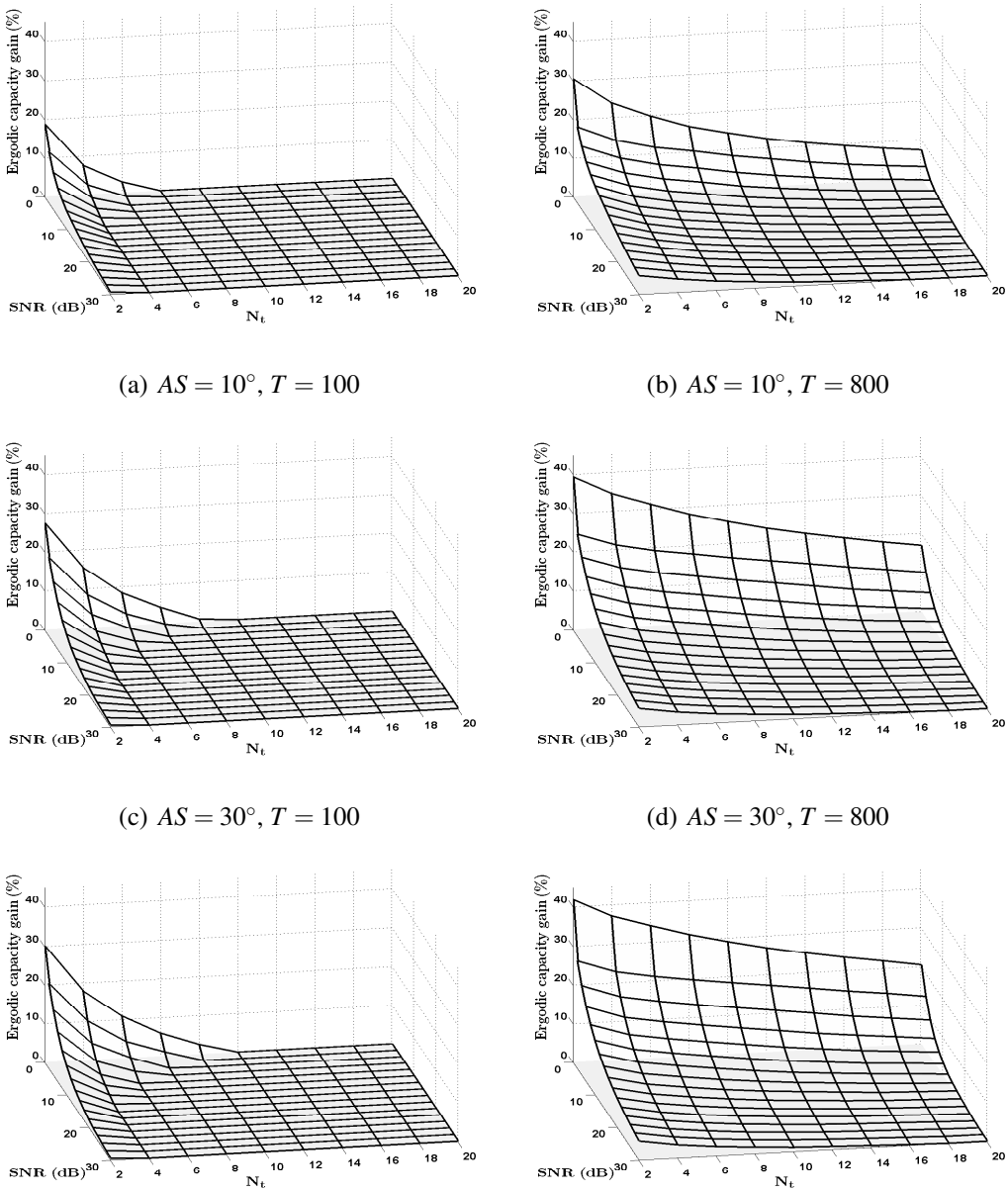

(a) $AS = 10^\circ$, $T = 100$

(b) $AS = 10^\circ$, $T = 800$

(c) $AS = 30^\circ$, $T = 100$

(d) $AS = 30^\circ$, $T = 800$

(e) uncorrelated., $T = 100$

(f) uncorrelated., $T = 800$

Figure 4.19: Achievable ergodic capacity gain for the optimally-trained system as a function of N_t, and SNR under different spatially correlated Rayleigh fading. The nontransparent plane represents the numerical value, zero

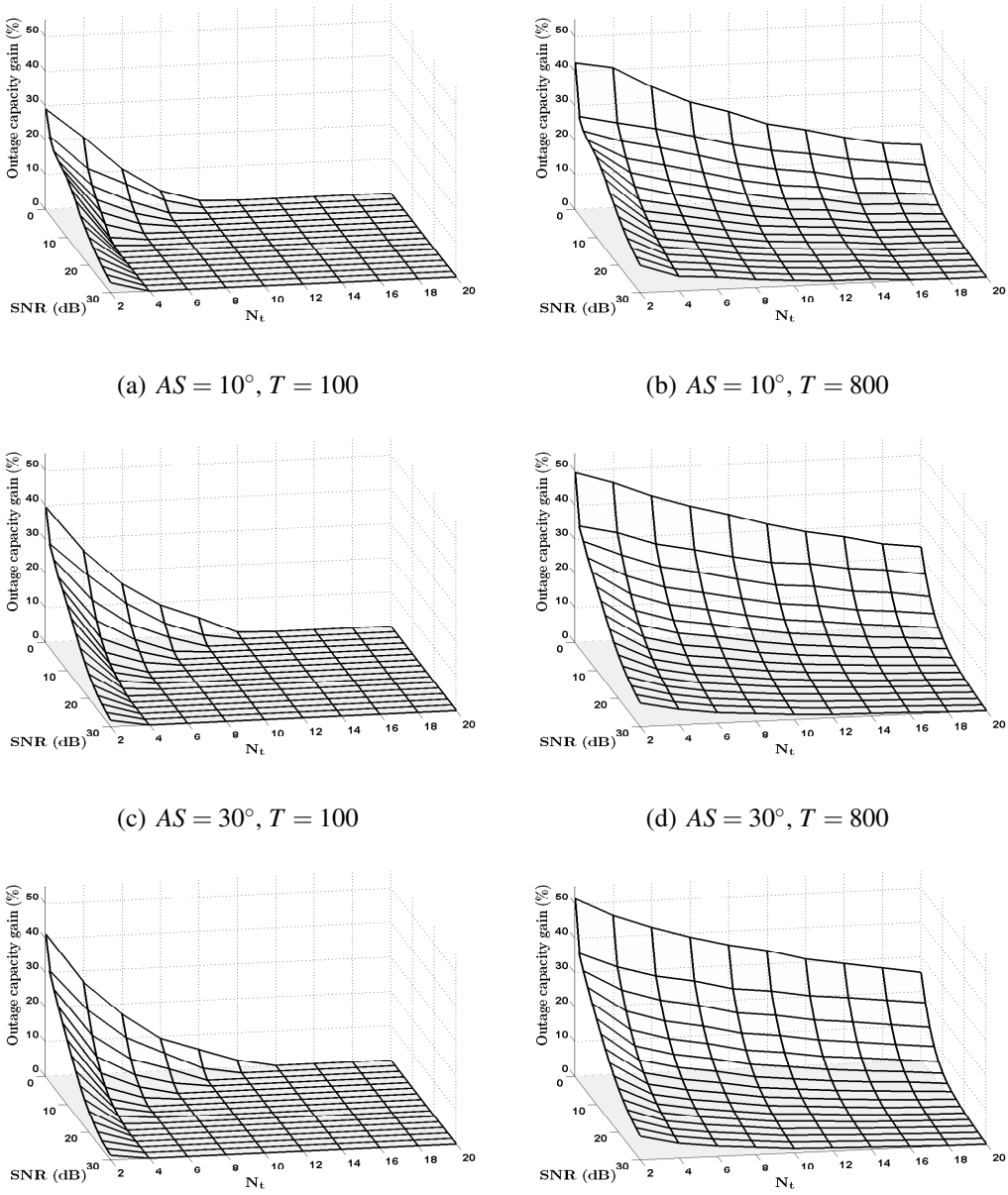

(a) $AS = 10^{\circ}$, $T = 100$

(b) $AS = 10^{\circ}$, $T = 800$

(c) $AS = 30^{\circ}$, $T = 100$

(d) $AS = 30^{\circ}$, $T = 800$

(e) uncorrelated., $T = 100$

(f) uncorrelated., $T = 800$

Figure 4.20: Achievable outage capacity gain for the optimally-trained system as a function of N_t, and SNR under different spatially correlated Rayleigh fading. The nontransparent plane represents the numerical value, zero

4.3 Chapter Summary

The performance of the training-based Alamouti space-time coded MIMO with transmit antenna selection in terms of ergodic capacity and outage capacity is evaluated by extensive Monte Carlo analysis. The marginal gain in capacity due to additional transmit antennas are shown for various SNR, block lengths, channel spatial correlations, and training strategies. The discussions in Section 3.8 have been validated by the results from Monte Carlo analysis. The capacity is a concave function of both the number of available transmit antenna and training length. The spatial correlation does not always lower the capacity.

Chapter 5

Summary, Conclusions and Future Work

5.1 Summary and Conclusions

This thesis investigated the performance of antenna selection for both OSTBC MIMO and OSTBC MIMO-OFDM system under a more realistic scenario. After providing motivation and background in Chapter 1 and Chapter 2, the N_t-by-two training-based Alamouti space-time coded MIMO with transmit antenna selection under study is defined in Chapter 3. In the same chapter, we conduct the performance analysis with focus on LMMSE channel estimation. In Section 3.3, we show that the LMMSE channel estimation provides a source for the correlated noise at the receiver. This justifies the need for a whitening operation for the OSTBC decoding. The antenna selection technique for the system with a specific channel estimator is also developed in Section 3.5. Although conceptually similar to the prior selection techniques, it is the first one that takes both the instantaneous channel estimate and spatial channel correlation into account in the selection criterion.

Chapter 4 shows the numerical performance analysis in terms of ergodic capacity and

outage capacity based on extensive Monte Carlo simulation of realization of channel matrices. The marginal gain in capacities due to additional transmit antennas are shown for various SNR, block lengths, channel spatial correlations, and training strategies. It is shown that both ergodic capacity and outage capacity increase most significantly when a small number of transmit antennas ($N_t = 4$) are used. The capacity may even decrease or have negligible gain when the number of available transmit antennas is increased further. The one exception is that when SNR is extremely low (0 dB), $N_t = 6$ has a significant gain. It is also found that the channel spatial correlation does not always decrease ergodic capacity even for systems without antenna selection under very high correlation (AS $= 10^\circ$). Also even in the operating region that the spatial correlation has negative influence, less than 5% decrease in the ergodic capacity due to correlation is observed. However, the spatial channel correlation does not benefit antenna selection performance in terms of outage capacity. The outage capacity seems to be degraded by spatial correlation more significantly and a 20% decrease is observed in low SNR regions. Those results are opposite to some prior understanding [64] since channel spatial correlation enhances the channel estimation quality. Also we note that the training length should be longer than N_t because capacity can still benefit from longer training length at high SNR (30 dB). The capacity improvement margin due to longer training length is more significant when considering outage performance.

In Section 3.7, we show that the percentage marginal capacity gain due to additional transmit antenna for the OSTBC MIMO-OFDM system with antenna selection is shown to be upper bounded by marginal gain for an OSTBC MIMO system with antenna selection if the channel on each subcarrier has identical spatial correlation as the channel at an OSTBC MIMO system. Therefore a desirable number of transmit antennas for OSTBC MIMO-OFDM systems with antenna selection is four ($N_t = 4$) as well.

5.2 Future Directions

In this section, several recommendations are suggested for future research.

- The wireless channel in this study is assumed to be quasi-static and the time variation of the channel is simulated by adjusting the block length T. A more realistic channel that models the temporal correlation could be considered.

- We can see that the training overhead is a key issue that forbids antenna selection system to benefit from a higher spatial dimension. An antenna selection algorithm that requires less training overhead could be a promising research area.

- In this thesis, we only state the performance enhancement for the OSTBC MIMO-OFDM with antenna selection due to an additional transmit antenna is upper bounded by the equivalent MIMO system, if the channel observed at each subcarrier of MIMO--OFDM is statistically identical to the MIMO system. A further analysis on order statistics could lead to the quantification of actual performance loss.

- The MIMO-OFDM system in this study is independently processed at each subcarrier. A system with joint space-time-frequency signal processing could be considered.

- Transmit antenna selection due its feedback requirement is only suitable under slow fading channels. Channel dynamic range is reduced by both space-time coding and antenna selection. Slowing fading channel and limited channel dynamic range place a challenge to scheduling under multiuser environment, since the same user remains to be the best for a very long time. Opportunistic beamforming is introduced [72] to resolve the fairness issue by randomizing the transmit power and phase. The user is scheduled when it is closest to the beam. In this configuration, the only

feedback information is the SNR from each user. However the performance only improves significantly when the number of users is sufficiently large. Antenna selection combined with opportunistic beamforming can be beneficial for a small number of users [73, 78]. However additional information is required for the transmitter to perform antenna selection, which produce additional feedback information. One possible system setup to maintain the reduced feedback information is to randomize the antenna subset. Therefore the resulting system would transmit to the user that is closest to the beam on the randomized antenna subset. The performance of this setup in a multiuser environment could be study further.

Appendix A

Some Matrix Properties [47]

- The Kronecker product of two matrices $\boldsymbol{A}(m \times n)$ and $\boldsymbol{B}(p \times q)$ is defined as

$$\boldsymbol{A} \otimes \boldsymbol{B} \triangleq \begin{pmatrix} a_{11}\boldsymbol{B} & \dots & a_{1n}\boldsymbol{B} \\ \vdots & \ddots & \vdots \\ a_{m1}\boldsymbol{B} & \dots & a_{mn}\boldsymbol{B} \end{pmatrix}. \tag{A.1}$$

  where a_{ij} is the $(i,j)^{th}$ element of the matrix $\boldsymbol{A}$.

- $$(\boldsymbol{A} \otimes \boldsymbol{B})(C \otimes D) = \boldsymbol{A}C \otimes \boldsymbol{B}D. \tag{A.2}$$

- $$(\boldsymbol{A} \otimes \boldsymbol{B})^{\dagger} = \boldsymbol{A}^{\dagger} \otimes \boldsymbol{B}^{\dagger}. \tag{A.3}$$

- $$(\boldsymbol{A} \otimes \boldsymbol{B})^{-1} = \boldsymbol{A}^{-1} \otimes \boldsymbol{B}^{-1}. \tag{A.4}$$

- For matrices $\boldsymbol{A_l}$, $\boldsymbol{B_l}$, $\boldsymbol{X}$, and $\boldsymbol{Y}$,

$$\text{if} \quad \boldsymbol{Y} = \sum_{l=0}^{L-1} \boldsymbol{A}_l \boldsymbol{X} \boldsymbol{B}_l \quad \text{then} \quad \boldsymbol{y} = \left(\sum_{l=0}^{L-1} \boldsymbol{B}_l^T \otimes \boldsymbol{A_l} \right) \boldsymbol{x}. \tag{A.5}$$

  $\boldsymbol{x}$ and $\boldsymbol{y}$ are the vector representations of $\boldsymbol{X}$ and $\boldsymbol{Y}$, respectively.

Appendix B

Burg's Maximum Entropy Theorem [12]

The maximum entropy rate stochastic process X_i satisfying the constraints

$$E\left[X_i X_{i+k}\right] = a_k, k = 0, 1, ..., p, \forall i, \tag{B.1}$$

is the p-th order Gaussian-Markov process of the form

$$X_i = -\sum_{k-1}^{p} a_k X_{i-k} + Z_i, \tag{B.2}$$

where the Z_i are i.i.d. $\backsim N(0, \sigma^2)$ and $a_1, a_2, ..., a_p, \sigma^2$ are chosen to satisfy Eq. (B.1). X_i does not need to be 1) zero mean, 2) Gaussian, 3) wide-sense stationary.

Appendix C

Transmit Correlation Matrices

In this appendix, a set of channel correlation matrices at the transmitter $\boldsymbol{R_{Tx}}$ are presented for each Azimuth Spread. The size of the matrix correspond to the number of available transmit antennas. We consider a downlink wireless communication link. Therefore the basestation acts as the transmitter. Only the case for 20 transmit antennas is presented. However for scenarios with fewer antennas, the correlation matrices can be obtained by partitioning the 20-by-20 matrix, i.e. for a system with $N_t \leq 20$ transmit antennas, the correlation matrix is the most up-left N_t-by-Nt sub-matrix of the 20-by-20 matrix.

C.1 Azimuth Spread: 10°

$$
\begin{bmatrix}
1.0000 & 0.8739 & 0.6268 & 0.4239 & 0.2921 & 0.2089 & 0.1551 & 0.1190 & 0.0938 & 0.0756 & 0.0622 & 0.0517 & 0.0418 & 0.0274 & 0.0051 & -0.0110 & -0.0019 & 0.0078 & -0.0045 & -0.0012 \\
0.8739 & 1.0000 & 0.8739 & 0.6268 & 0.4239 & 0.2921 & 0.2089 & 0.1551 & 0.1190 & 0.0938 & 0.0756 & 0.0622 & 0.0517 & 0.0418 & 0.0274 & 0.0051 & -0.0110 & -0.0019 & 0.0078 & -0.0045 \\
0.6268 & 0.8739 & 1.0000 & 0.8739 & 0.6268 & 0.4239 & 0.2921 & 0.2089 & 0.1551 & 0.1190 & 0.0938 & 0.0756 & 0.0622 & 0.0517 & 0.0418 & 0.0274 & 0.0051 & -0.0110 & -0.0019 & 0.0078 \\
0.4239 & 0.6268 & 0.8739 & 1.0000 & 0.8739 & 0.6268 & 0.4239 & 0.2921 & 0.2089 & 0.1551 & 0.1190 & 0.0938 & 0.0756 & 0.0622 & 0.0517 & 0.0418 & 0.0274 & 0.0051 & -0.0110 & -0.0019 \\
0.2921 & 0.4239 & 0.6268 & 0.8739 & 1.0000 & 0.8739 & 0.6268 & 0.4239 & 0.2921 & 0.2089 & 0.1551 & 0.1190 & 0.0938 & 0.0756 & 0.0622 & 0.0517 & 0.0418 & 0.0274 & 0.0051 & -0.0110 \\
0.2089 & 0.2921 & 0.4239 & 0.6268 & 0.8739 & 1.0000 & 0.8739 & 0.6268 & 0.4239 & 0.2921 & 0.2089 & 0.1551 & 0.1190 & 0.0938 & 0.0756 & 0.0622 & 0.0517 & 0.0418 & 0.0274 & 0.0051 \\
0.1551 & 0.2089 & 0.2921 & 0.4239 & 0.6268 & 0.8739 & 1.0000 & 0.8739 & 0.6268 & 0.4239 & 0.2921 & 0.2089 & 0.1551 & 0.1190 & 0.0938 & 0.0756 & 0.0622 & 0.0517 & 0.0418 & 0.0274 \\
0.1190 & 0.1551 & 0.2089 & 0.2921 & 0.4239 & 0.6268 & 0.8739 & 1.0000 & 0.8739 & 0.6268 & 0.4239 & 0.2921 & 0.2089 & 0.1551 & 0.1190 & 0.0938 & 0.0756 & 0.0622 & 0.0517 & 0.0418 \\
0.0938 & 0.1190 & 0.1551 & 0.2089 & 0.2921 & 0.4239 & 0.6268 & 0.8739 & 1.0000 & 0.8739 & 0.6268 & 0.4239 & 0.2921 & 0.2089 & 0.1551 & 0.1190 & 0.0938 & 0.0756 & 0.0622 & 0.0517 \\
0.0756 & 0.0938 & 0.1190 & 0.1551 & 0.2089 & 0.2921 & 0.4239 & 0.6268 & 0.8739 & 1.0000 & 0.8739 & 0.6268 & 0.4239 & 0.2921 & 0.2089 & 0.1551 & 0.1190 & 0.0938 & 0.0756 & 0.0622 \\
0.0622 & 0.0756 & 0.0938 & 0.1190 & 0.1551 & 0.2089 & 0.2921 & 0.4239 & 0.6268 & 0.8739 & 1.0000 & 0.8739 & 0.6268 & 0.4239 & 0.2921 & 0.2089 & 0.1551 & 0.1190 & 0.0938 & 0.0756 \\
0.0517 & 0.0622 & 0.0756 & 0.0938 & 0.1190 & 0.1551 & 0.2089 & 0.2921 & 0.4239 & 0.6268 & 0.8739 & 1.0000 & 0.8739 & 0.6268 & 0.4239 & 0.2921 & 0.2089 & 0.1551 & 0.1190 & 0.0938 \\
0.0418 & 0.0517 & 0.0622 & 0.0756 & 0.0938 & 0.1190 & 0.1551 & 0.2089 & 0.2921 & 0.4239 & 0.6268 & 0.8739 & 1.0000 & 0.8739 & 0.6268 & 0.4239 & 0.2921 & 0.2089 & 0.1551 & 0.1190 \\
0.0274 & 0.0418 & 0.0517 & 0.0622 & 0.0756 & 0.0938 & 0.1190 & 0.1551 & 0.2089 & 0.2921 & 0.4239 & 0.6268 & 0.8739 & 1.0000 & 0.8739 & 0.6268 & 0.4239 & 0.2921 & 0.2089 & 0.1551 \\
0.0051 & 0.0274 & 0.0418 & 0.0517 & 0.0622 & 0.0756 & 0.0938 & 0.1190 & 0.1551 & 0.2089 & 0.2921 & 0.4239 & 0.6268 & 0.8739 & 1.0000 & 0.8739 & 0.6268 & 0.4239 & 0.2921 & 0.2089 \\
-0.0110 & 0.0051 & 0.0274 & 0.0418 & 0.0517 & 0.0622 & 0.0756 & 0.0938 & 0.1190 & 0.1551 & 0.2089 & 0.2921 & 0.4239 & 0.6268 & 0.8739 & 1.0000 & 0.8739 & 0.6268 & 0.4239 & 0.2921 \\
-0.0019 & -0.0110 & 0.0051 & 0.0274 & 0.0418 & 0.0517 & 0.0622 & 0.0756 & 0.0938 & 0.1190 & 0.1551 & 0.2089 & 0.2921 & 0.4239 & 0.6268 & 0.8739 & 1.0000 & 0.8739 & 0.6268 & 0.4239 \\
0.0078 & -0.0019 & -0.0110 & 0.0051 & 0.0274 & 0.0418 & 0.0517 & 0.0622 & 0.0756 & 0.0938 & 0.1190 & 0.1551 & 0.2089 & 0.2921 & 0.4239 & 0.6268 & 0.8739 & 1.0000 & 0.8739 & 0.6268 \\
-0.0045 & 0.0078 & -0.0019 & -0.0110 & 0.0051 & 0.0274 & 0.0418 & 0.0517 & 0.0622 & 0.0756 & 0.0938 & 0.1190 & 0.1551 & 0.2089 & 0.2921 & 0.4239 & 0.6268 & 0.8739 & 1.0000 & 0.8739 \\
-0.0012 & -0.0045 & 0.0078 & -0.0019 & -0.0110 & 0.0051 & 0.0274 & 0.0418 & 0.0517 & 0.0622 & 0.0756 & 0.0938 & 0.1190 & 0.1551 & 0.2089 & 0.2921 & 0.4239 & 0.6268 & 0.8739 & 1.0000
\end{bmatrix}
$$

C.2 Azimuth Spread: 20°

$$
\begin{bmatrix}
1.0000 & 0.6391 & 0.2839 & 0.1531 & 0.0933 & 0.0605 & 0.0451 & 0.0311 & 0.0267 & 0.0185 & 0.0178 & 0.0119 & 0.0123 & 0.0055 & 0.0028 & -0.0043 & 0.0010 & 0.0006 & 0.0002 & -0.0017 \\
0.6391 & 1.0000 & 0.6391 & 0.2839 & 0.1531 & 0.0933 & 0.0605 & 0.0451 & 0.0311 & 0.0267 & 0.0185 & 0.0178 & 0.0119 & 0.0123 & 0.0055 & 0.0028 & -0.0043 & 0.0010 & 0.0006 & 0.0002 \\
0.2839 & 0.6391 & 1.0000 & 0.6391 & 0.2839 & 0.1531 & 0.0933 & 0.0605 & 0.0451 & 0.0311 & 0.0267 & 0.0185 & 0.0178 & 0.0119 & 0.0123 & 0.0055 & 0.0028 & -0.0043 & 0.0010 & 0.0006 \\
0.1531 & 0.2839 & 0.6391 & 1.0000 & 0.6391 & 0.2839 & 0.1531 & 0.0933 & 0.0605 & 0.0451 & 0.0311 & 0.0267 & 0.0185 & 0.0178 & 0.0119 & 0.0123 & 0.0055 & 0.0028 & -0.0043 & 0.0010 \\
0.0933 & 0.1531 & 0.2839 & 0.6391 & 1.0000 & 0.6391 & 0.2839 & 0.1531 & 0.0933 & 0.0605 & 0.0451 & 0.0311 & 0.0267 & 0.0185 & 0.0178 & 0.0119 & 0.0123 & 0.0055 & 0.0028 & -0.0043 \\
0.0605 & 0.0933 & 0.1531 & 0.2839 & 0.6391 & 1.0000 & 0.6391 & 0.2839 & 0.1531 & 0.0933 & 0.0605 & 0.0451 & 0.0311 & 0.0267 & 0.0185 & 0.0178 & 0.0119 & 0.0123 & 0.0055 & 0.0028 \\
0.0451 & 0.0605 & 0.0933 & 0.1531 & 0.2839 & 0.6391 & 1.0000 & 0.6391 & 0.2839 & 0.1531 & 0.0933 & 0.0605 & 0.0451 & 0.0311 & 0.0267 & 0.0185 & 0.0178 & 0.0119 & 0.0123 & 0.0055 \\
0.0311 & 0.0451 & 0.0605 & 0.0933 & 0.1531 & 0.2839 & 0.6391 & 1.0000 & 0.6391 & 0.2839 & 0.1531 & 0.0933 & 0.0605 & 0.0451 & 0.0311 & 0.0267 & 0.0185 & 0.0178 & 0.0119 & 0.0123 \\
0.0267 & 0.0311 & 0.0451 & 0.0605 & 0.0933 & 0.1531 & 0.2839 & 0.6391 & 1.0000 & 0.6391 & 0.2839 & 0.1531 & 0.0933 & 0.0605 & 0.0451 & 0.0311 & 0.0267 & 0.0185 & 0.0178 & 0.0119 \\
0.0185 & 0.0267 & 0.0311 & 0.0451 & 0.0605 & 0.0933 & 0.1531 & 0.2839 & 0.6391 & 1.0000 & 0.6391 & 0.2839 & 0.1531 & 0.0933 & 0.0605 & 0.0451 & 0.0311 & 0.0267 & 0.0185 & 0.0178 \\
0.0178 & 0.0185 & 0.0267 & 0.0311 & 0.0451 & 0.0605 & 0.0933 & 0.1531 & 0.2839 & 0.6391 & 1.0000 & 0.6391 & 0.2839 & 0.1531 & 0.0933 & 0.0605 & 0.0451 & 0.0311 & 0.0267 & 0.0185 \\
0.0119 & 0.0178 & 0.0185 & 0.0267 & 0.0311 & 0.0451 & 0.0605 & 0.0933 & 0.1531 & 0.2839 & 0.6391 & 1.0000 & 0.6391 & 0.2839 & 0.1531 & 0.0933 & 0.0605 & 0.0451 & 0.0311 & 0.0267 \\
0.0123 & 0.0119 & 0.0178 & 0.0185 & 0.0267 & 0.0311 & 0.0451 & 0.0605 & 0.0933 & 0.1531 & 0.2839 & 0.6391 & 1.0000 & 0.6391 & 0.2839 & 0.1531 & 0.0933 & 0.0605 & 0.0451 & 0.0311 \\
0.0055 & 0.0123 & 0.0119 & 0.0178 & 0.0185 & 0.0267 & 0.0311 & 0.0451 & 0.0605 & 0.0933 & 0.1531 & 0.2839 & 0.6391 & 1.0000 & 0.6391 & 0.2839 & 0.1531 & 0.0933 & 0.0605 & 0.0451 \\
0.0028 & 0.0055 & 0.0123 & 0.0119 & 0.0178 & 0.0185 & 0.0267 & 0.0311 & 0.0451 & 0.0605 & 0.0933 & 0.1531 & 0.2839 & 0.6391 & 1.0000 & 0.6391 & 0.2839 & 0.1531 & 0.0933 & 0.0605 \\
-0.0043 & 0.0028 & 0.0055 & 0.0123 & 0.0119 & 0.0178 & 0.0185 & 0.0267 & 0.0311 & 0.0451 & 0.0605 & 0.0933 & 0.1531 & 0.2839 & 0.6391 & 1.0000 & 0.6391 & 0.2839 & 0.1531 & 0.0933 \\
0.0010 & -0.0043 & 0.0028 & 0.0055 & 0.0123 & 0.0119 & 0.0178 & 0.0185 & 0.0267 & 0.0311 & 0.0451 & 0.0605 & 0.0933 & 0.1531 & 0.2839 & 0.6391 & 1.0000 & 0.6391 & 0.2839 & 0.1531 \\
0.0006 & 0.0010 & -0.0043 & 0.0028 & 0.0055 & 0.0123 & 0.0119 & 0.0178 & 0.0185 & 0.0267 & 0.0311 & 0.0451 & 0.0605 & 0.0933 & 0.1531 & 0.2839 & 0.6391 & 1.0000 & 0.6391 & 0.2839 \\
0.0002 & 0.0006 & 0.0010 & -0.0043 & 0.0028 & 0.0055 & 0.0123 & 0.0119 & 0.0178 & 0.0185 & 0.0267 & 0.0311 & 0.0451 & 0.0605 & 0.0933 & 0.1531 & 0.2839 & 0.6391 & 1.0000 & 0.6391 \\
-0.0017 & 0.0002 & 0.0006 & 0.0010 & -0.0043 & 0.0028 & 0.0055 & 0.0123 & 0.0119 & 0.0178 & 0.0185 & 0.0267 & 0.0311 & 0.0451 & 0.0605 & 0.0933 & 0.1531 & 0.2839 & 0.6391 & 1.0000
\end{bmatrix}
$$

C.3 Azimuth Spread: 30°

$$
\begin{bmatrix}
1.0000 & 0.4227 & 0.1562 & 0.0618 & 0.0560 & 0.0157 & 0.0322 & 0.0028 & 0.0228 & -0.0021 & 0.0180 & -0.0043 & 0.0149 & -0.0066 & 0.0100 & -0.0104 & 0.0087 & -0.0078 & 0.0080 & -0.0085 \\
0.4227 & 1.0000 & 0.4227 & 0.1562 & 0.0618 & 0.0560 & 0.0157 & 0.0322 & 0.0028 & 0.0228 & -0.0021 & 0.0180 & -0.0043 & 0.0149 & -0.0066 & 0.0100 & -0.0104 & 0.0087 & -0.0078 & 0.0080 \\
0.1562 & 0.4227 & 1.0000 & 0.4227 & 0.1562 & 0.0618 & 0.0560 & 0.0157 & 0.0322 & 0.0028 & 0.0228 & -0.0021 & 0.0180 & -0.0043 & 0.0149 & -0.0066 & 0.0100 & -0.0104 & 0.0087 & -0.0078 \\
0.0618 & 0.1562 & 0.4227 & 1.0000 & 0.4227 & 0.1562 & 0.0618 & 0.0560 & 0.0157 & 0.0322 & 0.0028 & 0.0228 & -0.0021 & 0.0180 & -0.0043 & 0.0149 & -0.0066 & 0.0100 & -0.0104 & 0.0087 \\
0.0560 & 0.0618 & 0.1562 & 0.4227 & 1.0000 & 0.4227 & 0.1562 & 0.0618 & 0.0560 & 0.0157 & 0.0322 & 0.0028 & 0.0228 & -0.0021 & 0.0180 & -0.0043 & 0.0149 & -0.0066 & 0.0100 & -0.0104 \\
0.0157 & 0.0560 & 0.0618 & 0.1562 & 0.4227 & 1.0000 & 0.4227 & 0.1562 & 0.0618 & 0.0560 & 0.0157 & 0.0322 & 0.0028 & 0.0228 & -0.0021 & 0.0180 & -0.0043 & 0.0149 & -0.0066 & 0.0100 \\
0.0322 & 0.0157 & 0.0560 & 0.0618 & 0.1562 & 0.4227 & 1.0000 & 0.4227 & 0.1562 & 0.0618 & 0.0560 & 0.0157 & 0.0322 & 0.0028 & 0.0228 & -0.0021 & 0.0180 & -0.0043 & 0.0149 & -0.0066 \\
0.0028 & 0.0322 & 0.0157 & 0.0560 & 0.0618 & 0.1562 & 0.4227 & 1.0000 & 0.4227 & 0.1562 & 0.0618 & 0.0560 & 0.0157 & 0.0322 & 0.0028 & 0.0228 & -0.0021 & 0.0180 & -0.0043 & 0.0149 \\
0.0228 & 0.0028 & 0.0322 & 0.0157 & 0.0560 & 0.0618 & 0.1562 & 0.4227 & 1.0000 & 0.4227 & 0.1562 & 0.0618 & 0.0560 & 0.0157 & 0.0322 & 0.0028 & 0.0228 & -0.0021 & 0.0180 & -0.0043 \\
-0.0021 & 0.0228 & 0.0028 & 0.0322 & 0.0157 & 0.0560 & 0.0618 & 0.1562 & 0.4227 & 1.0000 & 0.4227 & 0.1562 & 0.0618 & 0.0560 & 0.0157 & 0.0322 & 0.0028 & 0.0228 & -0.0021 & 0.0180 \\
0.0180 & -0.0021 & 0.0228 & 0.0028 & 0.0322 & 0.0157 & 0.0560 & 0.0618 & 0.1562 & 0.4227 & 1.0000 & 0.4227 & 0.1562 & 0.0618 & 0.0560 & 0.0157 & 0.0322 & 0.0028 & 0.0228 & -0.0021 \\
-0.0043 & 0.0180 & -0.0021 & 0.0228 & 0.0028 & 0.0322 & 0.0157 & 0.0560 & 0.0618 & 0.1562 & 0.4227 & 1.0000 & 0.4227 & 0.1562 & 0.0618 & 0.0560 & 0.0157 & 0.0322 & 0.0028 & 0.0228 \\
0.0149 & -0.0043 & 0.0180 & -0.0021 & 0.0228 & 0.0028 & 0.0322 & 0.0157 & 0.0560 & 0.0618 & 0.1562 & 0.4227 & 1.0000 & 0.4227 & 0.1562 & 0.0618 & 0.0560 & 0.0157 & 0.0322 & 0.0028 \\
-0.0066 & 0.0149 & -0.0043 & 0.0180 & -0.0021 & 0.0228 & 0.0028 & 0.0322 & 0.0157 & 0.0560 & 0.0618 & 0.1562 & 0.4227 & 1.0000 & 0.4227 & 0.1562 & 0.0618 & 0.0560 & 0.0157 & 0.0322 \\
0.0100 & -0.0066 & 0.0149 & -0.0043 & 0.0180 & -0.0021 & 0.0228 & 0.0028 & 0.0322 & 0.0157 & 0.0560 & 0.0618 & 0.1562 & 0.4227 & 1.0000 & 0.4227 & 0.1562 & 0.0618 & 0.0560 & 0.0157 \\
-0.0104 & 0.0100 & -0.0066 & 0.0149 & -0.0043 & 0.0180 & -0.0021 & 0.0228 & 0.0028 & 0.0322 & 0.0157 & 0.0560 & 0.0618 & 0.1562 & 0.4227 & 1.0000 & 0.4227 & 0.1562 & 0.0618 & 0.0560 \\
0.0087 & -0.0104 & 0.0100 & -0.0066 & 0.0149 & -0.0043 & 0.0180 & -0.0021 & 0.0228 & 0.0028 & 0.0322 & 0.0157 & 0.0560 & 0.0618 & 0.1562 & 0.4227 & 1.0000 & 0.4227 & 0.1562 & 0.0618 \\
-0.0078 & 0.0087 & -0.0104 & 0.0100 & -0.0066 & 0.0149 & -0.0043 & 0.0180 & -0.0021 & 0.0228 & 0.0028 & 0.0322 & 0.0157 & 0.0560 & 0.0618 & 0.1562 & 0.4227 & 1.0000 & 0.4227 & 0.1562 \\
0.0080 & -0.0078 & 0.0087 & -0.0104 & 0.0100 & -0.0066 & 0.0149 & -0.0043 & 0.0180 & -0.0021 & 0.0228 & 0.0028 & 0.0322 & 0.0157 & 0.0560 & 0.0618 & 0.1562 & 0.4227 & 1.0000 & 0.4227 \\
-0.0085 & 0.0080 & -0.0078 & 0.0087 & -0.0104 & 0.0100 & -0.0066 & 0.0149 & -0.0043 & 0.0180 & -0.0021 & 0.0228 & 0.0028 & 0.0322 & 0.0157 & 0.0560 & 0.0618 & 0.1562 & 0.4227 & 1.0000
\end{bmatrix}
$$

C.4 Azimuth Spread: 40°

$$
\begin{bmatrix}
1.0000 & 0.2523 & 0.1241 & 0.0068 & 0.0588 & -0.0159 & 0.0414 & -0.0201 & 0.0335 & -0.0207 & 0.0288 & -0.0203 & 0.0256 & -0.0203 & 0.0217 & -0.0214 & 0.0200 & -0.0191 & 0.0188 & -0.0187 \\
0.2523 & 1.0000 & 0.2523 & 0.1241 & 0.0068 & 0.0588 & -0.0159 & 0.0414 & -0.0201 & 0.0335 & -0.0207 & 0.0288 & -0.0203 & 0.0256 & -0.0203 & 0.0217 & -0.0214 & 0.0200 & -0.0191 & 0.0188 \\
0.1241 & 0.2523 & 1.0000 & 0.2523 & 0.1241 & 0.0068 & 0.0588 & -0.0159 & 0.0414 & -0.0201 & 0.0335 & -0.0207 & 0.0288 & -0.0203 & 0.0256 & -0.0203 & 0.0217 & -0.0214 & 0.0200 & -0.0191 \\
0.0068 & 0.1241 & 0.2523 & 1.0000 & 0.2523 & 0.1241 & 0.0068 & 0.0588 & -0.0159 & 0.0414 & -0.0201 & 0.0335 & -0.0207 & 0.0288 & -0.0203 & 0.0256 & -0.0203 & 0.0217 & -0.0214 & 0.0200 \\
0.0588 & 0.0068 & 0.1241 & 0.2523 & 1.0000 & 0.2523 & 0.1241 & 0.0068 & 0.0588 & -0.0159 & 0.0414 & -0.0201 & 0.0335 & -0.0207 & 0.0288 & -0.0203 & 0.0256 & -0.0203 & 0.0217 & -0.0214 \\
-0.0159 & 0.0588 & 0.0068 & 0.1241 & 0.2523 & 1.0000 & 0.2523 & 0.1241 & 0.0068 & 0.0588 & -0.0159 & 0.0414 & -0.0201 & 0.0335 & -0.0207 & 0.0288 & -0.0203 & 0.0256 & -0.0203 & 0.0217 \\
0.0414 & -0.0159 & 0.0588 & 0.0068 & 0.1241 & 0.2523 & 1.0000 & 0.2523 & 0.1241 & 0.0068 & 0.0588 & -0.0159 & 0.0414 & -0.0201 & 0.0335 & -0.0207 & 0.0288 & -0.0203 & 0.0256 & -0.0203 \\
-0.0201 & 0.0414 & -0.0159 & 0.0588 & 0.0068 & 0.1241 & 0.2523 & 1.0000 & 0.2523 & 0.1241 & 0.0068 & 0.0588 & -0.0159 & 0.0414 & -0.0201 & 0.0335 & -0.0207 & 0.0288 & -0.0203 & 0.0256 \\
0.0335 & -0.0201 & 0.0414 & -0.0159 & 0.0588 & 0.0068 & 0.1241 & 0.2523 & 1.0000 & 0.2523 & 0.1241 & 0.0068 & 0.0588 & -0.0159 & 0.0414 & -0.0201 & 0.0335 & -0.0207 & 0.0288 & -0.0203 \\
-0.0207 & 0.0335 & -0.0201 & 0.0414 & -0.0159 & 0.0588 & 0.0068 & 0.1241 & 0.2523 & 1.0000 & 0.2523 & 0.1241 & 0.0068 & 0.0588 & -0.0159 & 0.0414 & -0.0201 & 0.0335 & -0.0207 & 0.0288 \\
0.0288 & -0.0207 & 0.0335 & -0.0201 & 0.0414 & -0.0159 & 0.0588 & 0.0068 & 0.1241 & 0.2523 & 1.0000 & 0.2523 & 0.1241 & 0.0068 & 0.0588 & -0.0159 & 0.0414 & -0.0201 & 0.0335 & -0.0207 \\
-0.0203 & 0.0288 & -0.0207 & 0.0335 & -0.0201 & 0.0414 & -0.0159 & 0.0588 & 0.0068 & 0.1241 & 0.2523 & 1.0000 & 0.2523 & 0.1241 & 0.0068 & 0.0588 & -0.0159 & 0.0414 & -0.0201 & 0.0335 \\
0.0256 & -0.0203 & 0.0288 & -0.0207 & 0.0335 & -0.0201 & 0.0414 & -0.0159 & 0.0588 & 0.0068 & 0.1241 & 0.2523 & 1.0000 & 0.2523 & 0.1241 & 0.0068 & 0.0588 & -0.0159 & 0.0414 & -0.0201 \\
-0.0203 & 0.0256 & -0.0203 & 0.0288 & -0.0207 & 0.0335 & -0.0201 & 0.0414 & -0.0159 & 0.0588 & 0.0068 & 0.1241 & 0.2523 & 1.0000 & 0.2523 & 0.1241 & 0.0068 & 0.0588 & -0.0159 & 0.0414 \\
0.0217 & -0.0203 & 0.0256 & -0.0203 & 0.0288 & -0.0207 & 0.0335 & -0.0201 & 0.0414 & -0.0159 & 0.0588 & 0.0068 & 0.1241 & 0.2523 & 1.0000 & 0.2523 & 0.1241 & 0.0068 & 0.0588 & -0.0159 \\
-0.0214 & 0.0217 & -0.0203 & 0.0256 & -0.0203 & 0.0288 & -0.0207 & 0.0335 & -0.0201 & 0.0414 & -0.0159 & 0.0588 & 0.0068 & 0.1241 & 0.2523 & 1.0000 & 0.2523 & 0.1241 & 0.0068 & 0.0588 \\
0.0200 & -0.0214 & 0.0217 & -0.0203 & 0.0256 & -0.0203 & 0.0288 & -0.0207 & 0.0335 & -0.0201 & 0.0414 & -0.0159 & 0.0588 & 0.0068 & 0.1241 & 0.2523 & 1.0000 & 0.2523 & 0.1241 & 0.0068 \\
-0.0191 & 0.0200 & -0.0214 & 0.0217 & -0.0203 & 0.0256 & -0.0203 & 0.0288 & -0.0207 & 0.0335 & -0.0201 & 0.0414 & -0.0159 & 0.0588 & 0.0068 & 0.1241 & 0.2523 & 1.0000 & 0.2523 & 0.1241 \\
0.0188 & -0.0191 & 0.0200 & -0.0214 & 0.0217 & -0.0203 & 0.0256 & -0.0203 & 0.0288 & -0.0207 & 0.0335 & -0.0201 & 0.0414 & -0.0159 & 0.0588 & 0.0068 & 0.1241 & 0.2523 & 1.0000 & 0.2523 \\
-0.0187 & 0.0188 & -0.0191 & 0.0200 & -0.0214 & 0.0217 & -0.0203 & 0.0256 & -0.0203 & 0.0288 & -0.0207 & 0.0335 & -0.0201 & 0.0414 & -0.0159 & 0.0588 & 0.0068 & 0.1241 & 0.2523 & 1.0000
\end{bmatrix}
$$

C.5 Azimuth Spread: 50°

$$
\begin{bmatrix}
1.0000 & 0.1253 & 0.1252 & -0.0337 & 0.0720 & -0.0412 & 0.0552 & -0.0397 & 0.0466 & -0.0371 & 0.0412 & -0.0347 & 0.0372 & -0.0330 & 0.0332 & -0.0324 & 0.0310 & -0.0298 & 0.0292 & -0.0287 \\
0.1253 & 1.0000 & 0.1253 & 0.1252 & -0.0337 & 0.0720 & -0.0412 & 0.0552 & -0.0397 & 0.0466 & -0.0371 & 0.0412 & -0.0347 & 0.0372 & -0.0330 & 0.0332 & -0.0324 & 0.0310 & -0.0298 & 0.0292 \\
0.1252 & 0.1253 & 1.0000 & 0.1253 & 0.1252 & -0.0337 & 0.0720 & -0.0412 & 0.0552 & -0.0397 & 0.0466 & -0.0371 & 0.0412 & -0.0347 & 0.0372 & -0.0330 & 0.0332 & -0.0324 & 0.0310 & -0.0298 \\
-0.0337 & 0.1252 & 0.1253 & 1.0000 & 0.1253 & 0.1252 & -0.0337 & 0.0720 & -0.0412 & 0.0552 & -0.0397 & 0.0466 & -0.0371 & 0.0412 & -0.0347 & 0.0372 & -0.0330 & 0.0332 & -0.0324 & 0.0310 \\
0.0720 & -0.0337 & 0.1252 & 0.1253 & 1.0000 & 0.1253 & 0.1252 & -0.0337 & 0.0720 & -0.0412 & 0.0552 & -0.0397 & 0.0466 & -0.0371 & 0.0412 & -0.0347 & 0.0372 & -0.0330 & 0.0332 & -0.0324 \\
-0.0412 & 0.0720 & -0.0337 & 0.1252 & 0.1253 & 1.0000 & 0.1253 & 0.1252 & -0.0337 & 0.0720 & -0.0412 & 0.0552 & -0.0397 & 0.0466 & -0.0371 & 0.0412 & -0.0347 & 0.0372 & -0.0330 & 0.0332 \\
0.0552 & -0.0412 & 0.0720 & -0.0337 & 0.1252 & 0.1253 & 1.0000 & 0.1253 & 0.1252 & -0.0337 & 0.0720 & -0.0412 & 0.0552 & -0.0397 & 0.0466 & -0.0371 & 0.0412 & -0.0347 & 0.0372 & -0.0330 \\
-0.0397 & 0.0552 & -0.0412 & 0.0720 & -0.0337 & 0.1252 & 0.1253 & 1.0000 & 0.1253 & 0.1252 & -0.0337 & 0.0720 & -0.0412 & 0.0552 & -0.0397 & 0.0466 & -0.0371 & 0.0412 & -0.0347 & 0.0372 \\
0.0466 & -0.0397 & 0.0552 & -0.0412 & 0.0720 & -0.0337 & 0.1252 & 0.1253 & 1.0000 & 0.1253 & 0.1252 & -0.0337 & 0.0720 & -0.0412 & 0.0552 & -0.0397 & 0.0466 & -0.0371 & 0.0412 & -0.0347 \\
-0.0371 & 0.0466 & -0.0397 & 0.0552 & -0.0412 & 0.0720 & -0.0337 & 0.1252 & 0.1253 & 1.0000 & 0.1253 & 0.1252 & -0.0337 & 0.0720 & -0.0412 & 0.0552 & -0.0397 & 0.0466 & -0.0371 & 0.0412 \\
0.0412 & -0.0371 & 0.0466 & -0.0397 & 0.0552 & -0.0412 & 0.0720 & -0.0337 & 0.1252 & 0.1253 & 1.0000 & 0.1253 & 0.1252 & -0.0337 & 0.0720 & -0.0412 & 0.0552 & -0.0397 & 0.0466 & -0.0371 \\
-0.0347 & 0.0412 & -0.0371 & 0.0466 & -0.0397 & 0.0552 & -0.0412 & 0.0720 & -0.0337 & 0.1252 & 0.1253 & 1.0000 & 0.1253 & 0.1252 & -0.0337 & 0.0720 & -0.0412 & 0.0552 & -0.0397 & 0.0466 \\
0.0372 & -0.0347 & 0.0412 & -0.0371 & 0.0466 & -0.0397 & 0.0552 & -0.0412 & 0.0720 & -0.0337 & 0.1252 & 0.1253 & 1.0000 & 0.1253 & 0.1252 & -0.0337 & 0.0720 & -0.0412 & 0.0552 & -0.0397 \\
-0.0330 & 0.0372 & -0.0347 & 0.0412 & -0.0371 & 0.0466 & -0.0397 & 0.0552 & -0.0412 & 0.0720 & -0.0337 & 0.1252 & 0.1253 & 1.0000 & 0.1253 & 0.1252 & -0.0337 & 0.0720 & -0.0412 & 0.0552 \\
0.0332 & -0.0330 & 0.0372 & -0.0347 & 0.0412 & -0.0371 & 0.0466 & -0.0397 & 0.0552 & -0.0412 & 0.0720 & -0.0337 & 0.1252 & 0.1253 & 1.0000 & 0.1253 & 0.1252 & -0.0337 & 0.0720 & -0.0412 \\
-0.0324 & 0.0332 & -0.0330 & 0.0372 & -0.0347 & 0.0412 & -0.0371 & 0.0466 & -0.0397 & 0.0552 & -0.0412 & 0.0720 & -0.0337 & 0.1252 & 0.1253 & 1.0000 & 0.1253 & 0.1252 & -0.0337 & 0.0720 \\
0.0310 & -0.0324 & 0.0332 & -0.0330 & 0.0372 & -0.0347 & 0.0412 & -0.0371 & 0.0466 & -0.0397 & 0.0552 & -0.0412 & 0.0720 & -0.0337 & 0.1252 & 0.1253 & 1.0000 & 0.1253 & 0.1252 & -0.0337 \\
-0.0298 & 0.0310 & -0.0324 & 0.0332 & -0.0330 & 0.0372 & -0.0347 & 0.0412 & -0.0371 & 0.0466 & -0.0397 & 0.0552 & -0.0412 & 0.0720 & -0.0337 & 0.1252 & 0.1253 & 1.0000 & 0.1253 & 0.1252 \\
0.0292 & -0.0298 & 0.0310 & -0.0324 & 0.0332 & -0.0330 & 0.0372 & -0.0347 & 0.0412 & -0.0371 & 0.0466 & -0.0397 & 0.0552 & -0.0412 & 0.0720 & -0.0337 & 0.1252 & 0.1253 & 1.0000 & 0.1253 \\
-0.0287 & 0.0292 & -0.0298 & 0.0310 & -0.0324 & 0.0332 & -0.0330 & 0.0372 & -0.0347 & 0.0412 & -0.0371 & 0.0466 & -0.0397 & 0.0552 & -0.0412 & 0.0720 & -0.0337 & 0.1252 & 0.1253 & 1.0000
\end{bmatrix}
$$

C.6 Azimuth Spread: 60°

$$
\begin{bmatrix}
1.0000 & 0.0322 & 0.1358 & -0.0641 & 0.0860 & -0.0611 & 0.0682 & -0.0553 & 0.0584 & -0.0504 & 0.0520 & -0.0465 & 0.0473 & -0.0436 & 0.0430 & -0.0418 & 0.0401 & -0.0388 & 0.0379 & -0.0370 \\
0.0322 & 1.0000 & 0.0322 & 0.1358 & -0.0641 & 0.0860 & -0.0611 & 0.0682 & -0.0553 & 0.0584 & -0.0504 & 0.0520 & -0.0465 & 0.0473 & -0.0436 & 0.0430 & -0.0418 & 0.0401 & -0.0388 & 0.0379 \\
0.1358 & 0.0322 & 1.0000 & 0.0322 & 0.1358 & -0.0641 & 0.0860 & -0.0611 & 0.0682 & -0.0553 & 0.0584 & -0.0504 & 0.0520 & -0.0465 & 0.0473 & -0.0436 & 0.0430 & -0.0418 & 0.0401 & -0.0388 \\
-0.0641 & 0.1358 & 0.0322 & 1.0000 & 0.0322 & 0.1358 & -0.0641 & 0.0860 & -0.0611 & 0.0682 & -0.0553 & 0.0584 & -0.0504 & 0.0520 & -0.0465 & 0.0473 & -0.0436 & 0.0430 & -0.0418 & 0.0401 \\
0.0860 & -0.0641 & 0.1358 & 0.0322 & 1.0000 & 0.0322 & 0.1358 & -0.0641 & 0.0860 & -0.0611 & 0.0682 & -0.0553 & 0.0584 & -0.0504 & 0.0520 & -0.0465 & 0.0473 & -0.0436 & 0.0430 & -0.0418 \\
-0.0611 & 0.0860 & -0.0641 & 0.1358 & 0.0322 & 1.0000 & 0.0322 & 0.1358 & -0.0641 & 0.0860 & -0.0611 & 0.0682 & -0.0553 & 0.0584 & -0.0504 & 0.0520 & -0.0465 & 0.0473 & -0.0436 & 0.0430 \\
0.0682 & -0.0611 & 0.0860 & -0.0641 & 0.1358 & 0.0322 & 1.0000 & 0.0322 & 0.1358 & -0.0641 & 0.0860 & -0.0611 & 0.0682 & -0.0553 & 0.0584 & -0.0504 & 0.0520 & -0.0465 & 0.0473 & -0.0436 \\
-0.0553 & 0.0682 & -0.0611 & 0.0860 & -0.0641 & 0.1358 & 0.0322 & 1.0000 & 0.0322 & 0.1358 & -0.0641 & 0.0860 & -0.0611 & 0.0682 & -0.0553 & 0.0584 & -0.0504 & 0.0520 & -0.0465 & 0.0473 \\
0.0584 & -0.0553 & 0.0682 & -0.0611 & 0.0860 & -0.0641 & 0.1358 & 0.0322 & 1.0000 & 0.0322 & 0.1358 & -0.0641 & 0.0860 & -0.0611 & 0.0682 & -0.0553 & 0.0584 & -0.0504 & 0.0520 & -0.0465 \\
-0.0504 & 0.0584 & -0.0553 & 0.0682 & -0.0611 & 0.0860 & -0.0641 & 0.1358 & 0.0322 & 1.0000 & 0.0322 & 0.1358 & -0.0641 & 0.0860 & -0.0611 & 0.0682 & -0.0553 & 0.0584 & -0.0504 & 0.0520 \\
0.0520 & -0.0504 & 0.0584 & -0.0553 & 0.0682 & -0.0611 & 0.0860 & -0.0641 & 0.1358 & 0.0322 & 1.0000 & 0.0322 & 0.1358 & -0.0641 & 0.0860 & -0.0611 & 0.0682 & -0.0553 & 0.0584 & -0.0504 \\
-0.0465 & 0.0520 & -0.0504 & 0.0584 & -0.0553 & 0.0682 & -0.0611 & 0.0860 & -0.0641 & 0.1358 & 0.0322 & 1.0000 & 0.0322 & 0.1358 & -0.0641 & 0.0860 & -0.0611 & 0.0682 & -0.0553 & 0.0584 \\
0.0473 & -0.0465 & 0.0520 & -0.0504 & 0.0584 & -0.0553 & 0.0682 & -0.0611 & 0.0860 & -0.0641 & 0.1358 & 0.0322 & 1.0000 & 0.0322 & 0.1358 & -0.0641 & 0.0860 & -0.0611 & 0.0682 & -0.0553 \\
-0.0436 & 0.0473 & -0.0465 & 0.0520 & -0.0504 & 0.0584 & -0.0553 & 0.0682 & -0.0611 & 0.0860 & -0.0641 & 0.1358 & 0.0322 & 1.0000 & 0.0322 & 0.1358 & -0.0641 & 0.0860 & -0.0611 & 0.0682 \\
0.0430 & -0.0436 & 0.0473 & -0.0465 & 0.0520 & -0.0504 & 0.0584 & -0.0553 & 0.0682 & -0.0611 & 0.0860 & -0.0641 & 0.1358 & 0.0322 & 1.0000 & 0.0322 & 0.1358 & -0.0641 & 0.0860 & -0.0611 \\
-0.0418 & 0.0430 & -0.0436 & 0.0473 & -0.0465 & 0.0520 & -0.0504 & 0.0584 & -0.0553 & 0.0682 & -0.0611 & 0.0860 & -0.0641 & 0.1358 & 0.0322 & 1.0000 & 0.0322 & 0.1358 & -0.0641 & 0.0860 \\
0.0401 & -0.0418 & 0.0430 & -0.0436 & 0.0473 & -0.0465 & 0.0520 & -0.0504 & 0.0584 & -0.0553 & 0.0682 & -0.0611 & 0.0860 & -0.0641 & 0.1358 & 0.0322 & 1.0000 & 0.0322 & 0.1358 & -0.0641 \\
-0.0388 & 0.0401 & -0.0418 & 0.0430 & -0.0436 & 0.0473 & -0.0465 & 0.0520 & -0.0504 & 0.0584 & -0.0553 & 0.0682 & -0.0611 & 0.0860 & -0.0641 & 0.1358 & 0.0322 & 1.0000 & 0.0322 & 0.1358 \\
0.0379 & -0.0388 & 0.0401 & -0.0418 & 0.0430 & -0.0436 & 0.0473 & -0.0465 & 0.0520 & -0.0504 & 0.0584 & -0.0553 & 0.0682 & -0.0611 & 0.0860 & -0.0641 & 0.1358 & 0.0322 & 1.0000 & 0.0322 \\
-0.0370 & 0.0379 & -0.0388 & 0.0401 & -0.0418 & 0.0430 & -0.0436 & 0.0473 & -0.0465 & 0.0520 & -0.0504 & 0.0584 & -0.0553 & 0.0682 & -0.0611 & 0.0860 & -0.0641 & 0.1358 & 0.0322 & 1.0000
\end{bmatrix}
$$

Bibliography

[1] 3GPP, *Feasibility Study for Orthogonal Frequency Division Multiplexing (OFDM) for UTRAN Enhancement (Release 6) 3GPP TR 25.892*, 2004.

[2] F. Adachi, M. Feeny, A. Williamson, and J. Parsons, "Cross correlation between the envelopes of 900 mhz signal received at a mobile radio base station," *IEE Pt. F.*, vol. 133, pp. 506–512, Oct. 1986.

[3] S. M. Alamouti, "A simple transmitter diversity scheme for wireless communications," *IEEE J. Select. Areas Commun.*, vol. 16, no. 8, pp. 1451–1458, Oct. 1998.

[4] I. Bahceci, T. Duman, and Y. Altunbasak, "Performance of MIMO antenna selection for space-time coded OFDM systems," *Proc. IEEE Wireless Commun. Network Conf.*, vol. 2, pp. 987–992, Mar. 2004.

[5] I. Barhumi, G. Leus, and M. Moonen, "Optimal training design for MIMO OFDM systems in mobile wireless channel," *IEEE Trans. Signal Processing*, vol. 51, no. 6, pp. 1615–1624, June 2003.

[6] B.Hassibi and B. M.Hochwald, "How much training is needed in multiple-antenna wireless links?" *Trans. Inform. Theory*, vol. 43, no. 4, pp. 951– 963, Apr. 2003.

[7] M. Biguesh and A. B. Gershman, "Training-based mimo channel estimation: A study of estimator tradeoffs and optimal training signals,," *IEEE Trans. Signal Processing*, vol. 54, no. 3, pp. 884 – 893, Mar. 2006.

[8] H. Bölcskei, D. Gesbert, and A. J. Paulraj, "On capacity of OFDM-based spatial multiplexing systems," *IEEE Trans. Commun.*, vol. 50, no. 2, pp. 225–234, Feb. 2002.

[9] H. G. Booker, J. A. Rarcliff, and D. H. Shinn, "Diffraction from an irregular screen with application to ionospheric problems," *Trans. Roy. Soc. (London)*, vol. 262, no. A, pp. 579–607, June 1950.

[10] Y. Choi, A. Molisch, M. Win, and J. Winters, "Fast algorithms for antenna selection in MIMO systems," *Proc. of IEEE Vehic. Technol. Conf*, vol. 3, pp. 1733–1737, Sept. 2002-Fall.

[11] L. J. Cimini, "Analysis and simulation of a digital mobile channel using orthogonal frequency division multiplexing," *IEEE Trans. Commun.*, pp. 665–675, July. 1985.

[12] T. M. Cover and J. Y. Thomas, *Elements of Information Theory*, 1st ed. New York, NY: John Wiley & Sons, Inc, 1991.

[13] M. L. Doelz, E. T. Heald, and D. L. Martin, "Binary data transmission techniques for linear systems," *Proc. IRE*, vol. 45, pp. 656–661, May 1957.

[14] ETSI, *Radio Broadcasting Systems: Digital Audio Broadcasting (DAB) to Mobile, Portable and Fixed Receivers*, 1995.

[15] ——, *Digital Broadcasting Systems for Television, Sound, and Data Services: Framing Structure, Channel Coding and Modulation for Digital Terrestrial Television*, 1996.

[16] ——, *Broadband Radio Access Networks (BRAN); HIPERLAN Type 2; System Overview*, 2000.

[17] ——, *Universal Mobile Telecommunications System (UMTS); Physical channels and mapping of transport channels onto physical channels (FDD)*, version 6.5.0 release 6 ed., 2005.

[18] Y. Finkelstein, "Antenna selection in multicarrier communication systems," *Intel Tech. Jounal*, pp. 50–58, May 2003.

[19] G. J. Foschini and M. J. Gans, "On limits of wireless communications in a fading environment when using multiple antennas," *Wireless Pers. Commun.*, vol. 6, pp. 311–335, 1998.

[20] F. Frederiksen and R. Prasad, "An overview of OFDM and related techniques towards development of future wireless multimedia communications," *Proc. of IEEE Radio and Wireless Conf.*, vol. 3, pp. 19–22, Aug. 2002.

[21] D. Gesbert, H. Bolcskei, D. A. Gore, and A. J. Paulraj, "Outdoor mimo wireless channels: models and performance prediction," *IEEE Trans. Commun.*, vol. 50, no. 12, pp. 1926 – 1934, Dec. 2002.

[22] A. Ghrayeb and T. M. Duman, "Performance analysis of MIMO systems with antenna selection over quasi-static fading channels," *IEEE Trans.Veh. Technol.*, vol. 52, no. 2, pp. 281–288, Mar. 2003.

[23] D. Gore, R. Nabar, and A. Paulraj, "Selecting an optimal set of transmit antennas for a low rank matrix channel," *Proc. Int. Acoust. Speech and Signal Processing Conf.*, vol. 5, pp. 2785–2788, 5-9 June 2000.

[24] D. Gore and A. J. Paulraj, "MIMO antenna subset selection with space-time coding," *IEEE Trans. Signal Processing*, vol. 50, no. 10, pp. 2580–2588, Oct. 2002.

[25] A. Gorokhov, "Antenna selection algorithms for MEA transmision systems," *Proc. IEEE ICASSP Conf.*, vol. 3, pp. 2857–2860, May 2002.

[26] T. S. Group, *IEEE 802.11 Wireless LANs: TGn Sync Proposal Technical Speciffication*, 2005.

[27] H. Harter, *Order Statistics and Their Use in Testing and Estimation*. Wahington, DC: U.S. Govt. Press., 1973.

[28] R. Heath and A. Paulraj, "Antenna selection for spatial multiplexing systems based on minimum error rate," *Proc. IEEE Int. Contr. Conf.*, vol. 7, pp. 2276–2280, June 2001.

[29] IEEE, *Part 11: Wireless LAN Medium Access Control (MAC) and Physical Layer (PHY) Specifications: High-Speed Physical Layer in the 5 GHz Band*. IEEE Standard 802.11a, 1999.

[30] ——, *Part 11: Wireless LAN Medium Access Control (MAC) and Physical Layer (PHY) Specifications: Further Higher Data Rate Extension in the 2.4 GHz Band*. IEEE Standard 802.11g, 2003.

[31] W. C. Jacks, *Microwave Mobile Communications*. New York: IEEE Press, 1974.

[32] M. Jensen and M. Morris, "Efficient capacity-based antenna selection for MIMO systems," *IEEE Trans on Veh. Technol.*, vol. 1, pp. 110–126, Jan. 2005.

[33] S. M. Kay, *Fundamentals of Statistical Signal Processing: Estimation Theory*, 4th ed. Upper Saddle River, NJ: Prentice Hall, 1993.

[34] M. Kiessling, J. Speidel, I. Viering, and M. Reinhardt, "A closed-form bound on correlated MIMO channel capacity," *Proc. of IEEE Vehic. Technol. Conf.*, 2002.

[35] M. Klessling, J. Speidel, and Y. Chen, "MIMO channel estimation in correlated fading environments," *Proc. of IEEE Vehic. Technol. Conf.*, 2003.

[36] E. Knopp and P. A. Humblet, "On coding for block fading channels," *IEEE Trans. Info. Theory*, vol. 46, no. 1, pp. 189–205, Jan. 2000.

[37] E. G. Larsson and P. Stoica, *Space-Time Block Coding for Wireless Communications*. Cambridge: Cambridge University Press, 2003.

[38] J. Laurila, K. Kalliola, M. Toeltsch, K. Hugl, P. Vainikainen, and E. Bonek, "Wide-band 3-d characterization of mobile radio channels in urban environment," *IEEE Trans. Antennas Propagat.*, vol. 50, pp. 233– 243, Feb. 2002.

[39] J. L. Lawson and G. E. Uhlenbeck, *Threshold Signal*. New York: McGraw-Hill, 1950.

[40] K. F. Lee and D. S. Williams, "A space-time coded transmitter diversity technique for frequency selective fading channels," *Proc. IEEE Sensor Array and Multichannel Signal Processing Workshop*, vol. 2, pp. 15–18, Aug. 2002.

[41] W. C. Y. Lee, "Comparison of an energy density antenna system with predectection combining systems for mobile radio," *IEEE Trans. Commun. Technol.*, vol. 17, no. 2, pp. 277–284, Apr. 1969.

[42] ——, "Effects on correlation between two mobile radio base-station antennas," *IEEE Trans. Commun.*, vol. 21, no. 11, pp. 1214–1224, Nov. 1973.

[43] Y. Li, "Simplified channel estimation for OFDM systems with multiple transmit antennas," *IEEE Trans. Commun.*, vol. 1, no. 1, pp. 67–75, Jan. 2002.

[44] Y. Li, N. Seshadri, and S. Ariyavisitakul, "Channel estimation for OFDM system with transmitter diversity in mobile wireless channels," *IEEE J. Select Areas Commun.*, vol. 17, no. 3, pp. 461–470, Mar. 1999.

[45] Y. Li, J. Winters, and N. Sollenberger, "MIMO-OFDM for wireless communication: signal detection with enhanced channel estimation," *IEEE Trans. Commun.*, vol. 50, no. 9, pp. 1471– 1477, Sept. 2002.

[46] S. Loyka and A. Kouki, "On the use of Jensen's inequality for MIMO channel capacity estimation," *Can. Conf. Elect. Comput. Eng.*, vol. 1, pp. 475–480, May 2001.

[47] H. Lütkepohl, *Handbook of Matrices*. John Wiley & Sons, Inc, 1996.

[48] T. L. Marzetta, "BLAST training: Estimating channel characteristics for high-capacity space-time wireless," *Proc. 37th Annual Allerton Conference on Communications, Control, and Computing*, pp. 958–966, 1999.

[49] A. Molisch, M. Win, and J. Winters, "Capacity of MIMO systems with antenna selection," *Proc. IEEE Int. Contr. Conf.*, vol. 2, pp. 570–574, June 2001.

[50] A. F. Molisch and M. Z. Win, "MIMO systems with antenna selection," *IEEE Microwave*, vol. 5, no. 1, pp. 46– 56, Mar. 2004.

[51] A. F. Molisch, M. Z. Win, and J. H. Winters, "Performance of reduced-complexity transmit/receive-diversity systems," *Proc. IEEE Wireless Personal Multimedia Conf*, vol. 2, pp. 738–742, Oct. 2002.

[52] ——, "Reduced-complexity transmit/receive-diversity systems," *IEEE Trans. Signal Processing*, vol. 51, pp. 2729–2738, Nov. 2003.

[53] J. Moon, H. Jin, T. Jeon, and S. Lee, "Channel estimation for MIMO-OFDM systems employing spatial multiplexing," *Proc. of IEEE Vehic. Technol. Conf.*, 2004.

[54] K. I. Pedersen, P. E. Mogensen, and B. H. Fleury, "Spatial channel characteristics in outdoor enviroments and their impact on bs antenna system performance," *Proc. of IEEE Vehic. Technol. Conf.*, vol. 2, pp. 719–723, May 1998.

[55] J. G. Proakis, *Digital Communications*, 4th ed. New York, NY: McGraw-Hill, 2001.

[56] D. G. R. Nabar and A. Paulraj, "Antenna selection algorithms for mea transmision systems," *Proc. of IEEE ICT*, pp. 567–571, May 2000.

[57] G. G. Raleigh and J. M. Cioffi, "Spatio-temporal coding for wireless communications," *IEEE Trans. Commun.*, vol. 46, no. 3, pp. 357–366, Mar. 1996.

[58] J. Salz and J. Winters, "Effect of fading correlation on adaptive arrays in digital mobile radioe," *IEEE Trans. Veh. Technol.*, vol. 43, pp. 1049–1057, Nov. 1994.

[59] S. Sandhu, R. Nabar, D. Gore, and A. Paulraj, "Near-optimal selection of transmit antenna for a MIMO channel based on Shannon capacity," *Proc. Asilomar Conf. Signals Syst. Comput. Conf.*, vol. 1, pp. 567–571, Oct. 2000.

[60] S. Sandhu and A. Paulraj, "Space-time block codes: a capacity perspective," *IEEE Commun. Lett.*, vol. 4, no. 12, pp. 384–386, Dec. 2000.

[61] L. Schumacher, J. P. Kermoal, F. Frederiksen, K. I. Pedersen, and P. E. Mogensen, "MIMO channel characterisation," *European IST-1999-11729 Project METRA*, Feb. 2001.

[62] L. Schumacher, K. I. Pedersen, and P. E. Mogensen, "From antenna spacings to theoretical capacities-guidelines for simulating MIMO systems," *Proc. IEEE Int. Pers. Indoor Mobile Radio Communi.*, vol. 2, pp. 587–592, Sept. 2002.

[63] H. Shin and J. H. Lee, "Capacity of multiple-antenna fading channels: spatial fading correlation, double scattering, and keyhole," *IEEE Trans. Info. Theory*, vol. 49, no. 10, pp. 2636–2647, Oct. 2003.

[64] D. Shiu, G. J. Foschini, M. J. Gans, and J. M. Kahn, "Fading correlation and its effect on the capacity of multielement antenna systems," *IEEE Trans. Commun.*, vol. 48, no. 3, pp. 502–513, Mar. 2000.

[65] G. Stuber, J. Barry, S. McLaughlin, Y. Li, M. Ingram, and T. Pratt, "Broadband MIMO-OFDM wireless communications," vol. 92, no. 2, pp. 271–294, Feb. 2004.

[66] G. Taricco and E. Biglieri, "Space-Time decoding with imperfect channel estimation," *IEEE Trans. Wireless Commun.*, vol. 4, no. 4, pp. 1874–1888, July 2005.

[67] V. Tarokh, H. Jafarkhani, and A. Calderbank, "Space-time block codes from orthogonal design," *IEEE Trans. Info. Theory*, vol. 45, pp. 1456–1467, July 1999.

[68] V. Tarokh, N. Seshadri, and A. Calderbank, "Space-time codes for high data rate wireless communication: performance criterion and code construction," *IEEE Trans. Info. Theory*, vol. 44, no. 2, pp. 744–765, Mar. 1998.

[69] E. Telatar, "Capacity of multi-antenna Gaussian channels," *European Trans. Telecommun.*, vol. 10, no. 6, pp. 585–595, Nov.-Dec. 1999.

[70] D. Tse and P. Viswanath, *Fundamentals of Wireless Communication, Ch. 3*, 1st ed. United Kingdom: Cambridge University Press, 2005.

[71] S. Verdú and T. S. Han, "A general formula for channel capacity," *Trans. Inform. Theory*, vol. 40, pp. 1147–1157, July 1994.

[72] P. Viswanath, D. N. C. Tse, and R. Laroia, "Opportunistic beamforming using dumb antenna," *Trans. Inform. Theory*, vol. 48, pp. 1277–1294, June 2002.

[73] X. Wang, K. Niu, and W. Wu, "Performance of antenna selection transmit diversity with opportunistic beamforming in slow fading channels," *Proc. of IEEE Vehic. Technol. Conf.*, 2005.

[74] S. B. Weinstein and P. M. Ebert, "Data transmission by frequency-division multiplexing using discrete Fourier transform," *IEEE Trans. Commun. Technol.*, vol. COM-19, pp. 628–632, Oct. 1971.

[75] J. H. Winters, "Wireless PHX/LAM system with optimum combining," *United States Patent*, Dec. 1984.

[76] W. H. Wong and E. G. Larrson, "Orthogonal space-time block coding with antenna selection and power allocation," *IEE Elect. Lett*, vol. 39, no. 4, pp. 379–381, Feb. 2003.

[77] K. Yu, M. Bengtsson, B. Ottersten, D. McNamara, P. Karlsson, and M. Beach, "Modeling of wide-band MIMO radio channels based on nlos indoor measurements," *IEEE Trans. Veh. Technol.*, vol. 53, no. 3, pp. 655–665, May 2004.

[78] L. Zan and S. A. Jafar, "Combined opportunistic beamforming and receive antenna selection [cellular downlink applications]," *Proc. of IEEE Wireless Communications and Networking Conf.*, vol. 2, pp. 1007–1011, Mar. 2005.

[79] X. N. Zeng and A. Ghrayeb, "Antenna selection for space-time block codes over correlated Rayleigh fading channels," *Can. J. Elect. Comput. Eng.*, vol. 29, no. 4, pp. 219–226, Oct. 2004.

[80] Z. Zhou, Y. Dong, X. Zhang, W. Wang, and Y. Zhang, "A novel antenna selection scheme in MIMO systems," *Proc. IEEE Int. Conf. Communications, Circuits and Systems*, vol. 1, pp. 190–194, June 2004.